NASA CONTRACTOR REPORT

NASA CR-1067

INFRARED RADIOMETRIC STRESS INSTRUMENTATION APPLICATION RANGE STUDY

by Milo H. Belgen

Prepared by

NORTH AMERICAN AVIATION, INC.

Columbus, Ohio

for Langley Research Center

NATIONAL AERONAUTICS AND SPACE ADMINISTRATION • WASHINGTON, D. C. • MAY 1968

NASA CR-1067

INFRARED RADIOMETRIC STRESS INSTRUMENTATION APPLICATION RANGE STUDY

By Milo H. Belgen

Prepared under Contract No. NAS 1-6082 by
NORTH AMERICAN AVIATION, INC.
Columbus, Ohio

for Langley Research Center

NATIONAL AERONAUTICS AND SPACE ADMINISTRATION

For sale by the Clearinghouse for Federal Scientific and Technical Information
Springfield, Virginia 22151 – CFSTI price $3.00

CONTENTS

INFRARED RADIOMETRIC STRESS INSTRUMENTATION

APPLICATION RANGE STUDY

By Milo H. Belgen
North American Aviation, Inc.
Columbus Division

SUMMARY

The theory governing thermoelastic energy conversion was defined for adiabatic material elements subjected to oscillating stresses. The thermoelastic constants of four structural metals were measured. The thermoelastic constant is of significant magnitude for structural metals, and the energy conversion produces a small magnitude of temperature oscillation in an adiabatic material element subjected to oscillating stress. The oscillating radiant signal emitted by an adiabatic material element was theoretically defined for the oscillating stresses typical of fatigue, vibration and acoustic test parts. The frequency ranges of emitted signal losses due to non-adiabatic and high emissivity coating lag effects were theoretically defined and experimentally verified. The transient responses of high emissivity coatings were experimentally evaluated. This yielded quantitative definition of emitted radiant signals.

The signal attenuation by four diversely different pressure barrier windows was theoretically defined in terms of window pressure differential and other pertinent parameters. Radiometer performance was theoretically defined for optical collection systems and infrared detectors. The collection parameters were correlated in terms of the compromises available relative to spatial resolution and signal power irradiating the detector. The performance characteristics of five diversely different infrared detectors were defined, and this was combined with the signal emission and loss analysis to evaluate a "detectable stress". Detectable stress is the lower limit of stress oscillation likely to be detected (and the probable accuracy limit of measurements at greater stress levels).

The above research was utilized to develop a simplified method for evaluating infrared stress measurement applications and to study typical attainable spatial resolutions and detectable stresses (for selected detectors and windows) as a function of test part temperature and stress oscillation frequency. It appears that room temperature infrared measurements might have accuracies of the same general magnitude as conventional instrumentation, and infrared is likely to be more favorable than conventional instrumentation relative to accuracy and other factors at elevated temperatures. Since infrared measurements yield data on the sum of principal stresses, various combinations of infrared and conventional strain instrumentation could yield many (undefined) types of data not previously within the state-of-the-art. Infrared permits rapid spatial data acquisition by scanning with an analog electronic signal output.

INTRODUCTION

When a material is subjected to loads which change its volume, there is a conversion between the mechanical and thermal forms of energy. If the loads produce stress variations within the elastic limit of the material, the energy conversions are nearly reversible (or isentropic). The existence of this physical phenomena, commonly called the thermoelastic effect, has been recognized for many years (ref. 1). The thermoelastic effect has been incorporated into many diverse aspects of structural theory. The manner in which strain gage measurements are altered by the thermoelastic effect has been evaluated (ref. 2). The thermoelastic effect has been applied for measurement of dynamic stresses with thermocouples (ref. 3).

Application of the thermoelastic effect for measurement of dynamic stresses with an infrared radiometer was recently reported (ref 4 and 5). The non-contacting radiometric sensor with this technique has potential advantages over conventional structural instrumentation, such as strain gages, photoelastic coatings, and brittle coatings. The non-contacting sensor is suitable for rapid spatial data acquisition by surface scanning from relatively large stand-off distances. Since no sensor attachment to test parts is required, the radiometric technique circumvents sensor weight addition effects for dynamic tests and thermal degradation effects for elevated temperature tests. However, the potential advantages of radiometric stress measurements could not be quantitatively evaluated from the limited initial feasibility study of the technique.

Although the approximate magnitudes of adiabatic thermoelastic temperature changes could be theoretically predicted, quantitative experimental data were not available for common structural metals. Although non-adiabatic effects (signal losses due to heat transfer within test parts and between test parts and their environment) were expected at low frequencies, the magnitudes of these frequencies were unknown. Although coating thermal lag effects (signal losses due to high emissivity coatings which might be applied for radiation signal enhancement) were expected at high frequencies, the magnitudes of these frequencies were unknown. Although approximate magnitudes of attainable stress measurement accuracies were known for a specific simple radiometer, the magnitudes of accuracies for more sophisticated radiometers (with or without pressure barrier window attenuation) were unknown.

The primary purpose of the investigation reported herein was to define infrared radiometric stress instrumentation accuracy versus range parameters in terms of the direct signal factors identified above. A secondary purpose was to identify (but not develop) additional techniques required for direct stress read-out with radiometric sensors. The investigation was limited to unclassified data so that the results could be freely disseminated.

Mr. J. A. Daily is the author of Appendix E. Mr. Robert K. Hanning is co-author of Appendixes A and C. Mr. Ralph T. Rauch is co-author of Appendix F.

SYMBOLS

A_d	infrared detector sensitive surface area, millimeters^2
C_z	temperature increment signal ratio factor for bending stresses, seconds
C_x	temperature increment signal ratio factor for lateral stress gradients, seconds
C_e	temperature increment signal ratio factor for environmental heat transfer, seconds
C_c	temperature increment signal ratio factor for a coating, seconds
c	specific heat of test part material (approximate value of c_p for conductance and environmental analysis), joules/degree Kelvin gram
c_v	specific heat at constant volume of a test part material, joules/degree Kelvin gram
c_p	specific heat at constant pressure of a test part material, joules/degree Kelvin gram
c_σ	effective specific heat of an adiabatic test part material element subjected to large stress increments within the elastic limit, joules/degree Kelvin gram
c_1	first radiation constant in Planck's equation 37 405 watts microns^5/centimeter^2 micron
c_2	second radiation constant in Planck's equation, 14 388 micron degrees Kelvin
D_o	radiometer optics aperture diameter, centimeters
D_w	diameter of a circular window, centimeters
$D^*_{\lambda r}$	spectral specific detectivity of an infrared detector at a reference frequency, centimeter $\sqrt{\text{hertz}}$/watt
E	Young's modulus of elasticity of a material, newtons/centimeter^2 (selected data in pounds/inch^2)
e'	sum of principal strain components in an adiabatic element, centimeters/centimeter
f	frequency of sinusoidal stress oscillation of a test part, hertz
f_o	radiometer optics focal length, centimeters
h	coefficient of heat transfer between a test part surface and its environment, watts/degree Kelvin centimeter^2

K_M	material thermoelastic constant, centimeters^2/newton (selected data in inches^2/pound)
K_o	a geometric optical function, steradians/centimeter
k	thermal conductivity of test part material, watts/degree Kelvin centimeter
L_o	stand-off distance (from a radiometer to its focal plane), centimeters
L_{or}	stand-off distance for maximum radiometric angular field with specific spatial resolution criteria, centimeters
q_t	instantaneous rate of thermoelastic energy conversion, watts/centimeter^3
q_x	maximum rate of thermoelastic energy conversion (for a selected time), watts/centimeter^3
q_z	maximum rate of thermoelastic energy conversion (for a selected time) at distance z below the surface of a test part, watts/centimeter^3
s_o	size of field of view at the focal plane of a radiometer, centimeters
s_{xy}	size of a radiometric field of view on a test part surface, centimeters
T	average temperature of a body subjected to an oscillating temperature variation, degrees Kelvin
t	time, seconds
t_c	thickness of a coating, centimeters (selected data in mils)
t_p	thickness of a test part, centimeters
t_w	thickness of a window, centimeters
(V_S/V_N)	overall radiometer signal-to-noise ratio, dimensionless
$V'_{\lambda r}$	integrated spectral signal-to-noise ratio parameter, $\sqrt{\text{hertz}}$/centimeter steradian
X_w	width of a rectangular window, centimeters
x_p	lateral distance between an instantaneous radiometric field of view and an infinite heat sink on a test part, centimeters
Y_w	length of a rectangular window, centimeters

ℓ	half-thickness of a plate type of test part, centimeters
z	distance between a substrate material element and the surface of a plate type of test part, centimeters
α_c	thermal diffusivity of a coating, centimeters^2/second
α_p	thermal diffusivity of a test part structural material, centimeters^2/second
α_x	linear thermal coefficient of expansion of a test part structural material, centimeters/centimeter degree Kelvin.
Δf	electronic filter equivalent rectangular bandwidth, hertz
ΔL_o	optical field depth (total) for a radiometer focused at stand-off distance L_o, centimeters
$\Delta N_{\lambda 1}$	spectral signal radiance emitted from a surface, watts/centimeter^2 steradian micron
$\Delta N_{\lambda 2}$	spectral signal radiance transmitted to the aperture of a radiometer, watts/centimeter^2 steradian micron
$\Delta P_{\lambda 3}$	spectral signal radiant power incident on an infrared detector sensitive surface, watts/micron
ΔP	pressure differential across a window, pounds/inch^2
δ_w	maximum deflection of a window, inches
ε_λ	spectral normal emissivity of a surface, dimensionless
$\bar{\varepsilon}_\lambda$	integrated average spectral emissivity in a selected important infrared detection wave length range, dimensionless
η_o	radiometer overall optical efficiency factor, dimensionless
η_d	ratio of detectivity at a frequency f and a reference frequency for an infrared detector, dimensionless
η_z	ratio of actual and adiabatic temperature oscillations (root-mean-square) for thermoelastic energy conversion with bending stresses, dimensionless
η_x	ratio of actual and adiabatic temperature oscillations (root-mean-square) for thermoelastic energy conversion with extreme lateral stress gradients, dimensionless
η_e	ratio of actual and adiabatic temperature oscillations (root-mean-square) for thermoelastic energy conversion with environmental heat transfer, dimensionless

η_c	ratio of surface and substrate temperature oscillations (root-mean-square) for a coating, dimensionless
η_p	emitted signal ratio at frequency f (η_z, η_x, η_e, or η_c), dimensionless
θ	peak-to-peak amplitude of temperature oscillation in an adiabatic material element due to a stress oscillation σ, degrees Kelvin
θ'	temperature increment (relative to a temperature level T) produced by stresses in an adiabatic material element, degrees Kelvin
θ'_p	temperature increment (relative to a temperature level T) produced by stresses in a non-adiabatic surface material element (within a radiometric field of view), degrees Kelvin
θ'_{pz}	temperature increment (relative to a temperature level T) produced by stresses in a non-adiabatic substrate material element, degrees Kelvin
λ	spectral infrared radiation wave length, microns
λ_L	Lame' constant, newtons/centimeter^2
μ_L	Lame' constant, newtons/centimeter^2
ν	Poisson's ratio of a material, dimensionless
ρ	density of test part material, grams/centimeter^3
σ	peak-to-peak amplitude of oscillation of the sum of principle stresses in a material element, newtons/centimeter^2 (selected data in pounds/inch^2)
σ^*	minimum detectable stress, newtons/centimeter^2 (selected data in pounds/inch^2)
σ_{ii}	principal stress components xx, yy, and zz in an adiabatic material element (plus convention for tension), newtons/centimeter^2
σ_w	maximum stress in a window, pounds/inch^2
τ_λ	transmittance of an infrared window, dimensionless
τ_c	time constant for thermal response of a coating surface, seconds
ϕ_o	detector plane angular field of view, milliradians
ϕ_{or}	maximum field with specific spatial resolution criteria, milliradians

RESULTS AND DISCUSSION

Test Part Signal Generation

Thermoelastic Energy Conversion. - The basic source of infrared stress measurement signals is the conversion between the mechanical and thermal forms of energy which occurs when changes of stresses within a material element alter its volume. The elastic and thermodynamic theory for a material element with isotropic properties yields the relations

$$(\sigma_{xx} + \sigma_{yy} + \sigma_{zz}) = 2\mu_L e' + 3\lambda_L e' - (2\mu_L + 3\lambda_L)\, 3\alpha_x \theta'$$

$$e' = \frac{\rho\, c_v\, \theta'}{100(2\mu_L + 3\lambda_L)\, \alpha_x T}$$

when expressed in terms of coefficient of linear thermal expansion α_x and mass specific heat at constant volume c_v with the selected dimensional units (ref. 6). The above equations can be combined and simplified to the relations

$$\theta' = - K_M T(\sigma_{xx} + \sigma_{yy} + \sigma_{zz})$$

$$K_M = \frac{100_x}{c_v + \dfrac{100(2\mu_L + 3\lambda_L)\, 3\alpha_x{}^2 T}{\rho}}$$

where K_M is a designated thermoelastic constant primarily dependent on test part material properties.

The equation for θ' above implies that adiabatic temperature increments for a specific material are a linear function of the temperature level and the sum of principal stresses. With a plus convention for tension stresses, the negative sign implies that tension produces decreases and compression produces increases of material temperatures (if K_M is positive, as it is for nearly all materials). This investigation is directed toward infrared measurements of oscillating stresses rather than step changes in stresses. For a peak-to-peak sinusoidal stress oscillation σ and an adiabatic temperature oscillation θ, thermoelastic energy conversion is defined by the relations

$$\theta = K_M T \sigma$$

$$\theta' = (\theta/2) \sin 2\pi ft$$

$$q_t = \rho c \frac{d\theta'}{dt} = (\pi \rho c \theta f) \cos 2\pi ft$$

in which the adiabatic heat storage rate q_t is the energy conversion rate. These equations are general in terms of stress oscillation about an arbitrary average magnitude (which is not necessarily zero).

The equation for K_M above contains properties requiring more careful definition for this instrumentation application than for the common engineering applications. For the adiabatic material elements most important relative to infrared stress measurement, the Lame' constants are defined by the relations

$$\mu_L = \frac{E}{2(1 + \nu)}$$

$$\lambda_L = \frac{E\nu}{(1 + \nu)(1 - 2\nu)} + \frac{\alpha_x E^2 T}{c_v (1 - 2\nu)^2}$$

which have been verified by adiabatic sound transmission experiments (ref. 7 and 8). However, the second term in λ_L can be shown to have a negligible effect on thermoelastic constants for common materials, and dropping it yields the relation

$$K_M = \frac{100\alpha_x}{\rho \left[c_v + 100 \frac{3E\alpha_x{}^2 T}{\rho(1 - 2\nu)} \right]}$$

applicable for the isothermal Lame' constants. The quantity in brackets is the theroretical expression for the specific heat at constant pressure for a solid. This can be verified from the basic theory (ref. 9 and 10), noting that the 100 is a units conversion factor, density is the reciprocal of specific volume, and cubical expansion is three times linear expansion. These considerations yield the relation

$$K_M = \frac{100\alpha_x}{\rho\, c_p}$$

which is considered applicable for small stress increments. However, large stress increments produce both volume and pressure changes in solid materials, and an effective specific heat c_σ must then be introduced. This yields the relation

$$K_M = \frac{100\alpha_x}{\rho\, c_\sigma}$$

in the form sometimes shown in the literature (ref. 11). Most of the specific heat experiments reported in the literature were performed at constant (zero) pressure, and no exact definition of c_σ is known to exist. However, the known qualitative trends in compressibility of solids indicates that specific heat increases with pressure for some materials and decreases with pressure for other materials (ref. 10).

The theory on thermoelastic constants was derived with the assumption that all pertinent material properties are isotropic properties. Poisson's ratio is known to be somewhat anisotropic and to vary slightly with strain (within the elastic limit) for aluminum, magnesium, and titanium (ref. 12). Although small variations of Poisson's ratio would have little numerical effect on isotropic thermoelastic constants, the anistropic effects not included in the theory could be significant.

Experimental data indicate that there are some second order variations in material thermoelastic constants. (See section on "Thermoelastic Experiments", p. 95). These variations are probably due to the effects of stress on specific heat and/or Poisson's ratio (with anistropic materials). The second order variations can be neglected in evaluating infrared stress detection ranges, but must be considered in evaluating accuracy. Some infrared stress data corrections can be made for the second order variations with the results of the current investigation (See section on "Instrumentation System Methodology", p. 62). Ultimate accuracy would require more complete definition of the second order variations (See section on "Recommended Future Work", p. 86).

Infrared Radiation Signal Magnitudes.- The most important infrared stress measurement applications will involve a small surface element that is flat (or nearly flat) and is viewed perpendicular, (or nearly perpendicular) to its surface plane with the surface element completely filling a radiometer field of view. It is desirable to select signal parameters that are exact for the most important applications and have small magnitudes of variation for wide ranges of surface flatness and viewing angle. On this basis, the most suitable parameters are surface normal radiance and emissivity.

For a diffuse radiator, the radiance signal is independent of surface flatness and viewing angle. Lambert's law of cosines shows the radiance per unit surface area to vary directly as the cosine of viewing angle (ref. 13, p. 25). The area of any surface element completely filling a radiometer field of view will vary inversely as the cosine of viewing angle. The diffuse signal radiance is therefore independent of angular factors, but the surface area within the radiometer field of view is a function of viewing angle. (See section on Optical Collection Parameters", p. 38).

For real surfaces, the actual angular radiation does not conform exactly with Lambert's law of cosines when the angles are more than twenty degrees from perpendicular to the surface. The deviations are greatest for angles exceeding sixty degrees (reference 14, pp.41-51) which are not viewing angles of interest in this application. However, the summation of angular effects in a hemispherical field is significant for most real surfaces, and normal emissivity is a significantly more accurate surface property parameter than hemispherical (or total) emissivity for this application (ref.14, p. 52).

Thermoelastic energy conversion produces temperature increments which are small compared with temperature levels T. For a black body, the rate of hemispherical (or total) spectral radiant emittance change with temperature is a function of temperature level and wave length (ref.13, p. 24). The radiance (or radiant intensity) in the direction normal to a surface is $1/\pi$ times the hemispherical (or total) power radiated by the surface (ref.15, pp 332). For a real surface of emissivity ϵ_λ, the spectral radiance charge $\Delta N_{\lambda 1}$ is defined by the relation

$$(\Delta N_{\lambda 1}/\epsilon_\lambda \theta) = \frac{c_1 c_2}{\pi} \frac{e^{c_2/\lambda T}}{T^2 \lambda^6 (e^{c_2/\lambda T} - 1)^2}$$

where c_1 and c_2 are constants (ref. 13, pp. 13-19 and ref. 16, p. 5). The above equation in terms of adiabatic thermoelastic temperature increments yields the relation

$$(\Delta N_{\lambda 1}/\epsilon_\lambda K_M \sigma) = \frac{c_1 c_2}{\pi} \frac{e^{c_2/\lambda T}}{T \lambda^6 (e^{c_2/\lambda T} - 1)^2}$$

defining the basic infrared stress signal parameter. (See section on "Thermoelastic Energy Conversion", pp. 7).

The magnitude and spectral energy distribution of the thermoelastic signal parameter varies with temperature (fig. 1). The thermoelastic spectral energy distribution is the same function of temperature level as other infrared sources of small temperature increments. The magnitudes of thermoelastic signals (at constant stress increment) increase more rapidly with temperature than signals from other infrared sources (at constant temperature increment). Thermoelastic signal radiance is proportional to surface emissivity (as with other infrared sources) but is also proportional to test part thermoelastic constant (which is a function of certain material properties). This is expressed by the relation

$$\Delta N_{\lambda 1} = (\Delta N_{\lambda 1}/\epsilon_\lambda K_M \sigma)(\epsilon_\lambda)(K_M)(\sigma)$$

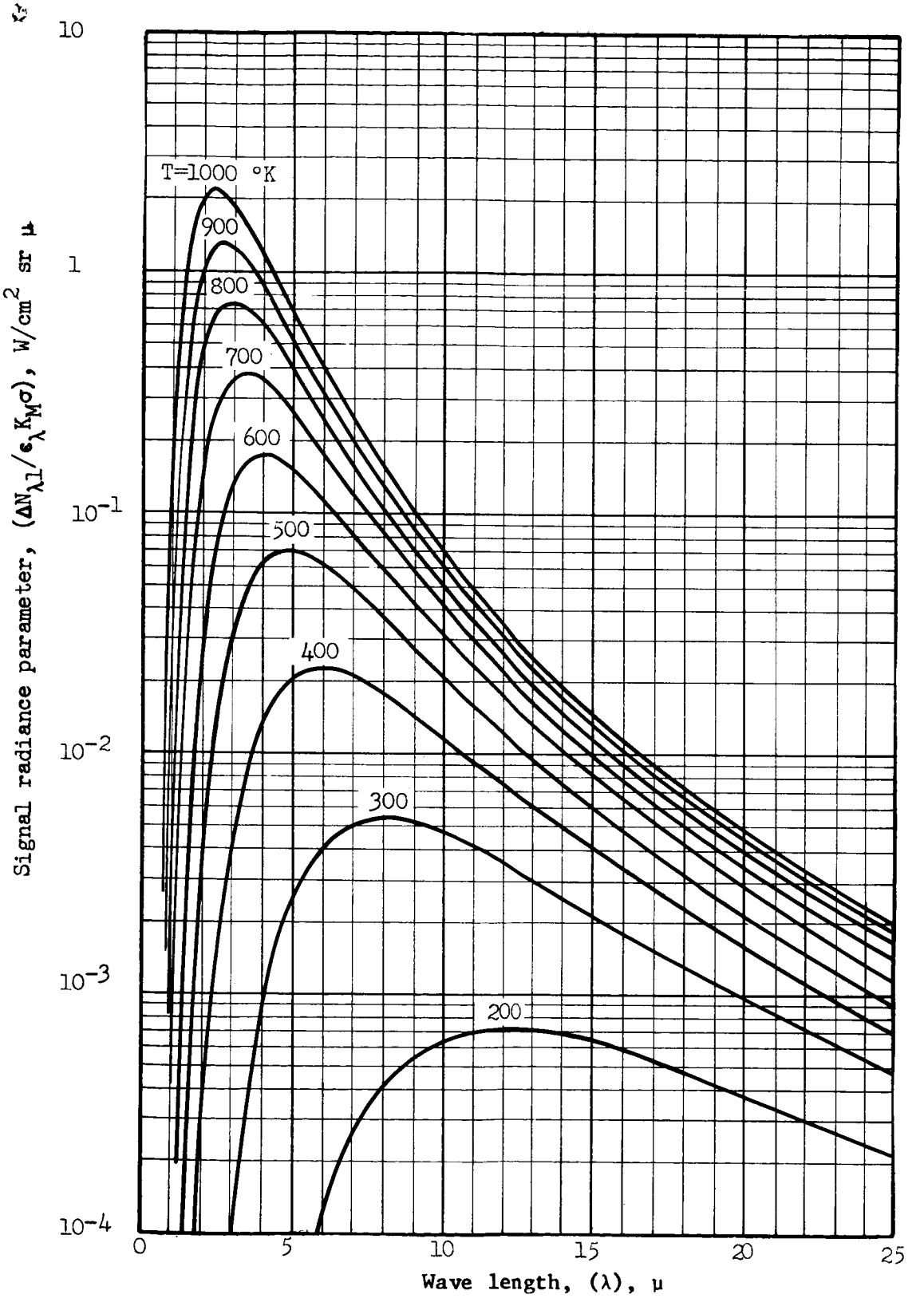

Figure 1.- Test part signal radiance emission parameter

which contains all factors necessary to define the signal radiance in terms of oscillating stress σ_o. The thermoelastic constant is applicable to adiabatic material elements and to the structural substrate of a coated test part. Actual signal radiance can be altered by non-adiabatic and coating response effects under some conditions. (See sections on "Substrate Conductance", "Lateral Conductance", "Environmental Radiation and Convection", and "Coating Thermal Response", pp. 12, 16, 21, and 25).

Substrate Conduction. - When a plate is subject to loading which changes its surface radius of curvature, bending stresses are produced within the plate. For pure bending, the stress varys linearly through the plate from a compression level at one surface to an equal tension level at the other surface (the plate mid-plane stress being zero). If the plate is vibrating in pure bending, the peak-to-peak stress oscillation varys directly with distance from the plate mid-plane (the highest magnitudes being at the surfaces). The oscillating thermoelastic energy conversion rate in this case will have maximum peak-to-peak magnitude at the surfaces, be zero at the mid-plane, and have opposite (positive-negative) sign on the two sides of the midplane at all times. (See section on "Thermoelastic Energy Conversion", p. 8). The energy conversion will therefore produce oscillating heat conduction between the two plate surfaces, and a radiometrically viewed surface element cannot be considered adiabatic when the heat transfer between the surface and its substrate is significant.

Since thermoelastic energy conversion is identical in magnitude and opposite in sign on the two sides of the mid-plane for a plate subjected to bending, the mid-plane will remain isothermal. When thermal gradients within the plate are significant, environmental heat transfer will be negligible compared with conduction, and the plate surfaces will be essentially adiabatic. The transient conduction equations of this thermal model have been solved for the case of an arbitrary spatial distribution of heat generation (that does not vary with time). With the symbols defined in this report, the relations

$$(\theta'_{pz})_{q_z} = \frac{4Z}{\pi^2 k} \sum_{n=0}^{\infty} \frac{(1 - e^{-\pi^2 \alpha_p F_1 t})(\cos F_1 \pi z)}{(2ZF_1)^2} \int_{-Z}^{Z} (q_z \cos F_1 \pi z) dz$$

$$F_1 = (2n+1)/2Z$$

are applicable (ref. 17, pp. 130-132), when it is noted that the summation from zero of (2n+1) is required in equation (10) as well as (7) and (9) of the reference. For a plate subjected to bending, the thermoelastic energy conversion will be a linear function of distance from the plate mid-plane, and the maximum rate will be ($\pi\rho c\theta f$) at the surfaces. (See section on "Thermoelastic Energy Conversion", p. 8). These considerations yield the relations

$$q_z = (\pi\rho c\theta f)(1 + z/Z) \qquad -Z<z<0$$

$$q_z = (\pi\rho c\theta f)(1 - z/Z) \qquad 0<z<Z$$

$$\int_{-Z}^{Z} (q_z \cos F_1\pi z)dz = \frac{2\rho c\theta f}{\pi Z F_1^2}$$

as the evaluation of the required spatial definite integral. Substitution into the heat conduction equation yields the relation

$$(\theta'_{pz})_{q_z} = \frac{2\theta f}{\pi^3 \alpha_p Z^2} \sum_{n=0}^{\infty} \frac{(\cos F_1\pi z)}{F_1^4} \left(1 - e^{-\pi^2\alpha_p F_1^2 t}\right)$$

defining transient temperatures versus time. The above equation would be applicable if the maximum energy conversion rates were instaneously applied within the plate and did not vary with time.

The equation for oscillating heat generation can be obtained from the equation for steady-state heat generation by applying Duhamel's theorem (ref. 17, pp. 30-31). For the portion of the equation dependent on time, this yields the relations

$$f(z,t) = \left(1 - e^{-\pi^2\alpha_p F_1^2 t}\right)$$

$$f(z,\tau,t-\tau) = \left\{1 - e^{-\pi^2\alpha_p F_1^2 (t-\tau)}\right\} (\cos 2\pi f\tau)$$

$$\frac{\partial f(z,\tau,t-\tau)}{\partial t} = (\pi^2\alpha_p F_1^2)(\cos 2\pi f\tau)e^{-\pi^2\alpha_p F_1^2 (t-\tau)}$$

$$f(z,t)_{q_t} = \int_0^t \frac{\partial f(z,\tau,t-\tau)}{\partial t} d\tau = \frac{F_2 F_3}{1 + F_2^2}$$

$$F_2 = \frac{\pi\alpha_p}{2f} \quad F_1^2 = \frac{\pi\alpha_p(2n+1)^2}{8fZ^2}$$

$$F_3 = (\sin 2\pi ft) + F_2 (\cos 2\pi ft) + F_2 e^{-\pi^2\alpha_p F_1^2 t}$$

applicable to sinusoidal variation of stress. Substitution of this time function for that in the complete equation for conduction with constant heat generation yields the relation

$$\theta'_{pz} = \frac{2\theta f}{\pi^3\alpha_p Z^2} \sum_{n=0}^{\infty} \frac{(\cos F_1\pi z)(F_2F_3)}{F_1^4 (1 + F_2^2)}$$

which is the general equation for transient temperatures throughout the vibrating plate. Substituting zero for **z** yields the relation

$$\theta'_p = \frac{\theta}{\pi^2 Z^2} \sum_{n=0}^{\infty} \frac{(\sin 2\pi ft) + F_2 (\cos 2\pi ft) - F_2 e^{-\pi^2\alpha_p F_1^2 t}}{F_1^2(1 + F_2^2)}$$

defining the plate surface temperature versus time.

The exponential term accounts for an initial transient disturbance which would occur if vibration were instanteously initiated in a test part. This disturbance would vanish during early vibration cycles, and the temperature oscillation amplitude would become constant. After steady-state vibration for a sufficient period of time, the surface transient temperature is defined by the relation

$$\theta'_p = \frac{\theta(\sin 2\pi ft)}{\pi^2 Z^2} \sum_{n=0}^{\infty} \frac{1 + F_2(\cot 2\pi ft)}{F_1^2(1 + F_2^2)}$$

in which the initial transient disturbance is neglected. The adiabatic and non-adiabatic temperatures can be compared with the relations

$$\theta' = (\theta/2)(\sin 2\pi ft)$$

$$\theta_p' = (\theta')(8/\pi^2) \sum_{n=0}^{\infty} \frac{1}{(2n+1)^2} \frac{1 + (F_4\alpha_p/fZ^2)(\cot 2\pi ft)}{1 + (F_4\alpha_p/fZ^2)^2}$$

$$F_4 = \pi(2n+1)^2/8$$

(See section on "Thermoelastic Energy Conversion", p. 7). The non-adiabatic effects are a function of the material thermal diffusivity, plate half-thickness, and oscillation frequency. These effects vanish (in conformance with the known physical trends) for zero diffusivity and for infinite thickness and frequency (because the summation becomes the reciprocal of the constant in the non-adiabatic relation).

The ratio of non-adiabatic and adiabatic (rms) temperatures yields the relations

$$\eta_z = \frac{\sqrt{f\int_0^{1/f} (\theta_p')^2 dt}}{\sqrt{f\int_0^{1/f} (\theta')^2 dt}}$$

$$\eta_z = \frac{8}{\pi^2} \sqrt{\left[\sum_{n=0}^{\infty} \frac{F_n}{(2n+1)^2}\right]^2 + (\pi/2C_z f)^2 \left[\sum_{n=0}^{\infty} F_n\right]^2}$$

$$F_n = \frac{1}{1 + (\pi/2C_z f)^2 (2n+1)^4}$$

$$C_z = (t_p^2/\alpha_p)$$

defining the substrate conduction effects on sinusoidal stress signals. The relations are considered exact because no simplifying approximations were necessary in their derivation.

The general relationships shown above provide a means of evaluating the signal ratios produced by substrate conduction (fig. 2). Frequency is the important independent test variable, and the signal ratio factor C_z

accounts for all other factors affecting substrate conduction.

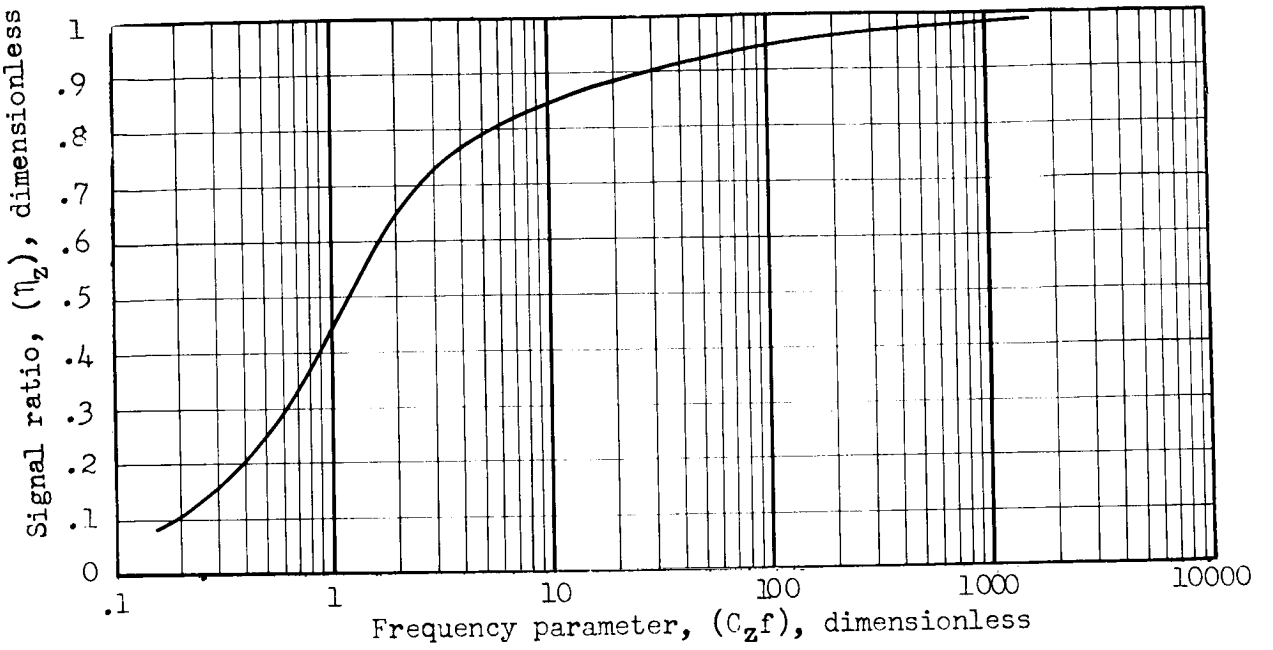

Figure 2.- Signal ratio parameters for substrate conduction

The signal loss by substrate conduction does not preclude acquisition of infrared stress data if the attenuated signal is strong enough for radiometric sensing. Observed data can be corrected when the frequency and test part characteristics are known. Such corrections would be exact in terms of their theoretical basis, and would be fairly accurate in terms of the observation of frequency, the measurement of test part thickness, and the evaluation of test part thermal diffusivity. However, the accuracy of corrections will sometimes be limited by uncertainty in the relative magnitude of the bending stress component (for parts not known to be subject to bending only), and this constitutes the basic lower frequency limitation imposed by substrate conduction.

In addition to the signal attenuation, substrate conduction alters the wave shape and phase angle of the adiabatic signal. These factors can be important in certain special applications (but not rms stress measurements).

Lateral Conduction. - When a thin plate is subjected to loading, the bending stress (and substrate conduction) is frequently small, and the biaxial stress field over the plate area is then of interest. The spatial stress distribution in this case is a function of the type of loading and the manner in which loads are transferred through the plate by shear stress

lag. The thermoelastic energy conversion rates with an oscillating biaxial stress field are therefore different for various portions of the plate. This will produce oscillating lateral heat conduction within the plate, and a radiometrically viewed plate area cannot be considered adiabatic when the heat transfer between the viewed area and the surrounding plate is significant.

The general case of lateral conduction with arbitrary biaxial stress fields is specific for each test application. However, a simplified maximum lateral conduction case can be selected as a means of evaluating ranges in which significant lateral conductance might be obtained. The selected case is a thin plate subjected to a finite (constant) oscillating stress with one edge of the plate connected to a semi-infinite solid which has small (negligible) stress and temperature oscillation. The transient conduction equations of this thermal model have been solved for the particular case of a constant spatial heat generation rate (that does not vary with time). With the symbols defined in this report, the relations

$$(\theta_p')_{q_x} = \frac{\alpha_p q_x}{k} \left[f(x,t)_{q_x} \right]$$

$$f(x,t)_{q_x} = (t + 2X^2)\operatorname{erf} \frac{X}{\sqrt{t}} + \frac{2X\sqrt{t}e^{-X^2/t}}{\sqrt{\pi}} - 2X^2$$

$$X = \frac{x_p}{2\sqrt{\alpha_p}}$$

are applicable (ref. 17, p. 79), when equation (2) of the reference is simplified to the case of zero initial temperatures. The maximum rate of thermoelastic energy conversion yields the relations

$$q_x = (\pi \rho c \theta f)$$

$$(\theta_p')_{q_x} = (\pi \theta f) \left[f(x,t)_{q_x} \right]$$

(See section on "Thermoelastic Energy Conversion", p. 8). The above equations define the transient temperatures which would be obtained if the maximum thermoelastic energy conversion rate was instantaneously applied within the plate and did not vary with time.

The equation for oscillating heat generation can be obtained from the equation for steady-state heat generation by applying Duhamel's theorem (ref. 17, pp. 30-31). For the portion of the equation dependent on time, this yields the relations

$$f(x,\tau,t-\tau) = \left[(t-\tau+2X^2)\ \mathrm{erf}\ \frac{X}{\sqrt{t-\tau}} + \frac{2X}{\sqrt{\pi}}\sqrt{t-\tau}\ e^{-\frac{X^2}{t-\tau}} - 2X^2 \right] (\cos 2\pi f\tau)$$

$$\frac{\partial f(x,t,t-\tau)}{\partial t} = \left[\mathrm{erf}\ \frac{X}{\sqrt{t-\tau}} \right] (\cos 2\pi f\tau)d\tau$$

$$f(x,t)_{q_t} = \int_o^t \frac{\partial f(x,t,t-\tau)}{\partial t}\, d\tau = \frac{(\sin 2\pi ft) - F_5 + F_6}{2\pi f}$$

$$F_5 = \left[\sin(2\pi ft) - 2X\sqrt{\pi f} \right] e^{-2X\sqrt{\pi f}}$$

$$F_6 = \frac{2}{\sqrt{\pi}} \int_o^{X/\sqrt{t}} \left[\sin 2\pi f \left\{ t - \frac{X^2}{\phi^2} \right\} \right] e^{-\phi^2}\, d\phi$$

$$\phi = \frac{X}{\sqrt{t-\tau}}$$

applicable to sinusoidal variation of stress. Substitution of this time function for that in the complete equation for conduction with constant heat generation yields the relation

$$\theta_p' = (\theta/2) \left[(\sin 2\pi ft) - F_5 + F_6 \right]$$

which is the general equation for transient temperatures throughout the vibrating plate.

The definite integral term F_6 accounts for an initial transient disturbance which would occur if vibration were instantaneously initiated in a test part. This disturbance would vanish during early vibration cycles (ref. 17, p. 65), and the temperature oscillation amplitude would become constant. After steady-state vibration for a sufficient period of time, the plate transient temperatures are defined by the relations

$$\theta_p' = (\theta/2)\ (\sin 2\pi ft)\left[1 - F_7F_8\left\{1 - F_9(\cot 2\pi ft)\right\}\right]$$

$$F_7 = e^{-2X\sqrt{\pi f}}$$

$$F_8 = (\cos 2X\sqrt{\pi f})$$

$$F_9 = (\tan 2X\sqrt{\pi f})$$

in which the initial transient disturbance is neglected. The adiabatic and non-adiabatic temperatures can be compared with the relations

$$\theta' = (\theta/2)(\sin 2\pi ft)$$

$$\theta_p' = \theta'\left[1 - \left\{1 - (\cot 2\pi ft)(\tan F_{10})\right\}\left\{\cos F_{10}\right\}\left\{e^{-F_{10}}\right\}\right]$$

$$F_{10} = 2X\sqrt{\pi f} = x_p\sqrt{\pi f/\alpha_p}$$

(See section on "Thermoelastic Energy Conversion", p. 7). The non-adiabatic effects are a function of the material thermal diffusivity, distance from an infinite heat sink, and oscillation frequency. These effects vanish (in accordance with known physical trends) for zero diffusivity and for infinite distance and frequency (because the exponential in the non-adiabatic relation becomes zero).

The ratio of non-adiabatic and adiabatic (rms) temperatures yields the relations

$$\eta_x = \frac{\sqrt{f\int_o^{1/f} (\theta_p')^2 \, dt}}{\sqrt{f\int_o^{1/f} (\theta')^2 \, dt}}$$

$$\eta_x = \sqrt{1 - e^{-\sqrt{\pi C_x f}} \left[2 \cos\sqrt{\pi C_x f} - e^{-\sqrt{\pi C_x f}} \right]}$$

$$C_x = (x_p^2/\alpha_p)$$

defining the lateral conduction effects on simusoidal stress signals. The relations are not exact in terms of thermoelastic energy conversion for any actual test part. The selected thermal model would be approximated in the regions of a thin plate near a rigid stiffener, but no stiffener would act as a completely infinite heat sink at stiffener-skin joint. Actual conduction effects will therefore be less than implied by the selected thermal model.

The general relationships shown above provide a means of evaluating the relative signal ratio magnitudes produced by lateral conduction (fig. 3). Frequency is the important independent test variable, and the signal ratio factor C_x accounts for all other variables affecting lateral conduction. The signal ratios greater than unity result from the node of the thermal conductance waves which would be generated by simusoidal thermoelastic energy conversion. For this application, the node is significant as a conductance error in the same manner as signal ratios less than unity.

The signal loss by substrate conduction does not preclude acquisition of infrared stress data if the attenuated signal is strong enough for radiometric sensing. Signal corrections for lateral conduction are probably feasible by use of auxiliary sensor and analog devices. (See section on "Recommended Future Work", p. 86). Without corrections, lateral conduction will impose signal ratios of unknown exact magnitudes in the vicinity of stiffeners, holes, stress nodes, and possibly other regions of flat plates with biaxial stress fields. The uncorrected data will be increasingly inaccurate as the radiometric field of view approaches these areas (with signal ratios deviating more from the unity asymptote), and this constitutes the basic lower frequency limitation imposed by lateral conduction.

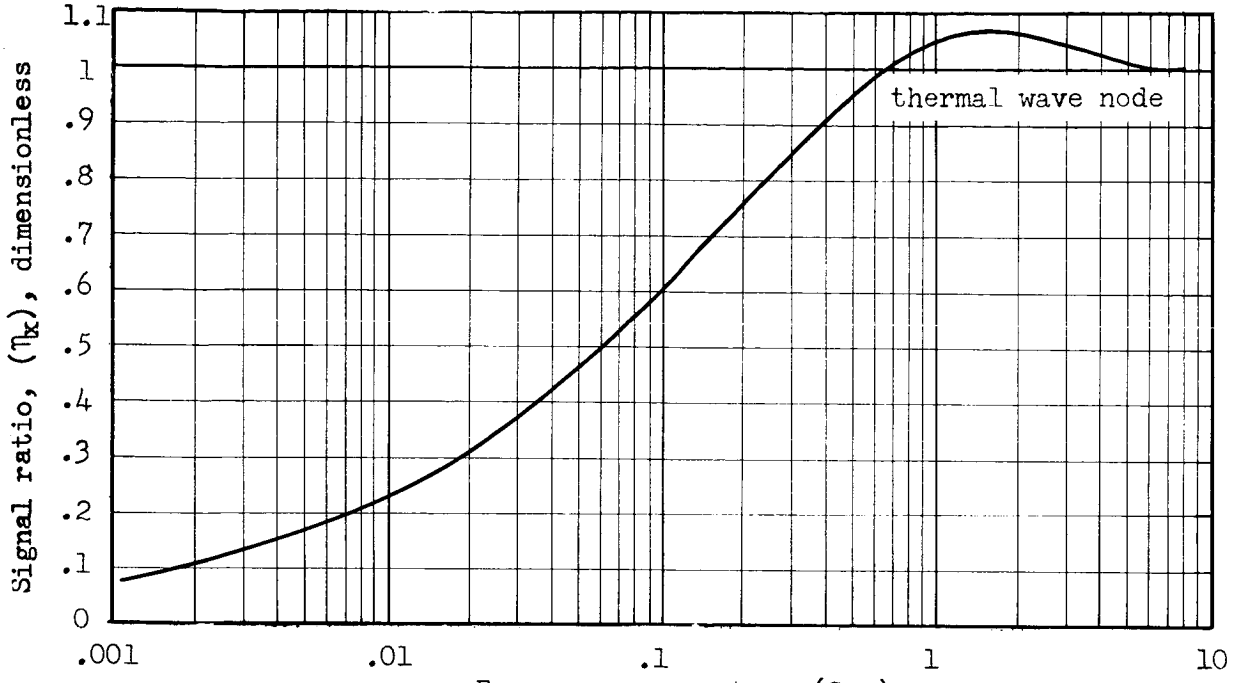

Figure 3.- Signal ratio parameters for lateral conduction

Environmental Radiation and Convection. - When a thin plate is subjected to oscillating loads, the test conditions may produce substrate and lateral conduction effects small enough to impose no limit on lower test frequencies. However, the oscillating temperatures due to thermoelastic energy conversion will cause periodic fluctuations of the temperature differences between the plate and its environment. This will produce oscillating heat transfer between the plate and its environment, and a radiometrically viewed plate area cannot be considered adiabatic when the oscillating heat transfer is significant. The term adiabatic is applied above in the sense of the period for each temperature oscillation (which directly affects infrared stress signals). There can be other non-adiabatic effects from differences between the environments on the two surfaces of the plate, changes in the environments, and transient response of the plate to environmental changes. However, the basic result of non-periodic heat transfer is a change of the average temperature level about which thermoelastic temperature oscillations occur. This has a known indirect effect on infrared signals. (See section on "Infrared Radiation Signal Magnitudes", p. 11). It has no direct non-adiabatic effect on the oscillating signals.

Heat can be transferred between a test part surface and its environment by radiation and convection. The radiation heat transfer rate (in general) is a function of the difference between the fourth powers of

the surface and environment temperatures, the emissivities of the surface and environment, and certain geometrical factors. However, for small temperature differences in a test part of small surface area (compared with its enclosure environment), radiation heat transfer becomes an (essentially) exact function of surface emissivity, surface temperature level, and the temperature difference between the surface and its environment (ref. 18, pp. 62-64). Therefore, the radiation and convection heat transfer relations become similar when the radiation heat transfer coefficient is defined as the product of the surface emissivity and the black body radiation (at the surface temperature level) per unit of temperature difference between the surface and its environment. With this approach, the total combined heat transfer coefficient is the sum of the radiation and convection coefficients (even if the two environmental temperatures are different). As the above discussion indicates, environmental radiation increases with surface emissivity, but the resultant increased non-adiabatic effects will usually be less important than the improved radiation signal accuracy associated with high emissivity surfaces. (See section on "Instrumentation System Methodology", p. 48).

The rate of heat storage in a vibrating plate element will be less than the thermoelastic energy conversion rate by an amount equal to the rate of heat transfer between the plate element and its environment. The heat storage rate for a plate element is equal to the product of its weight, specific heat, and rate of temperature change. The thermoelastic energy conversion rate for a plate element is equal to the product of its volume and volumetric energy conversion rate. The environmental heat transfer rate for a plate element is equal to the product of its exposed surface area, the coefficient of heat transfer, and the oscillating component of temperature difference between the plate element and its environment. These considerations yield the differential relation

$$t_p \rho c \frac{d\theta_p'}{dt} = t_p q_t - 2h\theta_p'$$

for a plate of any area (i.e. unity area) with both surfaces exposed to an average environmental heat transfer coefficient h. The magnitude of energy conversion for a vibrating plate is defined by the relation

$$q_t = (\pi \rho c \theta f)(\cos 2\pi ft)$$

(See section on "Thermoelastic Energy Conversion", p. 8). Substitution of this into the basic differential equation yields the relation

$$\frac{d\theta_p'}{dt} + \frac{2h}{t_p \rho c} \theta_p' = (\pi \theta f)(\cos 2\pi ft)$$

for the complete differential equation. This is readily solved to yield the relations

$$\theta_p' = \frac{(\pi\theta f)}{F_{11}^2 + (2\pi f)^2}\left[(2\pi f)(\sin 2\pi ft) + F_{11}(\cos 2\pi ft) - e^{-F_{11}t}\right]$$

$$F_{11} = (2h/t_p\rho c)$$

defining the plate transient temperature versus time.

The exponential term in the equation accounts for an initial transient disturbance which would occur if vibration were instantaneously initiated in a test part. This disturbance would vanish during early vibration cycles, and the temperature oscillation amplitude would become constant. After steady-state vibration for a sufficient period of time, the plate transient temperature is defined by the relation

$$\theta_p' = \frac{(\theta/2)(\sin 2\pi ft)}{1 + (F_{11}/2\pi f)^2}\left[1 + (F_{11}/2\pi f)(\cot 2\pi ft)\right]$$

in which the initial transient disturbance is neglected. The adiabatic and non-adiabatic temperatures can be compared with the relations

$$\theta' = (\theta/2)\ (\sin 2\pi ft)$$

$$\theta_p' = \theta'\left[1/(1 + F_{12}^2)\right]\left[1 + F_{12}(\cot 2\pi ft)\right]$$

$$F_{12} = (F_{11}/2\pi f) = (h/\pi\rho ct_p f)$$

(See section on "Thermoelastic Energy Conversion", p. 7). The non-adiabatic effects are a function of the material specific heat, material density, plate thickness, environmental heat transfer coefficient, and oscillation frequency. These effects vanish (in conformance with known physical trends) for zero heat transfer coefficient and for infinity density, specific heat, thickness and frequency (because all factors not unity in the non-adiabatic relation become zero).

The ratio of non-adiabatic and adiabatic (rms) temperatures yields the relations

$$\eta_e = \frac{\sqrt{f\int_o^{1/f} (\theta_p')^2\, dt}}{\sqrt{f\int_o^{1/f} (\theta')^2\, dt}}$$

$$\eta_e = \frac{1}{\sqrt{1 + (1/\pi C_e f)^2}}$$

$$C_e = (\rho c t_p/h)$$

defining the environmental heat transfer effects on sinusoidal stress signals. The relations are considered essentially exact because no significant simplifying assumptions were necessary in their derivation.

The general relationships shown above provide a means of evaluating the signal ratios produced by environmental heat transfer (fig. 4). Frequency is the important independent test variable, and the signal ratio factor C_e accounts for all other variables affecting environmental heat transfer.

The signal loss by environmental heat transfer does not preclude acquisition of infrared stress data if the attenuated signal is strong enough for radiometric sensing. Observed data can be corrected when the frequency, test part characteristics, and heat transfer coefficient are known. Such corrections would be essentially exact in terms of their theoretical basis, and would be fairly accurate in terms of the observation of frequency, the measurement of test part thickness, and the evaluation of test part material properties. However, the accuracy of corrections will usually be limited by uncertainty relative to exact heat transfer coefficients. Data corrected for environmental heat transfer will therefore be increasingly inaccurate as the magnitude of required corrections increases, and this constitutes the basic lower frequency limitation imposed by environmental radiation and convection.

In addition to signal attenuation, environmental heat transfer alters the phase angle (but not the wave shape) of the adiabatic signal. This can be important in certain special applications (but not rms stress measurements).

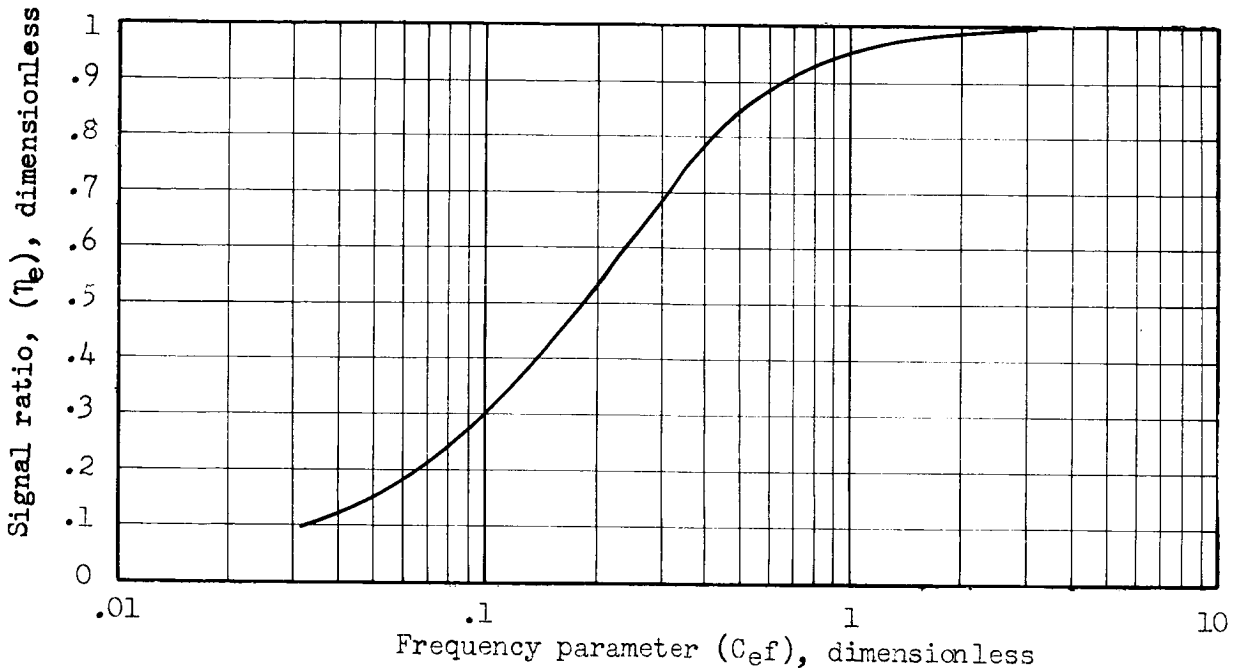

Figure 4.- Signal ratio parameters for environmental radiation and convection

Coating Thermal Response. - High emissivity coatings for infrared stress measurement applications will generally be as thin as practical (to obtain rapid thermal response), and the radiometric sensing will be in small surface elements that are flat (or nearly flat). The most appropriate geometric model for the coating is therefore an infinitely wide flat plate. For cases of interest in the application, the heat exchange between the coating surface and its environment will be negligible compared with the heat exchange between the coating and its substrate. The adiabatic coating surface is therefore similar to the adiabatic midplane of a plate which has the same thermal environment on both surfaces.

The response of a coating surface to a step change of substrate temperature would be approximately exponential with a time constant τ_c defined by the relation

$$\tau_c = 0.5\ t_c^2/\alpha_c$$

where α_c is thermal diffusivity and t_c is coating thickness (ref. 14, p. 266). For an exponential response characteristic, the coating surface-to-substrate (rms) temperature increment ratio η_c with sinusoidal substrate temperature oscillation is defined by the relation

$$\eta_c = \frac{1}{\sqrt{1 + (2\pi f \tau_c)^2}}$$

where f is the oscillation frequency (ref. 15, p. 252). Combining the above equations yields the relations

$$\eta_c = \frac{1}{\sqrt{1 + (\pi C_c f)^2}}$$

$$C_c = (t_c^2/\alpha_c)$$

defining the coating effects on sinusoidal oscillating temperature signals. The relations are fairly accurate, but they are not exact because the coating response is not exactly exponential.

The general relationships shown above provide a means of evaluating signal ratios produced by coating lag (fig. 5). Frequency is the important independent test variable, and the signal ratio factor C_c accounts for all other variables affecting thermal lag.

The signal loss by coating lag does not preclude acquisition of infrared stress data if the attenuated signal is strong enough for radiometric sensing. Observed data can be corrected for coating lag when the frequency and coating characteristics are known. Such corrections would be fairly accurate in terms of their theoretical basis, the observation of frequency and the evaluation of coating thermal diffusivity. However, the accuracy of corrections is limited by the uncertainty relative to exact coating thickness, particularly with thin coatings over large surface area (See section on "Recommended Future Work," p. 85). Data corrected for coating thermal lag will therefore be increasingly inaccurate as the magnitude of required corrections increase, and this constitutes the basic upper frequency limitation imposed by coatings.

In addition to the signal attenuation, coating thermal lag shifts the phase angle and slightly alters the wave shape of the substrate signal. These factors can be important in certain special applications (but not rms stress measurements).

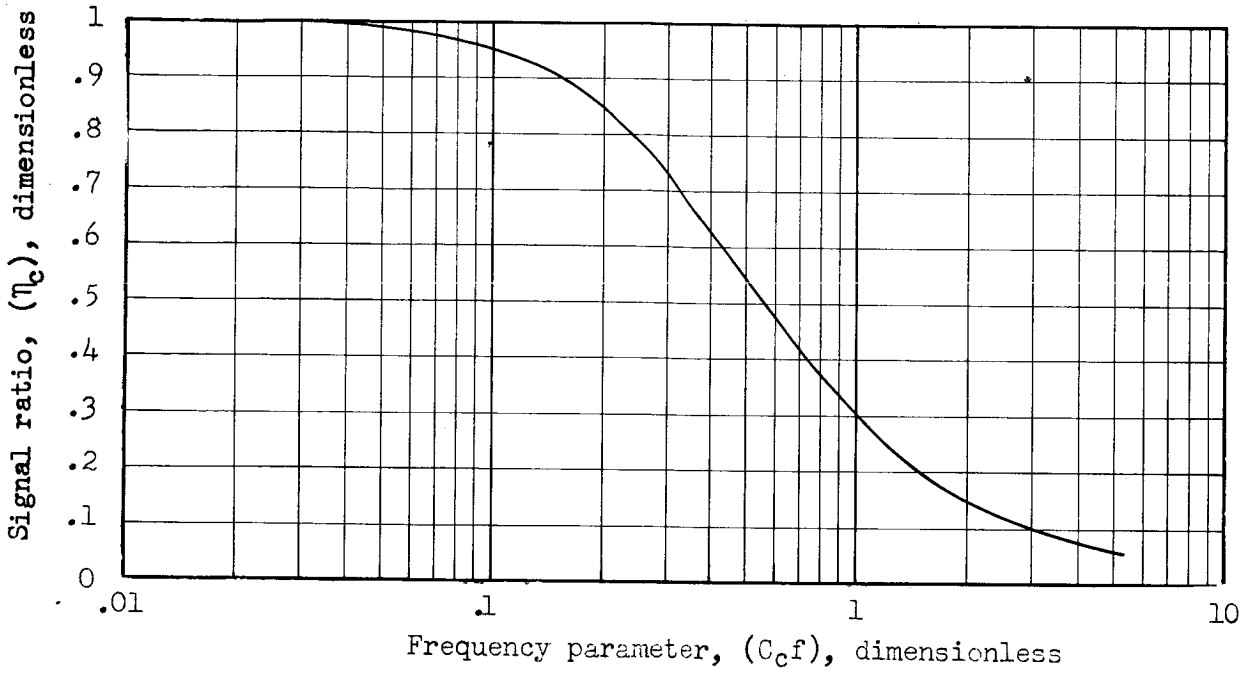

Figure 5.- Signal ratio parameters for coating thermal lag

Gaseous Media Attenuation. - It is desirable to place radiometric sensors for infrared stress measurements relatively close to the test parts for good spatial resolution of data. (See section on "Optical Collection Parameters", p. 40). However, various minimum stand-off distances may be required because of geometric arrangement of test facilities, size of surface area to be scanned, radiometric focal depth and other considerations. Infrared stress radiation signals can be attenuated during transmission through atmospheric air or gases within test cells, altitude chambers or wind tunnels.

The primary atmospheric constituents are nitrogen and oxygen, which do not significantly attenuate radiation in the near infrared wave lengths of infrared stress signals. Water vapor and carbon dioxide are the important gases of the ground level atmosphere which can attenuate signals. The concentrations of these gases vary in the atmosphere and in buildings due to various factors.

The average carbon dioxide content of the atmosphere is 0.033 percent by volume, and it is relatively constant (ref. 13, pp. 43-46). There is some evidence that the average concentration has increased slightly (15% in 50 years) due to burning of fossil fuels, and somewhat higher than average concentrations can be encountered in cities due to this and other industrial processes. The carbon dioxide concentration within occupied buildings will normally be slightly higher than the atmosphere because of human respiration products. The maximum recommended threshold limit in ventilation practice is 5,000 parts per million by volume (ref. 19, p. 152). This is considered representative of an extreme maximum concentration unlikely to be exceeded during infrared stress measurements. Typical normal carbon dicxide concentrations in the atmosphere and well ventilated buildings do not exceed one-fifth of the above extreme maximum.

The water vapor content of the atmosphere varies greatly with climatic condition and geographical location. Atmospheric dew points higher than 79°F (82°F wet bulb and 91°F dry bulb) are not encountered more than 30 hours per year anywhere in the continental United States and Canada (ref. 19, pp. 488-495). This dew point is considered representative of a typical extreme atmospheric water vapor concentration unlikely to be exceeded during infrared stress measurements. Atmospheric humidities are lower than this maximum most of the time (even for the most adverse locations and seasons), and humidities can be very low during cold weather. Buildings with simple heating and ventilating systems will have nearly the same inside humidity as the surrounding atmosphere. Buildings with air conditioning systems will normally have interior dew points lower than 56°F (50 percent relative humidity at 75° to 76° F air temperature) because of the dehumidification associated with the refrigeration (ref. 19, p. 494). Buildings with humidification equipment normally have sufficient water vapor addition to keep the interior dew point at approximately 56°F when atmospheric dew points are lower than this. Typical normal water

vapor concentrations do not exceed one-half of the above extreme maximum except in the atmosphere and buildings without air conditioning during humid weather periods.

A stand-off distance of 1000 centimeters is considered a typical maximum unlikely to be frequently exceeded in infrared stress measurements. The primary gaseous attenuation factors at this distance are 5 atmosphere centimeters of carbon dioxide and 0.025 precipitable centimeters of water vapor for the extreme maximum concentrations (5000 parts per million and 79°F dew point, respectively). Atmospheric transmittance data are available in terms of these primary factors for various atmospheric pressures and temperatures (ref. 20 and 21). For ground level infrared stress measurement applications, the atmospheric pressure and temperature effects on transmittance will be small compared with the carbon dioxide and water vapor concentration effects. The transmittance data for one atmosphere pressure and 300°K temperature were therefore used to evaluate atmospheric signal attenuation (ref. 13, pp. 74-87).

Both atmospheric transmittance and emitted infrared signal magnitudes vary with wave length. The spectral distribution of emitted signals is primarily a function of test part temperature. (See section on "Infrared Signal Magnitudes", p. 11). For a gray body test part surface at a given temperature, this distribution can be defined in terms of a relative emitted signal, which is the ratio of spectral signal radiance parameter and the maximum signal parameter for any wave length. The transmitted signal spectral distribution can then be computed as the product of emitted signal ratio and atmospheric transmittance. Evaluations of this type were carried out for 300 and 1000°K test part temperatures. The atmospheric signal attenuation was found to be significant in certain wave length regions at the extreme conditions assumed for the evaluations (fig. 6). However, the overall atmospheric attenuation is relatively small with stand-off distances less than 1000 centimeters (under the most adverse atmospheric conditions).

Transmission of infrared signals within test facilities (such as wind tunnels, altitude chambers, and test cells) can involve different gaseous attenuation considerations than the atmosphere. Enclosed test facilities can contain gases of different composition, pressure, and temperature than the atmosphere. Transmission path lengths in test facilities can be limited by test space configuration and operational constraints not encountered in atmospheric testing.

Most test facilities employ atmospheric air, but the composition, pressure, and temperature are sometimes altered in the facility test spaces. The gaseous transmittance in altitude chambers will be higher than atmospheric transmittance because of the sub-atmospheric pressures. The gaseous transmittance in conventional high speed wind tunnels will be higher than atmospheric transmittance because of the dehumidification (and heating) normally employed. In general, the gaseous transmittance within test facilities employing atmospheric air will be equal to or higher than atmospheric transmittance. Signal losses in these types of

———— emitted signals
– – – – – – transmitted signals

Note: Weak absorption bands have been omitted for clarity.

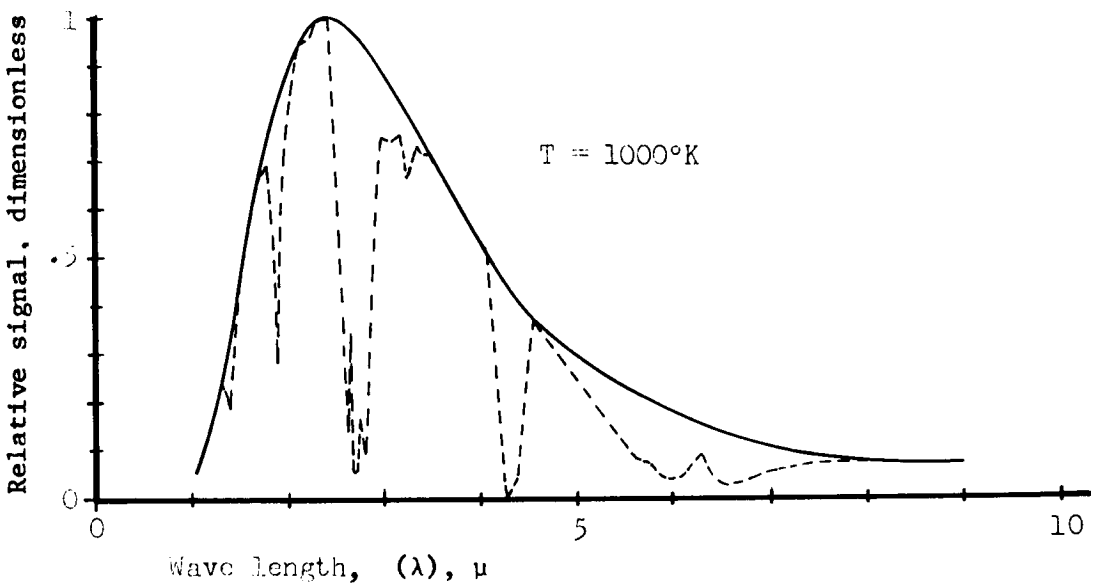

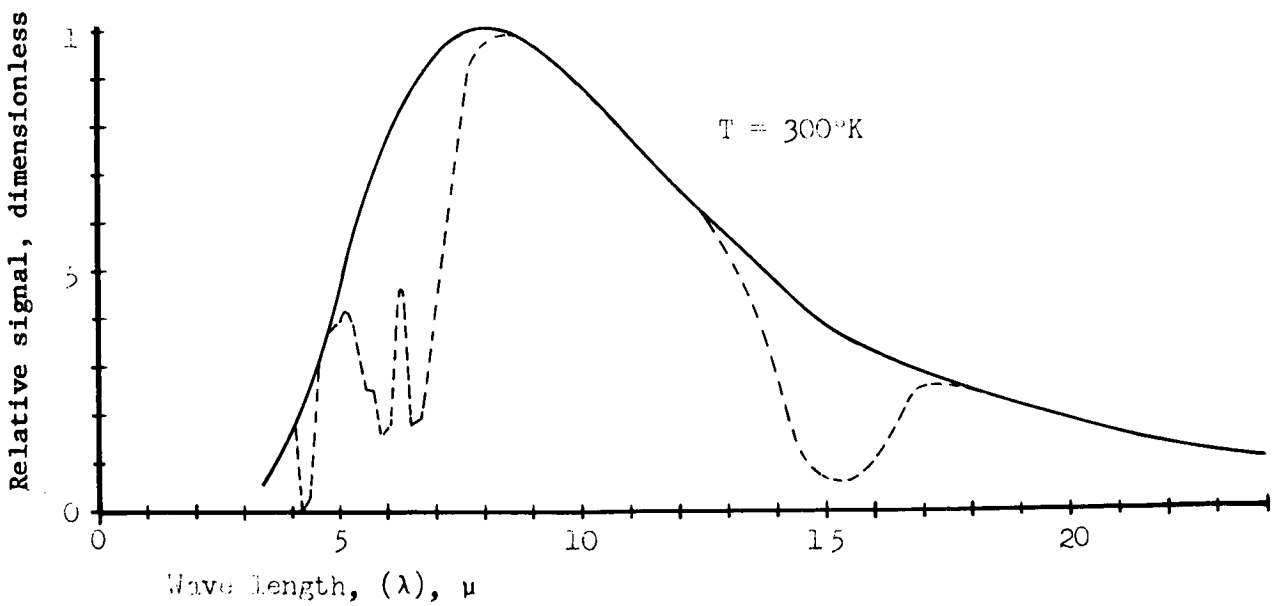

Figure 6.-Relative signals emitted and transmitted 1000 centimeters through an atmosphere of extremely high carbon dioxide and water vapor content

facilities will therefore tend to be less than atmospheric losses (fig. 6), particularly with the typically shorter transmission path lengths. The discussion above is not valid for facilities employing air (or nitrogen) at very high temperatures (such as electric arc and shock compression heating above 1000°K). Dissociation alters gas compositions at high temperatures, and the infrared transmittance criteria considered herein would not be applicable.

The attenuation of infrared stress signals by common gases will be small for most test applications of interest. Gaseous attenuation can usually be neglected in evaluating the stress detection limit for test applications, but it should be accounted for during calibration to assure valid interpretation of radiometric data in terms of stress. (See section on "Instrumentation System Methodology", p. 87).

Pressure Barrier Window Attenuation. - Although interior radiometric sensors are practical for some test facilities, windows and external sensors are desirable or necessary for many facilities. Pressure barrier windows are a means of avoiding aerodynamic flow disturbances by sensors in wind tunnels and isolating sensors from hostile environments, such as acoustic noise and heat. Most test facilities have glass windows for visual observation, photographic data acquisition, schlieren studies, and/or other purposes. Common glasses transmit optical and near infrared radiation, but they strongly attenuate wave lengths greater than approximately 2.7 microns. Certain modified glasses transmit moderately longer wave lengths, but other materials are necessary to achieve large spectral transmission ranges.

Glass windows would be adequate for certain test applications, such as measurement of high temperature signals with detectors sensitive to short infrared wave lengths. Infrared window materials will usually be necessary for transmission of the longer wave length signals from test parts near room temperature. In addition to being more costly than glasses, the infrared materials are limited relative to maximum available size (although larger sizes are likely to be available in the future). Because of this, multipane infrared windows are likely to be required for large radiometric apertures. A large number of materials transmit infrared radiation, but few of these have suitable strength and other physical properties for windows.

Four materials with different spectral transmittance ranges have been selected for this study on the basis of their general suitability as pressure barrier windows. (See appendix on "Window Design Analysis", p. 130). Crown glass is the material widely employed for schlieren and other optical windows, and its infrared transmittance is typical of that for common glasses. Modified glass (Corning Glass Works designation Cortran TM 9753) has infrared transmittance typical of the maximum spectral range currently feasible with glass. Polycrystalline magnesium fluoride (Eastman Kodak Company designation Irtran 1) is superior to glass in strength and spectral transmittance range, but it is relatively costly and is limited in maximum available size. Polycrystalline zinc selenide (Eastman Kodak Company

designation Irtran 4) is superior to magnesium fluoride in spectral transmission range, but it is less favorable relative to strength, cost, and maximum available size. Since window transmittance is a function of thickness, material strength is a factor in the attainable window transmittance.

Round windows are most directly compatible with radiometric collection mirrors, but square or rectangular windows may sometimes be desirable for multipane installations or for adaption to existing facility window frames. The maximum stress in a pressure barrier window is primarily a function of differential pressure and window dimensions. (See appendix on "Window Design Analysis", p. 131). Neglecting the secondary effects of variation in Poisson's ratio, the relation

$$\sigma_w = 0.3055\Delta P(D_w/t_w)^2$$

defines maximum stress for round windows. Based on a conservative (tenfold) factor of safety relative to modulus of rupture, the above equation yields specific thickness criteria for round windows of various materials (fig. 7). Actual applications may not require this factor of safety and may involve many other detailed considerations, such as deflection criteria (Appendix F).

Test data were available on the refractive index and the spectral transmittance for some thicknesses of the selected materials (ref. 22-27). The theoretical relations for radiation interface reflection (at normal incidence) and transmission through solids (ref. 15, pp. 234-236) were applied with the test data to estimate window transmittance as a function of wave length (fig. 8). The transmittance of zinc selenide can (and frequently should) be increased somewhat in a selected spectral range with antireflection coatings (not appropriate for the other materials). Neglecting attenuation by gaseous media, the signal radiance at a radiometer aperture is expressed by the relation

$$\Delta N_{\lambda 2} = \tau_\lambda(\Delta N_{\lambda 1})$$

in terms of window transmittance and emitted signal radiance.

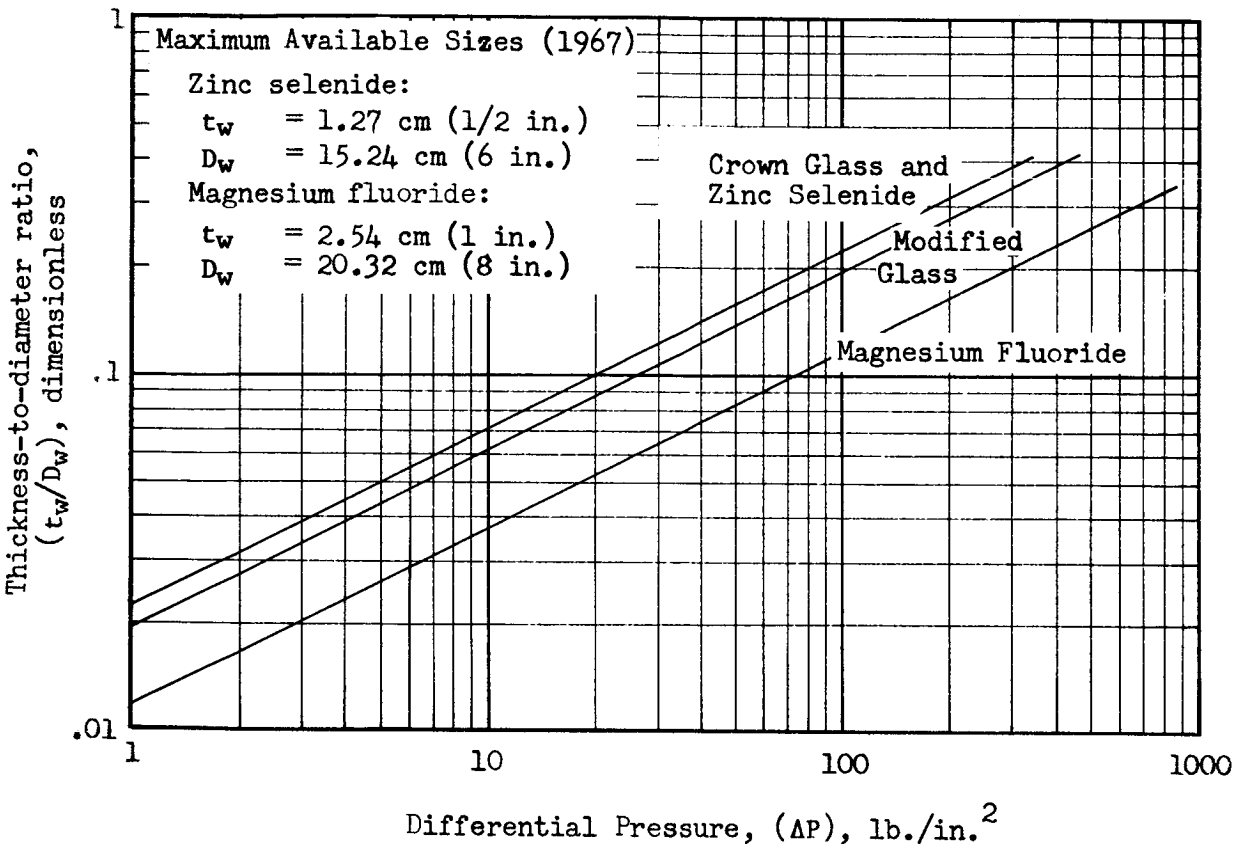

Figure 7. - Typical thickness criteria for tenfold factor of safety with round pressure barrier windows

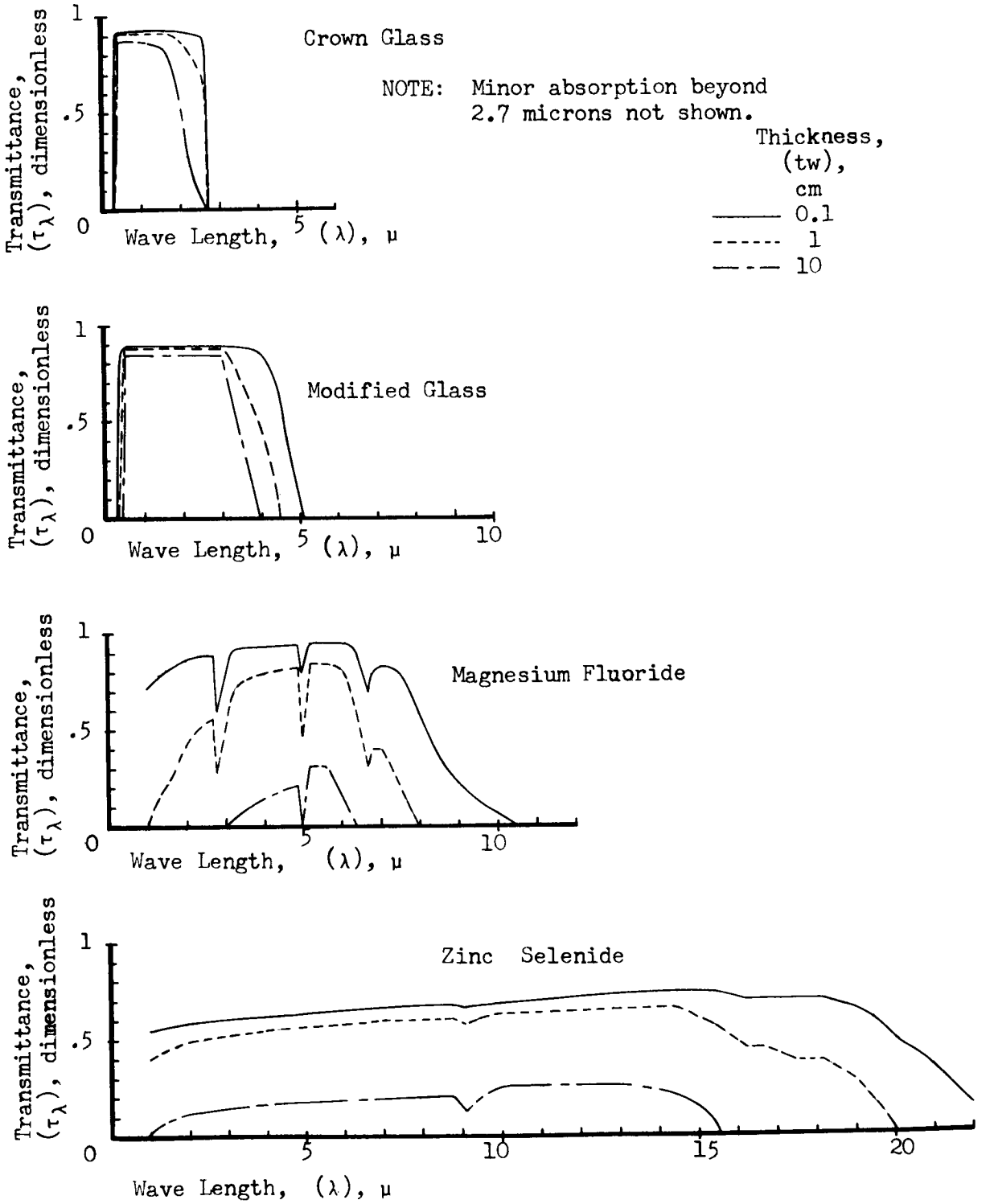

Figure 8 - Spectral transmittance for typical window materials of various thicknesses

Radiometric Instrumentation Performance

Optical Collection.- An infrared radiometer collects signal radiation from the test part and concentrates this energy on a detector. Various types and arrangements of components can be employed to collect radiation, but all collection systems involve the same basic performance considerations. Radiometer signal-to-noise ratio is normally a compromise relative to the attainable spatial resolution (instantaneous field of view) as well as the optical collection system size (and cost). However, the ultimate attainable signal-to-noise ratio and spatial resolution are limited by certain other unavoidable aspects of optical collection systems.

The wave length range useful for infrared detection is relatively large, and refractive optics are seldom employed because of transmission and chromatic aberration difficulties with available lense materials. The principal use of infrared lenses has been for immersion of detectors to improve their performance rather than for the primary radiometer optical collection function. Various types of reflective optics can be used, the important differences being in the focal plane (detector) location (ref. 13, pp. 219-222). Although other systems may be desirable for special test applications, the Cassegrainian system is most frequently used because of its compactness. This system employs a convex secondary mirror to concentrically fold rays from a concave primary mirror so that the collected radiation is concentrated on a detector behind the center of the primary mirror. The blockage by the secondary mirror is usually relatively high, but the component arrangement is convenient from the standpoint of fabrication, assembly, alignment and other factors. The Cassegrainian mirrors can be shaped for optimum optical collection at a selected stand-off distance, and it is normally focused for other distances by movement of the secondary mirror along the optical axis (with some resulting focal losses). Radiometer scanning is usually achieved by a movable flat mirror outside the collection system aperture. Different radiometers have some differences in blockage, reflectance, and focal losses, but the aperture diameter and optical focal length are the primary factors defining the basic performance for any optical collection system. Radiometers for infrared stress measurements would normally employ detectors with square sensitive areas to achieve a desirable (and practical) radiometric field of view.

The signal-to-noise ratio of an infrared detector is proportional to the ratio of the total signal power incident on the detector and the square root of detector area. (See section on "Infrared Detection", p. 43). The signal power collected and concentrated on the detector of a radiometer is equal to the product of the signal radiance incident at the radiometer aperture, the aperture area, the radiometric solid angular field, and the overall optical efficiency factor. The plane anglar dimensions of the radiometric solid angular field are proportional to the detector linear dimensions and inversely proportional to

the optical collection system focal length. For a square detector, the above considerations yield the relations

$$\Delta P_{\lambda 3} = (\Delta N_{\lambda 2})(0.25\pi D_o^2)(\phi_o/1000)^2(\eta_o)$$

$$\phi_o = 100\sqrt{A_d}/f_o$$

$$(\Delta P_{\lambda 3}/\sqrt{A_d}) = (\eta_o K_o D_o^2)(\Delta N_{\lambda 2})$$

$$K_o = (0.25\pi\phi_o/10^4 f_o)$$

which contain dimensional constants applicable to the conventional units convenient for infrared radiometric technology. These relations indicate that signal-to-noise ratio is directly proportional to the optical collection system efficiency factor, the aperture diameter squared, and a geometric optical function K_o involving the angular field of view.

Although large angular fields are desirable for high signal-to-noise ratios, small angular fields are desirable for favorable data spatial resolution (small instanteous fields of view on test parts). The minimum feasible angular field can be limited by diffraction of the infrared waves (ref. 13, pp. 212-216). The limit is a function of aperture diameter, and is defined by the relation

$$\phi_o = (1.22/D_o)$$

for a typical (ten micron) wave length of infrared radiation. The above relation would be approximately correct for detection of room temperature signal radiance with detectors of flat spectral response, and it would define more critical limits than actually exist for shorter wave length cases. However, the minimum feasible infrared detector size also imposes a limit on minimum angular field (fig. 9), and this will usually be more important than the diffraction limit. Angular fields larger than feasible minimums may be desirable for improved signal-to-noise ratios when the resultant compromises of spatial resolution are acceptable.

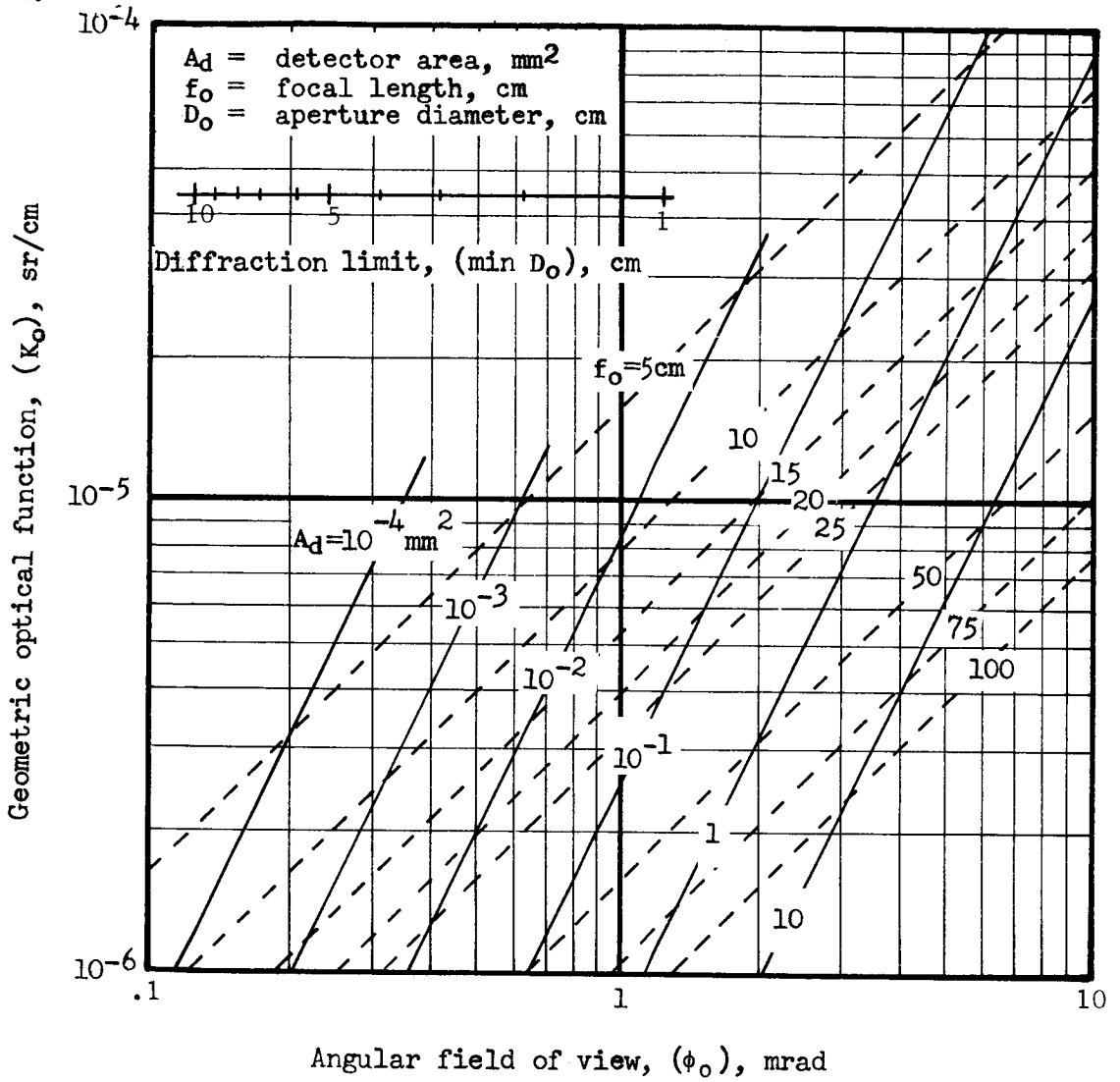

Figure 9. - Geometric function for optical collection systems of radiometers

For any specific angular field, the smallest attainable field of view on a surface is a function of the distance between the radiometer and the surface. The size of this minimum field (for small angles) is defined by the relation

$$S_o = L_o\phi_o/1000$$

which is applicable for the plane perpendicular to the optical axis at which the optics are focused. This relation would define effective

field of view on a test part surface if the surface was at the external radiometric focal plane. Actual radiometers do not usually have sharp uniform fields of view (because of minor optical diffraction and/or detector sensitivity variations). The effective field of view is commonly defined as the area in which the signal response is greater than half the peak value. However, the exact effective area is not important compared with field of view size changes due to other factors.

Scanning of contoured test part surfaces will be desirable for many infrared stress measurement applications. The scanning is usually achieved by angular motions of the optical axis. The instantaneous viewing angle and stand-off distance then vary for both flat and contoured test parts. A complex focal adjustment device would be necessary to maintain exact radiometric focus during scanning, and it will usually be desirable to employ a fixed focal adjustment. The maximum instanteous field of view on the test part surface will therefore be larger than at the external focal plane due to both angular and de-focusing effects.

Signal radiance magnitudes would not be significantly altered by relatively large variations of viewing angle. (See section on "Infrared Radiation Signal Magnitude", pp. 9-10). The field of view on the test part surface varies inversely with the cosine of deviation in viewing angle from perpendicular to the surface. The angular effects on the spatial resolution of infrared stress data will therefore be relatively small for viewing angles of primary interest in measurements (less than 30 percent change in resolution for viewing angles less than 45 degrees from perpendicular). The de-focusing effects on data resolution can be greater than the angular effects, and the optical field depth can be an important parameter in radiometric performance. If a radiometer is adjusted for an external focal plane distance L_o equal to the average test part stand-off distance, the required optical field depth ΔL_o will be the total variation of instantaneous stand-off distance involved with the scanning application. Neglecting certain secondary effects, the maximum increase of test part surface field of view can be defined by the relation

$$(s_{xy} - s_o) = (\Delta L_o/2)(D_o/L_o)$$

which is a linear function of radiometric aperture diameter. With the expression for focal plane size shown above, the size of the field of view on the test part surface is defined by the relation

$$s_{xy} = (L_o\phi_o/1000) + (\Delta L_o D_o/2L_o)$$

in terms of the angular field of view. This relation indicates that a required spatial resolution and depth of field can be obtained with various combinations of stand-off distance and angular field of view for a given aperture diameter.

It is normally desirable to optimize radiometric signal-to-noise ratio to the degree feasible within the constraints of the required spatial resolution (and possibly other factors). For a given focal length, signal-to-noise ratio is proportional to angular field of view (fig. 9). For a given optical collection system (diameter and focal length), signal-to-noise ratio is therefore proportional to the angular field relation

$$\phi_o = (1000/L_o)(s_{xy}) - (500\ D_o/L_o^2)(\Delta L_o)$$

in terms of required spatial resolution and depth of field. By setting the derivative of the angular field relation (with respect to stand-off distance) equal to zero, the relations

$$\frac{d\phi_o}{dL_o} = -(1000/L_o^2)(s_{xy}) + (1000\ D_o/L_o^3)(\Delta L_o)$$

$$L_{or} = D_o \Delta L_o / s_{xy}$$

define a reference stand-off distance at which maximum signal-to-noise ratio would be obtained. Substitution in the angular field equation yields the relation

$$\phi_{or} = 500\ s_{xy}^2 / D_o \Delta L_o$$

defining a reference maximum field of view (within the constraints of required resolution and depth of field) attainable at the reference stand-off distance.

Small fields of view on test parts can be obtained with small angular fields and short stand-off distances, but the depths of optical fields also tend to be small under these conditions (fig. 10). Any specific aperture diameter, depth of field and maximum field of view on a test part surface defines a specific reference angular field and stand-off distance at which maximum signal-to-noise ratio would be obtained.

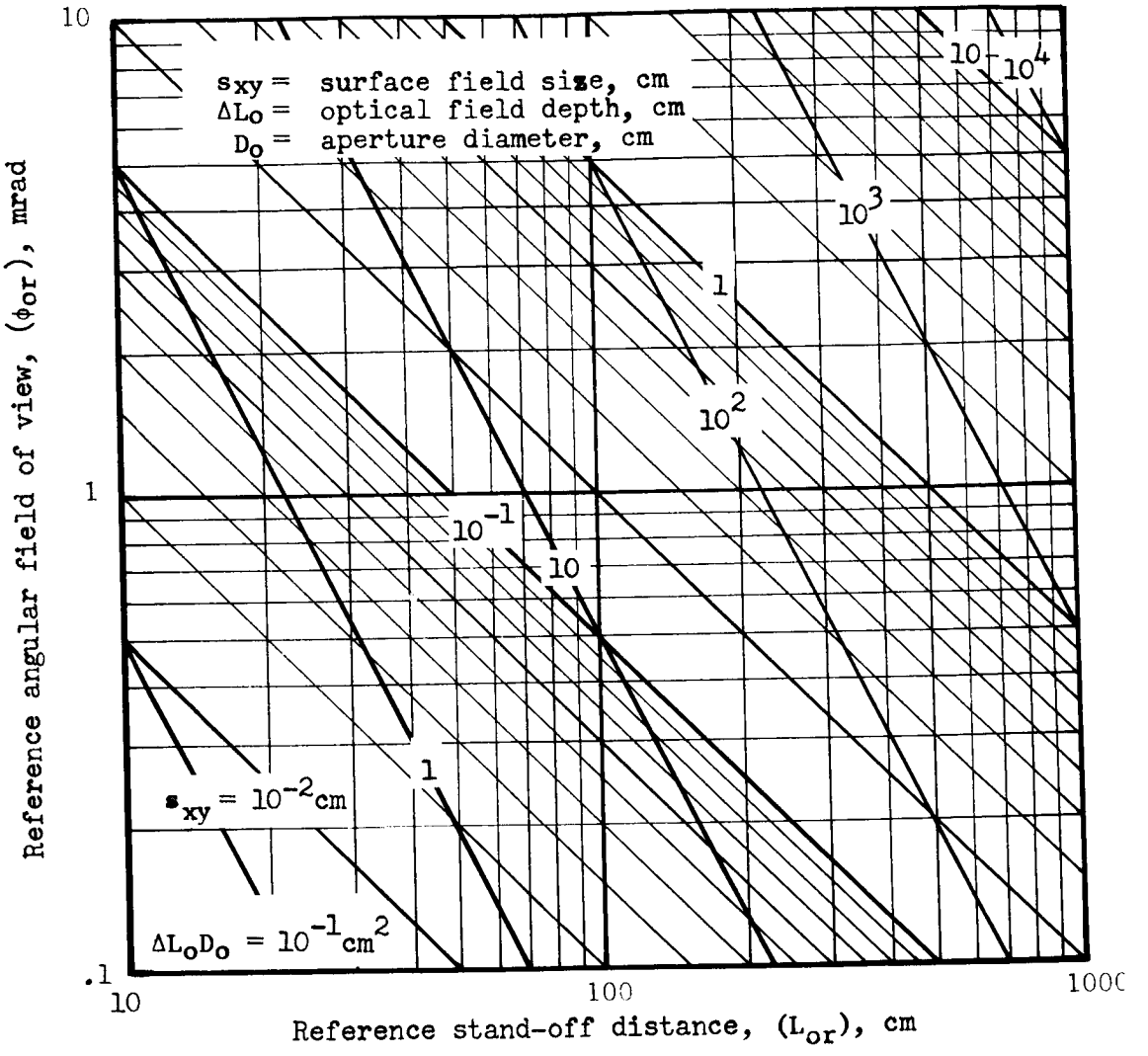

Figure 10. - Trends in field of view and stand-off distance with spatial resolution for combinations of optical field depth and aperture diameter

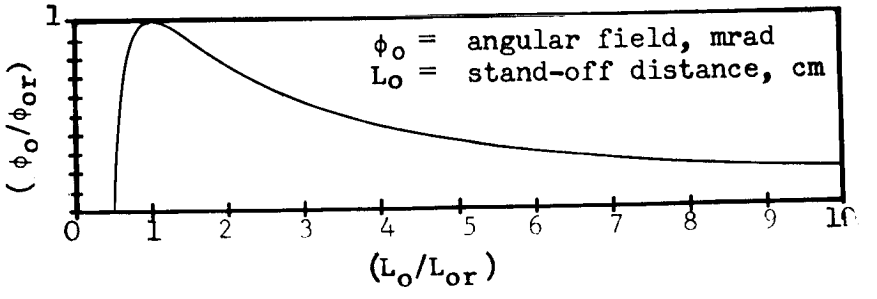

Figure 11. - Effect of stand-off distance of field of view

However, these specific reference parameters will not always fall within the other constraints of test applications. The equations for an arbitrary and the reference angular field yield the relation

$$(\phi_o/\phi_{or}) = 2(L_{or}/L_o) - (L_{or}/L_o)^2$$

correlating ratios of angular fields and stand-off distances. Stand-off distances less than the reference value can involve large signal losses (fig. 11), but short stand-off distances would seldom be required in test applications. Stand-off distances greater than the reference value involve relatively moderate signal losses and will frequently be desirable when the test applications have minimum stand-off distance constraints. However, the factors affecting minimum angular field (detector size and diffraction) will impose other limits on increases in stand-off distance feasible for a given spatial resolution criteria.

For a specific optical collection system focal length and aperture diameter D_o the geometric optical function K_o is defined in terms of any selected spatial resolution and stand-off distance criteria (fig. 9, 10, and 11). Signal-to-noise ratio is proportional to this function, the aperture diameter squared, and the overall optical efficiency factor η_o. Typical optical blockage losses are less than 25 percent (ref. 13, p. 222). Typical reflectance losses are less than 30 percent with three mirrors (two for collection and one for scanning), each having greater than 90 percent reflectivity (ref. 13, p. 220). Typical overall optical efficiency is therefore greater than 50 percent for a radiometer used at stand-off distances near that for which it was designed. Large focal losses can usually be avoided by using stand-off distances within the design range of the radiometer.

Infrared Detection. - Many materials can convert incident radiant energy into electrical signals by various physical mechanisms (ref. 13, pp. 123-140). All such materials also produce electrical noise due to various physical mechanisms (ref. 15, pp. 243-250). Signal-to-noise ratio is the ultimate index of infrared detection performance, but this cannot be directly defined for detection materials. Spectral specific detectivity is the most useful parameter for the detection performance of materials (ref. 13, pp. 140-151 and ref. 15, pp. 276-277). This parameter provides a fairly general index of spectral performance attainable with a material when employed in a specified manner. The effects of detector operating frequency (on both signal and noise) can be correlated independently of the spectral performance aspects. The detector area is a factor affecting signal-to-noise ratio, and the minimum feasible

TABLE I.- IDENTIFICATION OF SELECTED DETECTORS

Material	PbS	InSb-PV	Ge:Au	Ge:Hg	thermistor
Mode of operation	photo cond.	photo volt.	photo cond.	photo cond.	bolometer
Minimum area, mm^2	0.05	0.01	0.05	0.05	0.01
Operating temp., °K	77	77	77	28	300
Calibration freq., Hz	90	900	900	900	90

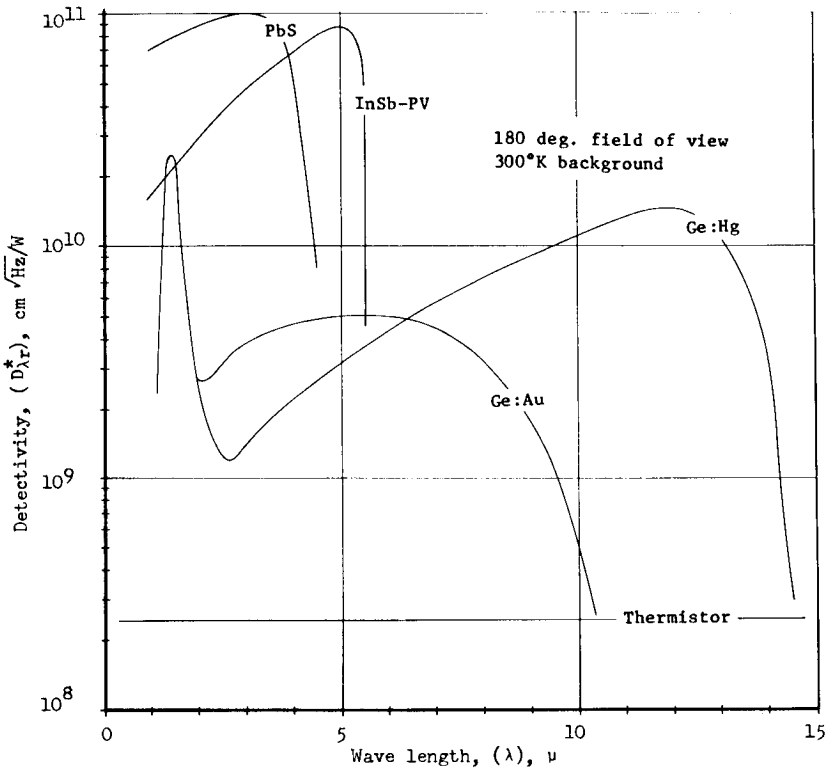

Figure 12.- Spectral response of selected detectors

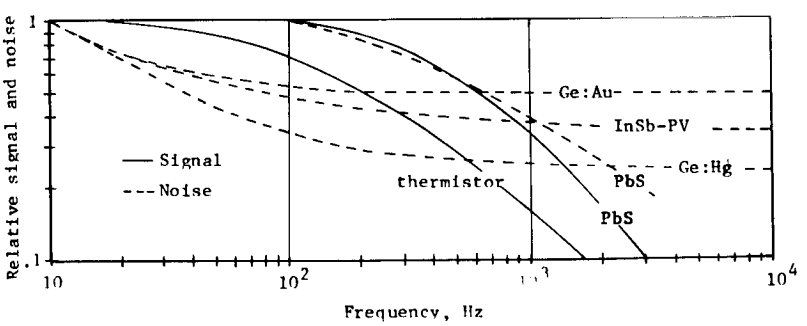

Figure 13.- Frequency effects for selected detectors

area for a given material usually imposes a limitation on attainable spatial resolution.

Common detector materials with diverse spectral response ranges were selected for the infrared stress application range study (Table I and fig. 12). The performance shown is for unimmersed detectors of production quality, and the performance is exactly applicable only for the specific selected time constant, field of view, chopping frequency, and other factors. (See section on "Infrared Detector Analysis", p. 120). The spectral performance of the selected detectors ranges from that for lead sulfide (PbS), which responds only in the short wave lengths, to that for the thermistor (or thermal) detector, which responds in all wave lengths. Indium antimonide (InSb-PV) responds to somewhat longer wave lengths than PbS. Gold activated germanium (Ge:Au) has the broadest spectral response of the detectors operating at 77°K (liquid nitrogen temperature). Mercury activated germanium (Ge:Hg) responds to relatively long wave lengths, but requires cooling to 28°K. Detectors responding to longer wave lengths (such as copper activated germanium at 10°K) are available (See section on "Infrared Detector Analysis", p. 121). Detector selection was based partly on the fact that many existing commercial radiometers have PbS, InSb, and thermistor detectors, which might be applied for infrared stress measurements.

Detectivities are applicable to specific chopping frequencies (Table I), and there are frequency effects on detector signals and noise (fig. 13). These effects can be combined to define a detector signal ratio n_d which is representative of the frequency effects on detectivity (fig. 14).

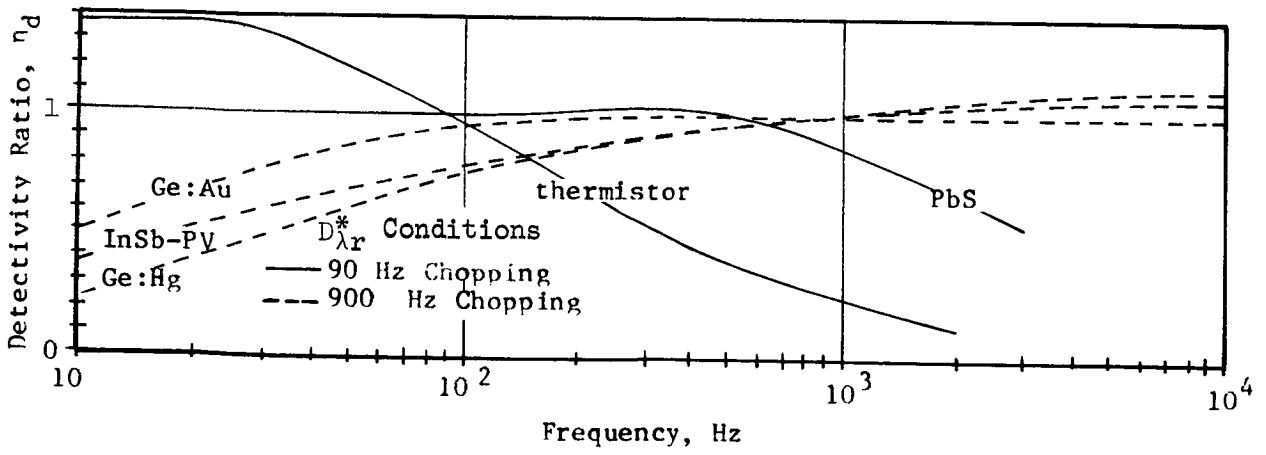

Figure 14.- Frequency effects on detectivity

Electrical signal is proportional to the product of detectivity and signal power irradiating the detector. Since both detectivity and signal irradiation usually vary with wave length, the total electrical signal is defined by the integral of the spectral values over the full range of wave lengths. Electrical noise (as normalized in the specific detectivity parameter) is proportional to the square root of detector area and electronic filter band width. These considerations yield the relation

$$(V_S/V_N) = \frac{\eta_d}{\sqrt{\Delta f}} \int_o^\infty (D^*_{\lambda r})(\Delta P_{\lambda 3}/\sqrt{A_d})\, d\lambda$$

in terms of the symbols identified herein (Ref. 13, p. 603). This conveniently separates the effects of electronic filtering, detector operating frequency, and infrared signal spectral detection.

The signal power irradiating a detector is defined by the relation

$$(\Delta P_{\lambda 3}/\sqrt{A_d}) = (\eta_o K_o D_o{}^2)(\Delta N_{\lambda 2})$$

(See section on "Optical Collection" p. 36). The radiometer aperture signal radiance is defined by the relation

$$\Delta N_{\lambda 2} = (\tau_\lambda)(\Delta N_{\lambda 1})$$

(See Section on "Pressure Barrier Window Attenuation, p. 32). The signal radiance emitted from a test part is defined by the relation

$$\Delta N_{\lambda 1} = (\Delta N_{\lambda 1}/\varepsilon_\lambda K_M \sigma)(\varepsilon_\lambda)(K_M \sigma)(\eta_p)$$

(See Section on "Test Part Signal Generation", pp. 10, 16, 21, 25 and 26). These considerations yield the relations

$$(V_S/V_N) = \sigma(K_M)(\eta_o K_o D_o{}^2)(\eta_p \eta_d)(V'_{\lambda r})/\sqrt{\Delta f}$$

$$V'_{\lambda r} = \int_o^\infty (D^*_{\lambda r})(\tau_\lambda)(\varepsilon_\lambda)(\Delta N_{\lambda 1}/\varepsilon_\lambda K_M \sigma)d\lambda$$

in terms of the appropriate infrared stress measurement parameters. The minimum detectable stress is defined by the relation

$$\sigma^* = \sqrt{\Delta f}/(K_M)(\eta_o K_o D_o{}^2)(\eta_p \eta_d)(V'_{\lambda r})$$

for which the signal-to-noise ratio is unity. The detectable stress limit is therefore dependent on the integrated spectral response of the detector to the radiant signal and several other factors related to the specific infrared stress measurement application.

The integrated spectral signal-to-noise ratio parameter $V'_{\lambda r}$ includes four quantities, and certain combinations of these quantities define different types of infrared stress measurement limits. The most important combination is the signal radiance parameter $(\Delta N_{\lambda 1}/\epsilon_\lambda K_M \sigma)$ and specific detectivity $D^*_{\lambda r}$ because the detector must have adequate response to the wave lengths in which there are significant test part signal emissions (fig. 1 and 12). If a pressure barrier window is necessary for the test application, the window transmittance becomes an important additional quantity because the window must transmit in the spectral range of the radiant signals (fig. 8). The test part emissivity is more important relative to general magnitude (in a range from nearly zero to nearly unity) than exact spectral variations. For a surface with gray body emissivity characteristics, the spectral integral can be simplified to the relation

$$(V'_{\lambda r}/\bar{\epsilon}_\lambda) = \int_0^\infty (D^*_{\lambda r})(\tau_\lambda)(\Delta N_{\lambda 1}/\epsilon_\lambda K_M \sigma)\, d\lambda$$

in which the three most important spectral quantities are integrated versus wave length. Window spectral transmittance ranges are dependent primarily on the material, but are also affected by window thickness. The integral can be evaluated for combinations of windows and detectors as a function of the test part temperature effects on signal radiance emission parameter (fig. 17).

It is usually desirable to apply high emissivity coatings on the surfaces of test parts for infrared stress measurements. Such coatings have approximately gray body properties in the infrared spectral range of interest (small variations of emissivity with wave length). Uncoated metals have relatively low emissivities that vary more significantly with wave length (fig. 18). An average emissivity $\bar{\epsilon}_\lambda$ for the wave length range most important in the specific application provides adequate definition of the detectable stress limit. Exact emissivity (over a large test part surface area) is important for the interpretation of radiometer signal data in terms of test part stress. (See section on "Instrumentation System Methodology", p. 63).

Signal Emission Frequency Ranges.- The frequency effects on infrared stress signal emission can be evaluated on the basis of test application requirements (fig. 15). For ranges with unity signal ratio, no signal emission roll-offs will be encountered. If the application requirements include frequencies in roll-off ranges, data can be left uncorrected if the resultant errors are acceptable, and data can be corrected for improved accuracy in some cases. Substrate conduction can be corrected for over a relatively large range of signal ratios if a known proportion of stress arises from bending (or if the test part is known to undergo pure bending). Lateral conductance corrections are generally not practical without an auxiliary sensor or analog device. Environmental heat transfer can be corrected for only at relatively high signal ratios, the correction accuracy being generally limited by uncertainties in heat transfer coefficients. Coating thermal response can be corrected for only at relatively high signal ratios the correction accuracy being generally limited by uncertainties in coating thicknesses. If severe frequency roll-off limitations are encountered, it may be desirable to consider alternate approaches relative to the test part, such as material, scale, or other factors affecting the sources of the frequency limitations. The above procedures yield test part signal attenuation η_p as a function of frequency f.

TABLE II. - TYPICAL TEST PART PROPERTIES

(From ref. 28)

Properties	Units	Materials			
		Magnesium (AZ31B)	Aluminum (7075)	Steel (4130)	Titanium (6AL-4V)
Conductivity (k)	W/°Kcm	0.967	1.315	0.380	0.0656
Density (ρ)	g/cm^3	1.775	2.80	7.84	4.44
Mass specific heat (c)	J/°Kg	1.048	0.965	0.479	0.567
Diffusivity($\alpha_p = k/\rho c$)	cm^2/sec	0.52	0.49	0.10	0.026
Vol. specific heat (ρc)	J/°Kcm^3	1.86	2.70	3.76	2.52

TABLE III. - TYPICAL COATING PROPERTIES

Properties	Units	Coatings						
		Black Velvet (101-C10)			Black Enamel (Q36K802)			
		4 mils	3 mils	2 mils[a]	0.9 mil	0.7 mil	0.5 mil	0.3 mil[b]
Diffuseness	-	high			unknown			
Emissivity	-	highest			high			
Signal factor (C_c)	sec	**0.019**	0.0102	0.0046	0.0024	0.0015	0.00075	0.00027

[a]Thinnest coating practical to apply (Appendix B).
[b]Thinnest coating opaque to infrared (Appendix C).

η_z = signal ratio, dimensionless
f = frequency, Hz
$C_z = (t_p^2/\alpha_p)$, sec
t_p = part thickness, cm
α_p = part diffusivity, (Table II), cm^2/sec

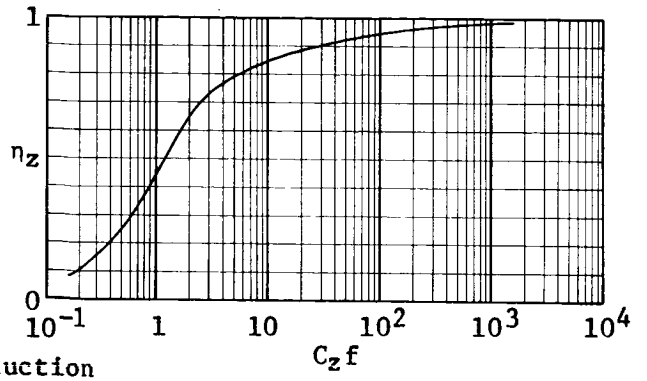

(a) Substrate conduction

η_x = signal ratio, dimensionless
f = frequency, Hz
$C_x = (x_p^2/\alpha_p)$, sec
x_p = lateral distance, cm
α_p = part diffusivity, (Table II), cm^2/sec

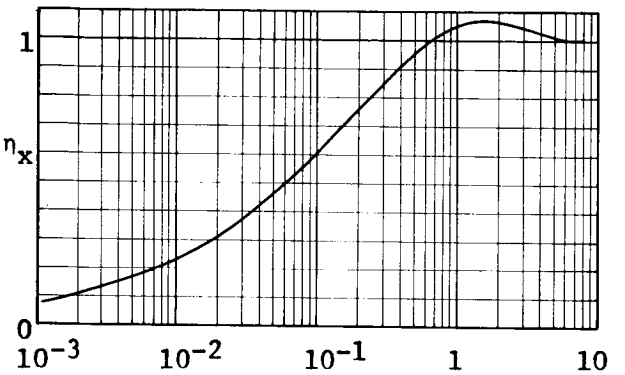

(b) Lateral conduction

η_e = signal ratio, dimensionless
f = frequency, Hz
$C_e = (\rho c t_p/h)$, sec
t_p = part thickness, cm
h = heat transfer coeff., $W/cm^2\ {}^oK$
ρ = part density, (Table II), g/cm^3
c = part specific heat, (Table II), $J/°Kg$

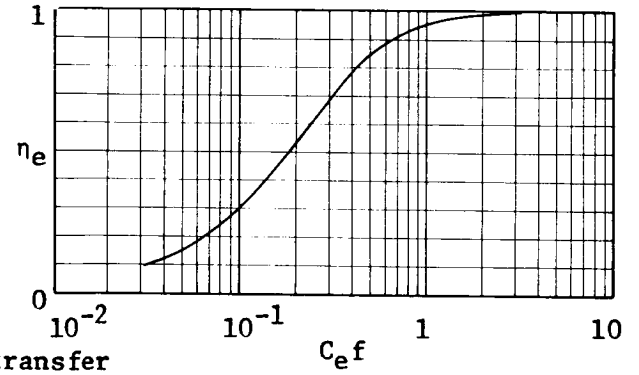

(c) Environmental heat transfer

η_c = signal ratio, dimensionless
f = frequency, Hz
$C_c = (t_c^2/\alpha_c)$, (Table III), sec
t_c = coating thickness, cm
α_c = coating diffusivity, cm^2/sec

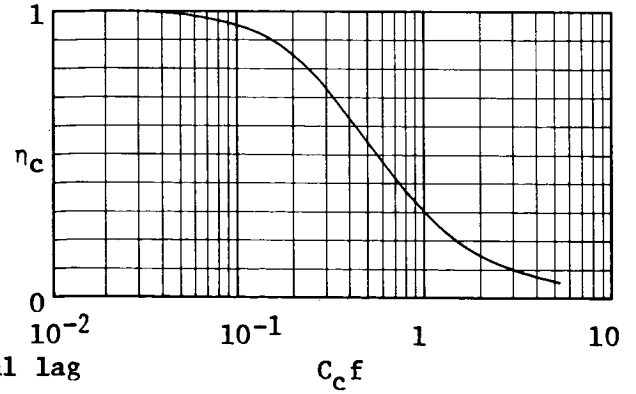

(d) Coating thermal lag

Figure 15.- Frequency effects on sinusoidal infrared stress signal emission

The thermoelastic temperature increments in the signal radiance parameter are based on adiabatic material elements. The test part surface material within the instantaneous radiometer field of view can be considered adiabatic if there is no significant heat transfer to or from that material element during the period of stress oscillation producing the signal. When the test part motions produce oscillating bending stresses, thermoelastic energy conversion will vary with depth below the surface, and there can be significant heat exchange by conduction between the surface element and the deeper substrate. When the test part oscillating surface stress distribution has gradients in magnitude, thermoelastic energy conversion will not be the same in all areas of the surface, and there can be significant heat exchange by conduction between the material element within the radiometer field of view and the laterally adjacent portions of the test part. When the test part stress oscillation produces surface temperature oscillation by thermoelastic energy conversion, there can be significant heat exchange by radiation and convection between surface material elements and their environment. These three possible types of heat exchange impose different limitations on the lower limits of test frequencies. (See sections on "Substrate Conduction", "Lateral Conduction", and "Environmental Radiation and Convection", pp. 16, 20, and 24).

The thermoelastic temperature increments in the signal radiance parameter are those which would be produced in the structural metals of test parts, and the signal radiance magnitudes are a direct function of test part surface emissivity. Metals typically have low emissivities which cannot be accurately predicted because of surface effects, such as oxidation and corrosion. High emissivities of known magnitudes can be obtained by applying certain coatings to test parts, and this tends to improve infrared stress data accuracy in several respects. The primary improvements are more accurate radiometric sensing (higher signal-to-noise ratio with higher emissivity) and more accurate data reduction (lower signal-to-stress conversion errors with lower unknown emissivity variations). Coatings also improve the diffuseness of test part radiation and the suppression of spurious environmental radiation (by reducing reflection from the test part into the radiometer). This may be important, particularly for room temperature test parts. A coating may impose testing temperature limitations if its thermal degradation threshold is more critical than the substrate metal, but the coating advantages are least important at elevated temperatures. A coating may reduce the useful frequency range of accurate measurements in two respects. High emissivity coating radiation to its environment may limit the lower frequency portion of the range. (See section on "Environmental Radiation and Convection", p. 22). This will usually be less important than the coating advantages. Coating thermal lag relative to its substrate may significantly limit the upper frequency portion of the range. (See section on "Coating Thermal Response", p. 26). Techniques to measure coating thickness and correct for coating thermal lag are required to achieve ultimate accuracies at high frequencies. (See section on "Recommended Future Work", p. 85).

Spectral Detection Factors. - The spectral aspects of signals, windows, and detectors are the most important factors relative to infrared stress detectability. Pressure barrier window thickness requirements can be evaluated on the basis of window diameter, material and differential pressure for test applications (fig. 16). The integral spectral effects of test part temperature can be evaluated for combinations of windows and detectors (fig. 17). The average surface emissivity can be evaluated for the test part surface of the application (fig. 18). If the integral spectral factors are excessively unfavorable with an existing test facility window (for all types of detectors), a window of different material may have to be installed to achieve desired stress detectability levels. Since window size imposes a limit on the radiometer aperture diameter, the stress detectivity for a given pressure barrier window material will vary with the window size as well as the thickness required for pressure integrity. The aperture diameter and type of detector can also impose non-spectral limitations on stress detectivity, spatial resolution, and depth of optical field, but these are usually less important than the spectral limitations. The above procedures yield the integrated parameter of the relation

$$V'_{\lambda r} = \bar{\varepsilon}_{\lambda} \left(V'_{\lambda r}/\bar{\varepsilon}_{\lambda}\right)$$

which is indicative of signal-to-noise ratio in terms of all spectral factors. The detector material defines a minimum detector area A_d, and the window size D_w defines a maximum aperture diameter D_o.

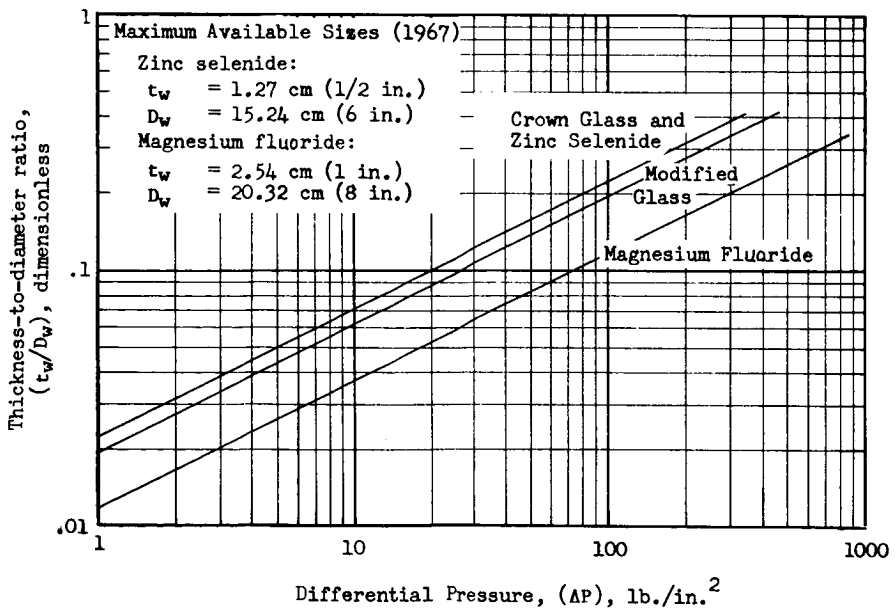

Figure 16. - Typical thickness criteria for tenfold factor of safety with round pressure barrier windows.

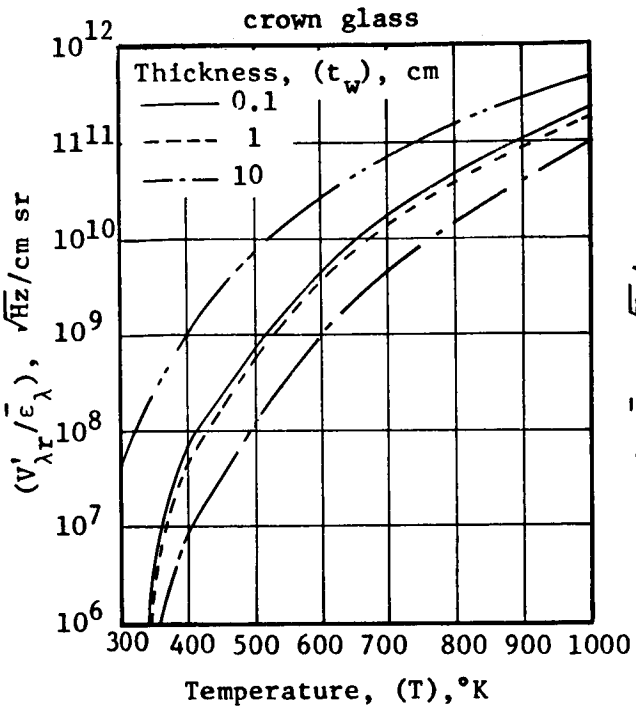

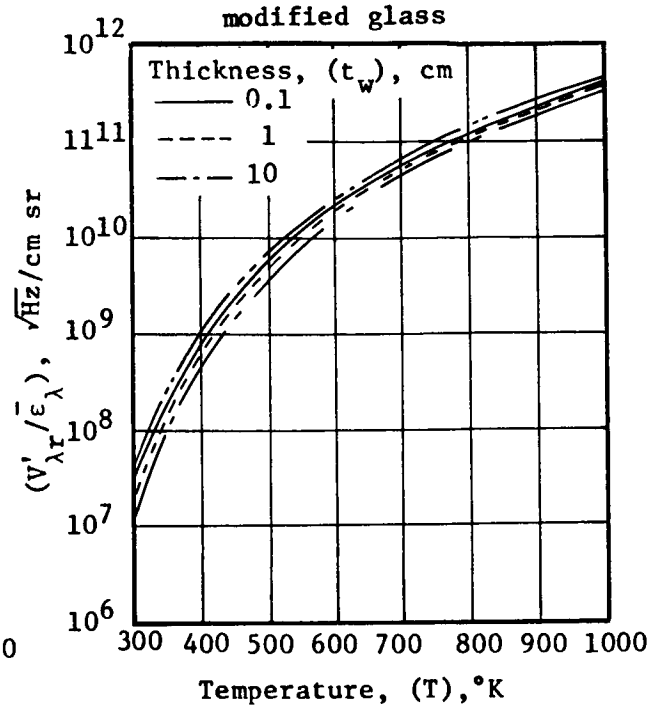

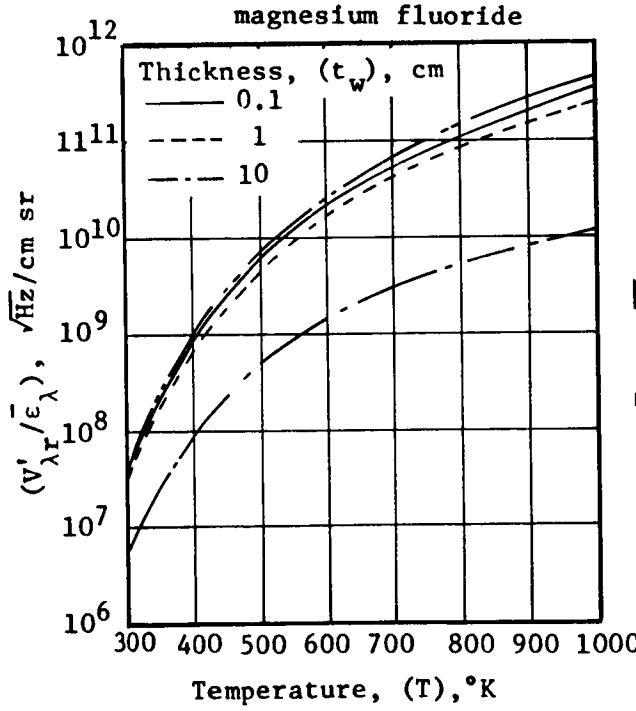

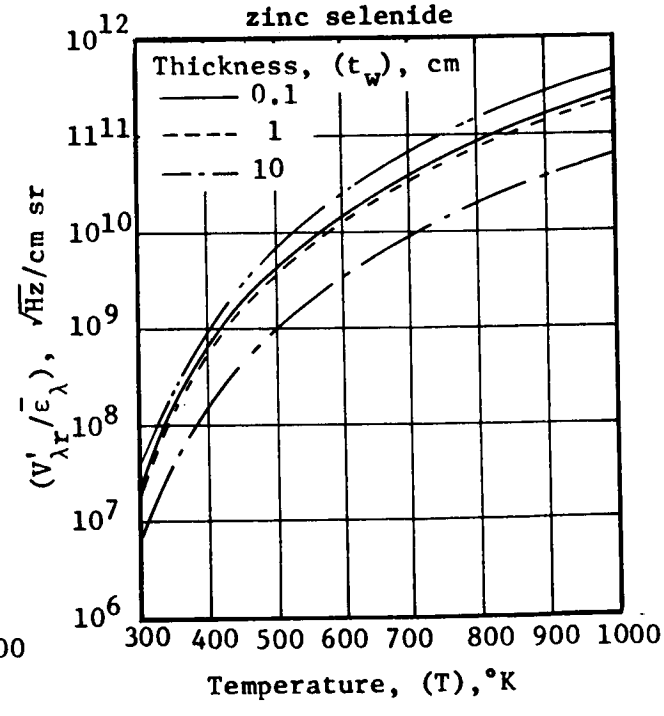

——·—— Spectral integrals with no windows

(a) Lead sulfide at 77°K.

Figure 17.- Spectral integrals for infrared stress detection

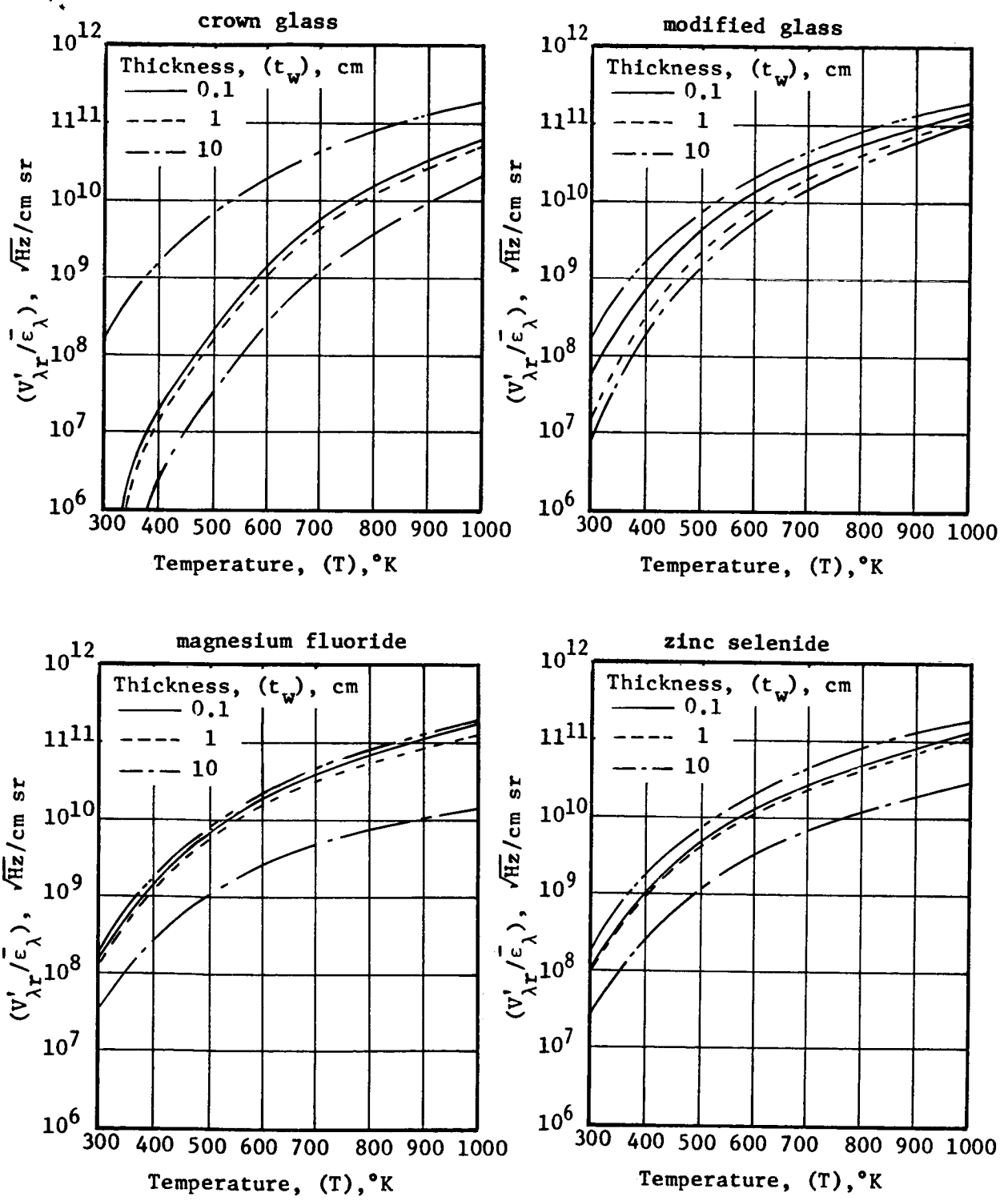

——·—— Spectral integrals with no windows

(b) Indium antimonide at 77°K

Figure 17.- Continued

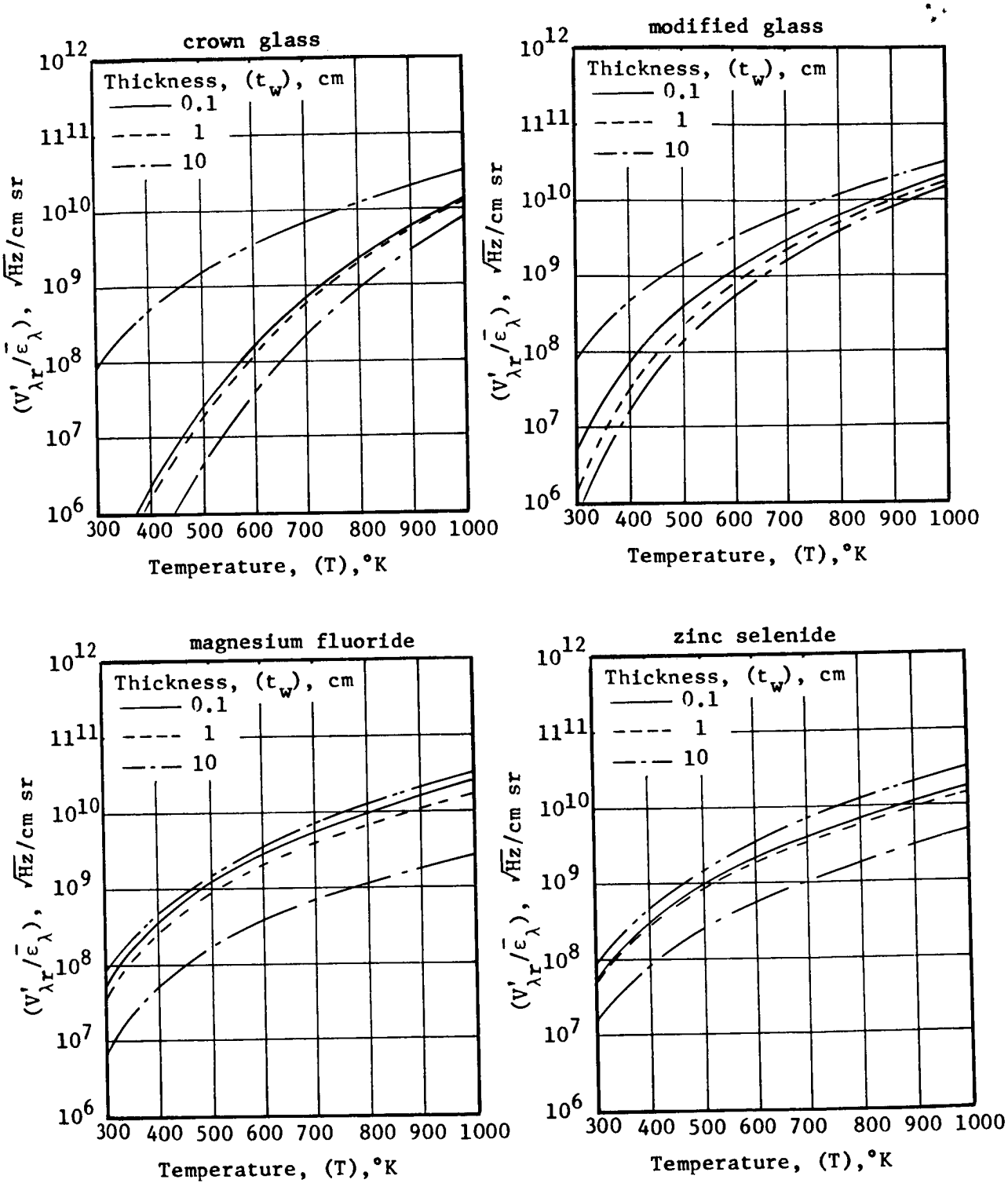

——·—— Spectral integrals with no windows

(c) Gold activated germanium at 77°K

Figure 17.- Continued

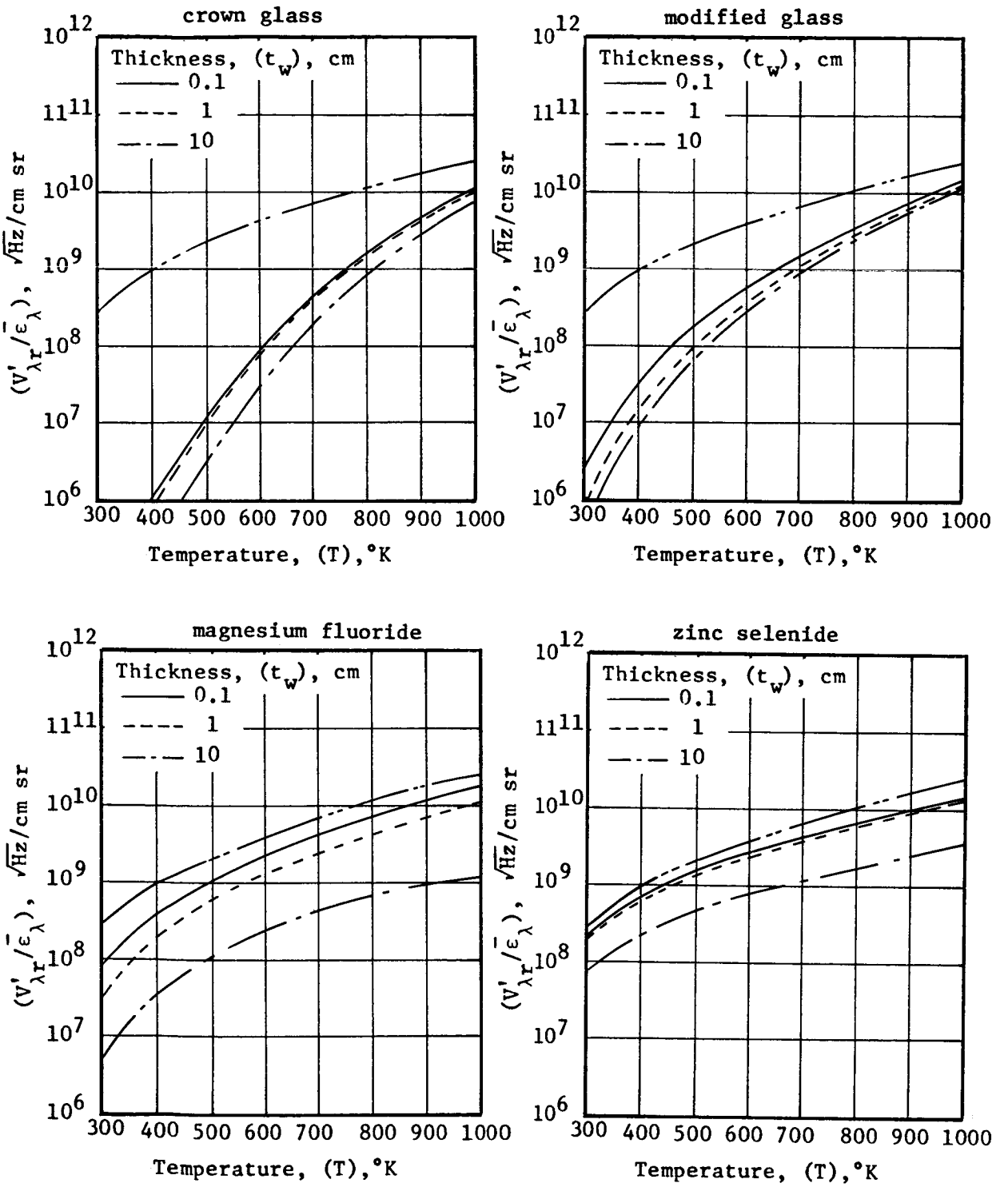

——·——·—— Spectral integrals with no windows

(d) Mercury activated germanium at 28°K

Figure 17.- Continued

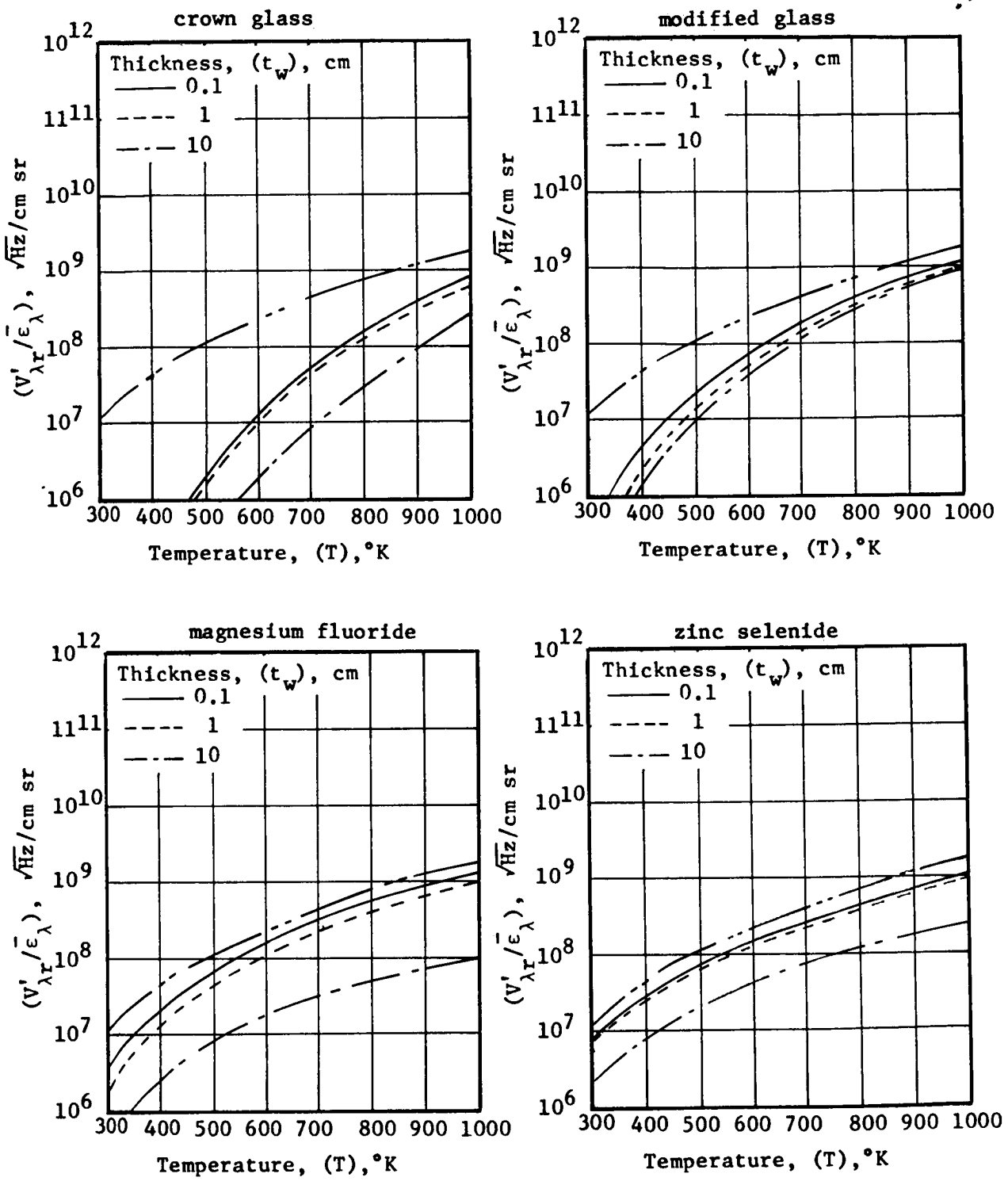

——·—— Spectral integrals with no windows

(e) Unimmersed thermistor at 300°K

Figure 17.- Concluded

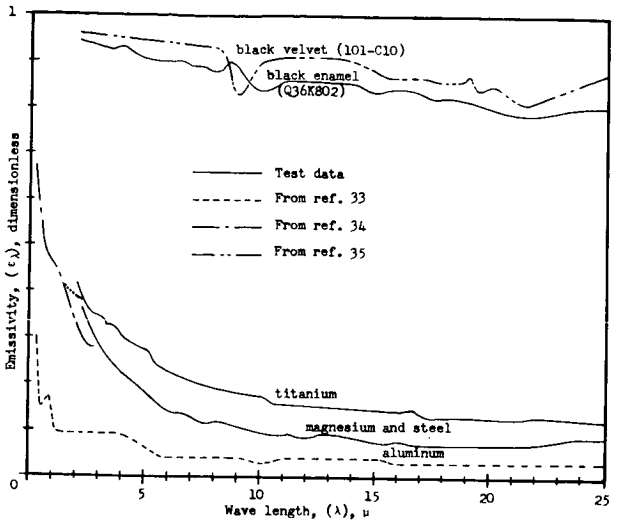

Figure 18. - Surface emissivities

Window losses can frequently be avoided by using an internal sensor when test facility environments are not hostile to the radiometer and the sensor does not interfere with the facility test simulation. (See section on "Pressure Barrier Window Attenuation", p. 31). When a window is necessary, its thickness should usually be minimized. Factors of safety less than ten are adequate for most applications. (See section on "Window Design Analysis", p. 130). Large window pressure differentials can usually be avoided by enclosing the sensor (and window) with a chamber controlled at nearly the same pressure as exists within the test facility. The transmission loss of zinc selenide windows can also be reduced by anti-reflection coatings peaked for an important spectral wave length range. Specific applications may require careful consideration of the above factors, window deflections and other aspects of window design (Appendix F).

The performance data for specific detectors were used to compute the signal integrals shown herein. (See section on "Infrared Detection", pp. 42-43). Spectral integrals for other detectors can be computed from this type of performance data or estimated on the basis of approximate performance differences relative to the specific detectors covered by this study. The exact performance of an infrared detector is dependent on many additional factors not included in the spectral integral computations. (See section on "Infrared Detector Analysis", p. 120). Individual detectors selected from production lots can usually be obtained at added cost, and their performance would be superior to that indicated herein for typical production detectors. Thermistor and lead sulfide detectors can be obtained with different time constants, and this affects detectivity as well as frequency response. Immersed detectors employ an integral lense to concentrate more signal energy on the detector material than would normally be obtained. The typical result of this is approximately three times the unimmersed detectivity and double the unimmersed plane angular field of view. Specific applications may require careful consideration of many aspects of detection performance (Appendix E).

Spectral emissivities are shown for polished uncoated metals. The emissivities of metals vary considerably with surface condition. (See section on "Signal Emission Frequency Ranges, p. 48).

Optical Collection Factors. - The improvement of signal strength by optical collection is a compromise relative to attainable spatial resolution, depth of optical field, and stand-off distance. The geometric aspects of signal gains can be evaluated relative to angular field of view (fig. 19). The spatial resolution and depth of optical field can be evaluated relative to angular field of view and stand-off distance (fig. 20). Specific test applications can involve constraints on the stand-off distance for a test facility and the aperture diameter, focal length, and/or detector area for radiometric equipment. Any combination of test application constraints can be applied to evaluation of geometric aspects of optical collection systems. When combined with a known optical collection system efficiency η_o, the above procedures yield the optical gain parameter $(\eta_o K_o D_o^2)$ and data spatial resolution s_{xy} for test applications.

detector	PbS	InSb	Ge:Au	Ge:Hg	Thermistor
min. A_d, mm^2	0.05	0.01	0.05	0.05	0.01

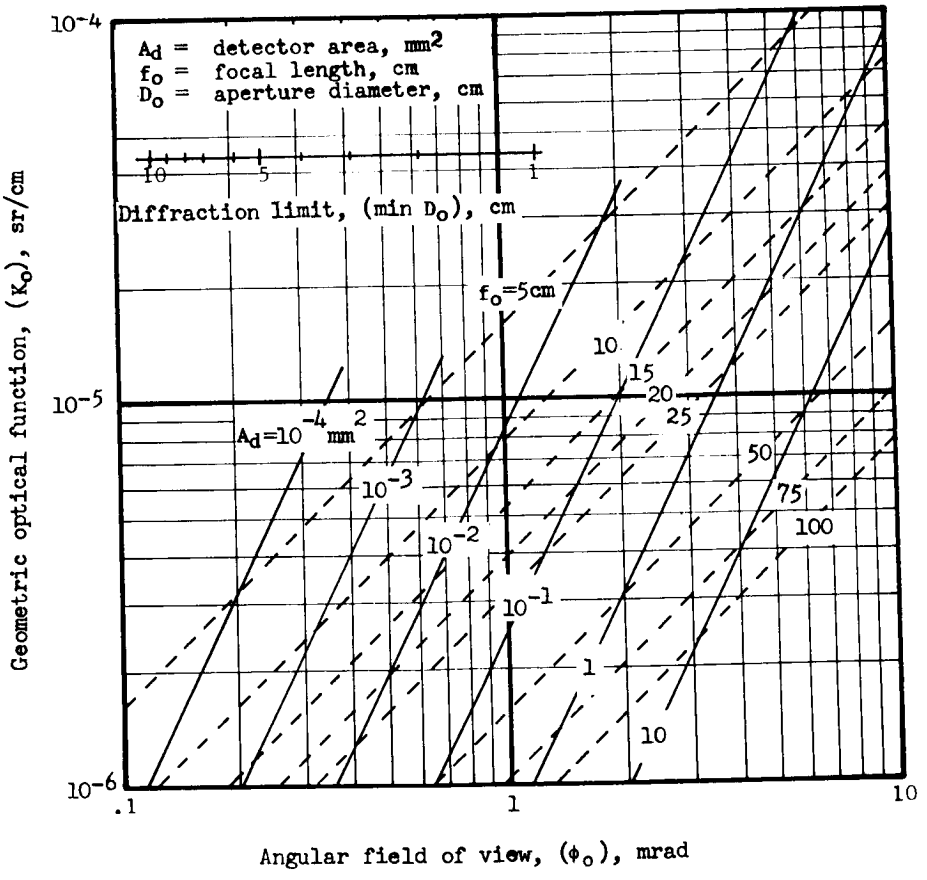

Figure 19.- Geometric optical function

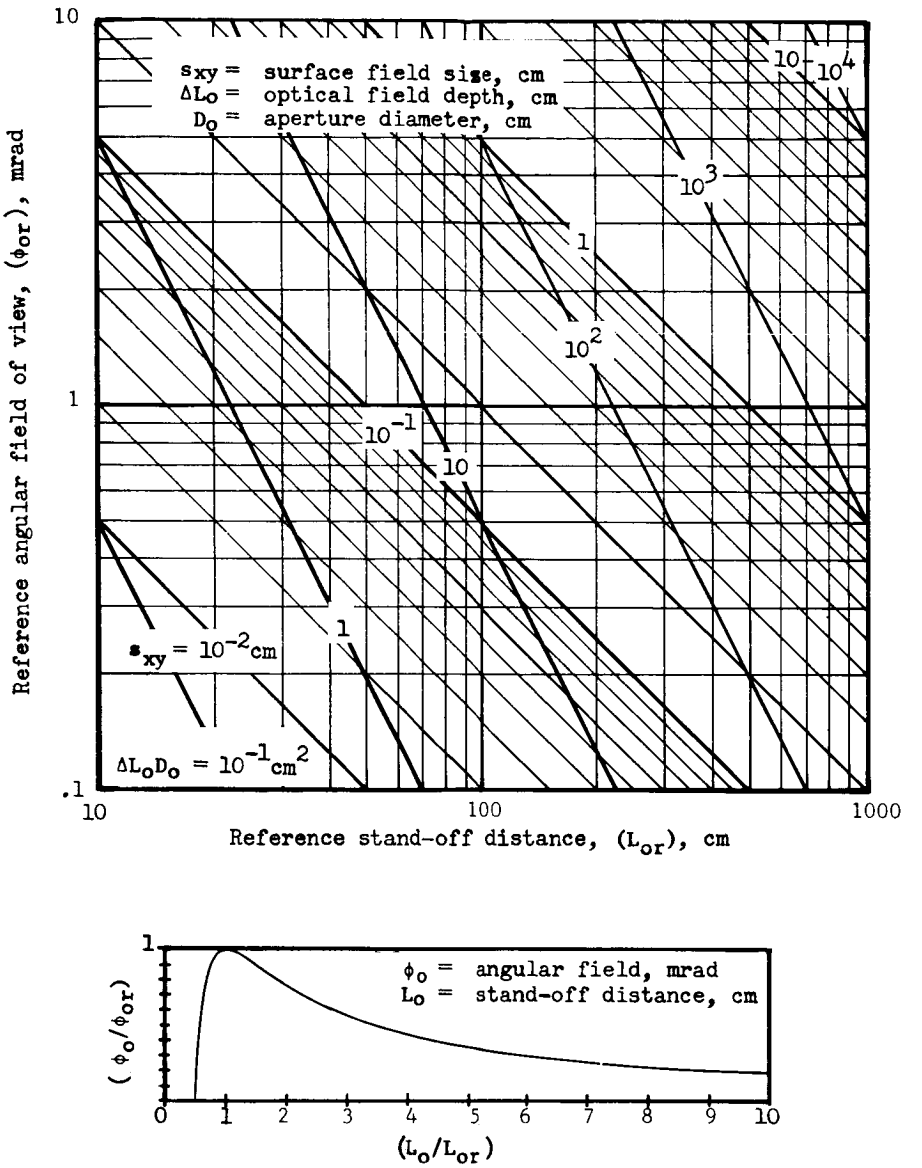

Figure 20. - Spatial resolution and depth of field

The angular field ϕ_o (Figure 19) is for unimmersed detectors. The angular field and detectivity of immersed detectors can be estimated from the immersion lense characteristics. (See section on "Spectral Detection Factors", p. 55).

A typical radiometer has an optical efficiency η_o of approximately 50 percent when focal losses are small. (See section on "Optical Collection", p. 41). However, focal losses can be

significant when a radiometer is used at stand-off distances greatly different than that for which it was designed. Many radiometers are designed for infinity stand-off distance (to avoid a maximum distance limit), but focal losses are then likely to be significant in the 100 to 1000 centimeter stand-off distance range most important for infrared stress measurements. Optical collection system mirrors can be optimized for finite stand-off distances important to specific applications, and focal losses are relatively small for a range of stand-off distances near the design optimum.

Spatial resolution is a function of required optical field depth s_{xy} (and other factors) when a surface is scanned with a fixed radiometer focal adjustment (fig. 20). The variations of instantaneous stand-off distance due to the angular scan motion of the radiometer axis is usually the major consideration relative to required optical field depth, but vibrating test part motions can also affect the required depth of optical field. Such motions can have an additional adverse effect on spatial resolution when there is a motion component perpendicular to the radiometer axis because data aquisition is then from a surface area larger than the maximum instantaneous field of view size s_{xy}. The factors discussed above may impose absolute (practical) limits on attainable spatial resolution for certain surface areas of specific test parts, but special scanning techniques can alleviate such limits in some cases. Multiple scans with various fixed focal adjustments provides improved spatial resolution at various discrete stand-off distances. Various (more favorable) test part viewing angles can sometimes be obtained by moving the radiometer, using more than one radiometer, or reflecting infrared signals with flat mirrors. Data on instantaneous location of surface field of view during scanning of moving parts can usually be obtained by applying a grid on the test part of different emissivity than the remainder of the test part surface.

When angular motion and stress oscillation of a test part occur at the same frequency, a non-uniform radiation environment can produce spurious signals. (See section on "Infrared Stress Measurement Experiments", p.118). This type of motion and stress oscillation is usually obtained with vibrating test parts for which infrared stress measurements are desirable. A high emissivity (low reflectivity) coating on the test part tends to directly suppress environmental radiation incident on the test part surface. The suppression is most effective if the coating is highly diffuse (rather than specular) because angular motion of a diffuse surface in a non-uniform radiation environment produces relatively small

changes of reflected energy in any one direction (except grazing angles). Of two available high emissivity coatings, black velvet has higher emissivity, and it probably is a more diffuse radiator, but it is limited relative to thermal response. (See section on "Coating Response Experiments", p.101). The other coating (black enamel) has faster response and nearly the same emissivity, but it probably is a more specular radiator than black velvet. Application of black velvet to test parts may suppress environment reflection more effectively than black enamel when the resultant upper frequency limitations are acceptable. (See section on "Signal Emission Frequency Ranges", pp. 46-47). In addition to direct suppression of reflection by coatings on test parts, non-uniformities in radiation environments can be reduced with diffuse high emissivity coatings. The most important radiation environment is that which would reflect radiation directly into the radiometer (the area around the radiometer aperture for viewing angles nearly perpendicular to test part surfaces). The degree of spurious signal suppression feasible by applying high emissivity coatings (as discussed above) is unknown. More exact techniques are required to achieve ultimate infrared stress reliability and accuracy with moving test parts. (See section on "Recommended Future Work", p. 85).

Signal Processing Factors.- Detector frequency effects and electronic bandwidth are the two signal processing factors most important relative to the detectable stress for specific test applications. The detector signal ratio can be evaluated for the frequency of radiant signal oscillation at the detector (fig. 21). At high test part stress oscillation frequencies, the detectors with low time constants are favorable. With low test part oscillation frequencies, it may be desirable to optically chop the radiant signal to improve the detector performance. It is usually necessary to use chopping at very low frequencies because of the difficulties with low frequency (or direct current) amplification.

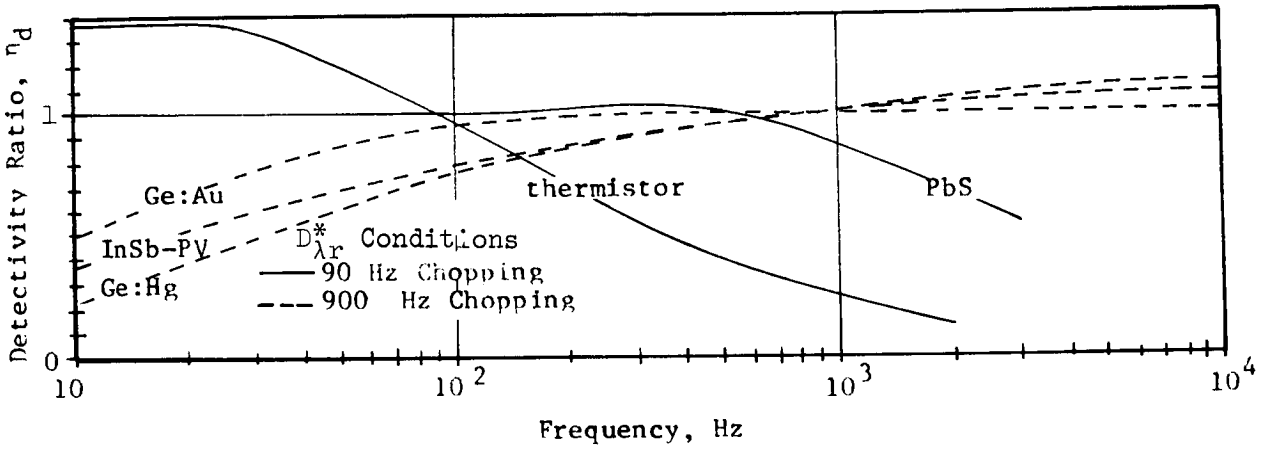

Figure 21. - Frequency effects for selected detectors

Narrow electronic bandwidths are desirable for filtering detector noise which would otherwise be present in the radiometer output signal. For non-scanning steady-state measurements, bandwidths approaching one hertz can be considered, but bandwidths less than two hertz require very complex techniques, and a typical standard wave analyzer might have a bandwidth of approximately 3.5 hertz (See section on "Infrared Stress Measurement Experiments," p. 111). Narrow bandwidth filters respond slowly to changes of signal magnitude, and are not desirable for transient signals which might be obtained from changes in test part stresses or rapid surface scanning. The bandwidth Δf is therefore normally a compromise relative to various aspects of the test application. An adjustable bandwidth is practical, and this would be desirable for infrared stress measurements. It would permit rapid scanning (with wide bandwidths) to map surface stress fields and more accurate non-scanning measurements (with narrow bandwidths) at selected test part surface locations.

Data Reduction. - Thermoelastic constants are dependent on the material of which the test part is composed. Values defined by thermoelastic experiments are available for common structural metals (Table IV). Values for other materials can be computed from the thermoelastic theory (pp. 8). The thermoelastic constant K_M yields the detectable stress of the relation

$$\sigma^* = \sqrt{\Delta f}/(K_M)(\eta_o K_o D_o^2)(\eta_p \eta_d)(V'_{\lambda r})$$

when combined with previously defined factors (pp. 46, 49, 56, and 60). For a magnitude of measured stress σ, the signal-to-noise ratio of the relation

$$(V_S/V_N) = (\sigma/\sigma^*)$$

defines an ultimate accuracy limit for infrared stress instrumentation.

TABLE IV.- TYPICAL THERMOELASTIC CONSTANTS FOR STRUCTURAL METALS

(From Appendix A)

Materials	Thermoelastic constants, (K_M)		Approximate variations, $\pm$ %[a]
	in^2/lb	cm^2/N	
Steel (4130)	2.22×10^{-8}	3.22×10^{-8}	6.4
Titanium (6AL-4V)	2.70	3.91	6.7
Aluminum (7075)	6.65	9.65	4.5
Magnesium (AZ31B)	9.90	14.37	1.5

[a] probable approximate variation for stresses less than 75 percent of yield strength with 299 to 368°K temperatures.

Certain types of test measurements can be made with detection threshold signal-to-noise ratios (as low as 2 or 3). Qualitative data of this type could be used to define instantaneous spatial stress nodes in vibrating parts and to study non-catastropic crack propagation patterns with time in fatigue test parts. However, quantitative stress data are desirable for most test applications, and data reduction factors (as well as signal-to-noise ratios) are then important.

The thermoelastic constants of structural metals vary significantly with stress and temperature level (Table IV). If these variations are acceptable in terms of desired data accuracy, the average thermoelastic constants can be applied in data reduction, and the additional accuracy considerations are then signal-to-noise ratio and several aspects of the specific application. These include accuracy of information on test part temperature level, test part surface emissivity, and transmission losses for the specific application. Transmission losses (and radiometer performance data) can be obtained for specific applications with pre-test (external) optical chopping calibrations. If other aspects of measurement accuracy are sufficiently favorable, some data corrections for second order thermoelastic variations may be appropriate (Appendix A, p.95).

The accuracy of scanning infrared stress measurements can be improved in another way when auxilliary single-point sensors can be attached to the test part. The desirable sensors are a strain gage rosette and thermocouple at a highly stressed point on the test part within the radiometric scanning field. This yields a calibration at the instrumentated point during each surface scan, and the calibration can be applied to improve the extensive spatial data acquired during the scan. The calibration is a direct measurement of the radiometric signal produced by a known stress at a known temperature level for the specific test set-up. It includes the overall effects of the specific test part material thermoelastic constant and surface emissivity, the gaseous transmission losses for the specific stand-off distance and gases, the specific facility window transmission losses, and the performance of the specific radiometer being used. This calibration data is superior to optical chopping calibration data from several different aspects. Thermoelastic constant and emissivity data are obtained for the specific test part. Gaseous transmission losses are evaluated instantaneously during data scans (rather than by pre-test calibration). Data are acquired on actual test part temperature during data scan. The data from single-point sensors on a test part are valuable as a drift check and/or calibration correction even with other more accurate calibration and data correction techniques (discussed below).

Thermoelastic constants have been measured for specific structural metals (Appendix A). However, the available data were obtained with only four test specimens. Thermoelastic constants for a specific alloy could vary somewhat due to small differences in minor constituents, heat treat level, rolling fabrication variables, and other factors. Thermoelastic constants could be different for specific alloys of the same general type. Exact thermoelastic constant data are not available for many materials which might be required for test applications. It is therefore desirable to utilize a calibration which incorporates the thermoelastic constant of the test part material for the specific application. The single-point auxiliary sensors (discussed above) do this, but better definition of stress and temperature

effects could be obtained by a pre-test absolute thermoelastic calibration with a specimen of the test part material. (See section on "Recommended Future Work, p. 86).

The inclusion of surface emissivity in calibrations is primarily for convenience, and it does not substantially improve scan data accuracy. Uncoated metals are likely to have spatial variations in emissivity which are not defined by a single-point calibration within a scan field. For ultimate accuracy, high emissivity coatings can be used, and the surface emissivity is then known. Coatings do impose upper frequency testing limitations. (See section on "Signal Emission Frequency Ranges", p. 48). However, these limitations could be alleviated by improved methods of application and thickness measurement for thin coatings. (See section on "Recommended Future Work", p. 85).

Gaseous transmission losses can vary with the level of certain minor constituents. (See section on "Gaseous Media Attenuation", pp. 28-31). If the magnitudes of the losses are significant and variations occur in important gaseous constituents, there can be different gaseous transmission losses during pre-test calibrations and various test scans for infrared stress data acquisition. The single-point auxiliary sensors (discussed above) provide a means of correcting the scan data for the actual gaseous losses that exist during the scan. Although gaseous loss variations appear to be the major source of signal drift with time, the single-point sensors would also detect drift from other sources and/or instrumentation malfunctions.

The temperature is important in the single-point auxiliary sensors (discussed above) primarily for definition of the temperature applicable to the single point calibration signal. The temperature sensor also provides some data on test part temperature level during test runs, but this data are not applicable to the entire scan field unless the test part is isothermal. Test part temperature gradients can be produced by vibration damping heat generation, environmental transients, and other factors. Scan data could be corrected for test part gradients by employing radiometric sensing of test part temperature levels. (See section on "Recommended Future Work", p. 86).

Typical Infrared Stress Application Ranges

The spatial resolution and detectable stress limits of test applications can be rapidly estimated with the technology shown herein. (See section "Instrumentation System Methodolgy", pp. 46-64). Many types of parametric studies could be made relative to overall infrared stress measurement application ranges for the numerous alternate test application and instrumentation conditions possible. It was considered desirable to show some of the more important application range trends herein. The intent was to emphasize those aspects of the infrared stress measurement technique which impose the primary limitations on application ranges.

Spatial resolution trends were evaluated for a radiometer of relatively large aperture diameter (20 cm) with 0.1, 1, and 10 milliradian assumed angular fields ϕ_o . The smallest angular field above would be within the diffraction limit, but could be attained only with small detector areas and/or long focal lengths (p. 56). The geometric optical function K_o would therefore tend to smaller for the smaller angular fields, and this indicates the signal losses typical for attaining ultimate spatial resolution.

Spatial resolution can be evaluated in terms of the maximum size s_{xy} of the radiometric field on the test part surface. This resolution is dependent on the stand-off distance L_o between the test part and radiometer and the optical field depth ΔL_o (p. 57). The required optical field depth is dependent on stand-off distance variations due to test part motions and/or fixed-focus scanning factors (p. 58).

The overall spatial resolution trends show the importance of small radiometric fields of view (fig. 22). There is an optimum stand-off distance for any required radiometer and optical field depth which yields the smallest field of view s_{xy} attainable on the test part. However, spatial resolution penalties are relatively small with moderate variations of stand-off distance for any required optical field depth. The most important test application factor relative to spatial resolution is the required optical field depth. For large optical field depths, best spatial resolution can only be obtained with small radiometric angular fields at large stand-off distances. Radiometers with smaller aperture diameters would be less critical relative to optical field depth (p. 57), but might be more critical relative to the diffraction limit (p. 56). Smaller apertures would also yield lower signal outputs (p. 55).

For an intermediate radiometric field of one milliradian, the spatial resolution would vary from 0.02 to 0.63 centimeters for optical field depths from 0.01 to 10 centimeters (fig. 22). Detectable stress

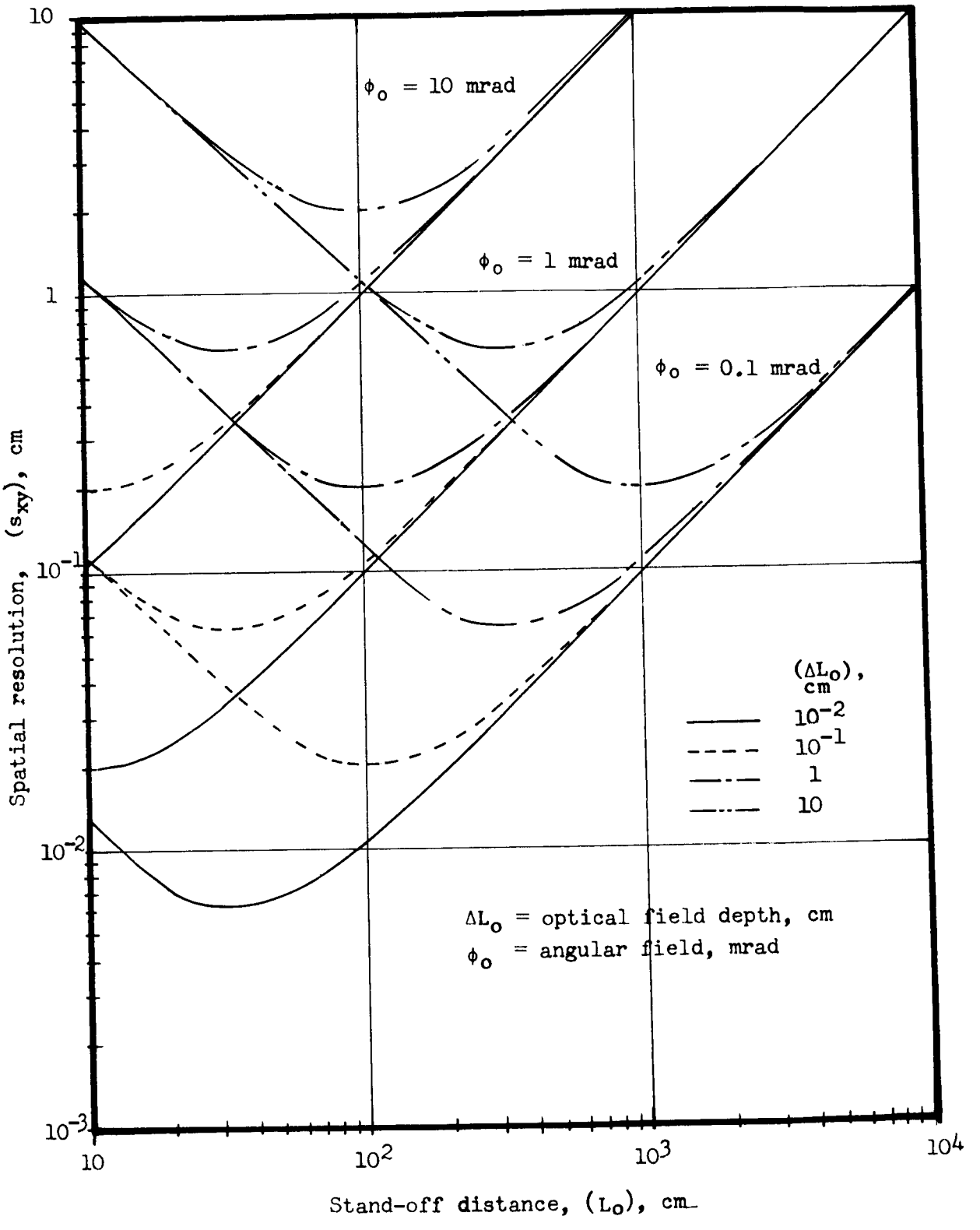

Figure 22. - Typical radiometer spatial resolution trends

trends were evaluated for a radiometer with this spatial resolution criteria and a typical focal length f_o of 20 centimeters. The one milliradian field implies a detector area of 0.05 square millimeters, and is not the minimum attainable with detectors in the selected radiometer (p. 56). However, the above criteria and an assumed optical efficiency η_o of 0.5 (p. 57) yield suitable parameters for evaluating typical infrared stress detectability trends (Table V).

TABLE V. - SELECTED TYPICAL RADIOMETER AND WINDOW PARAMETERS FOR DETECTABLE INFRARED TREND STRESS TREND STUDIES

Aperture diameter, D_o, (selected), cm	20
Focal length, f_o, (selected), cm	20
Angular field of view, ϕ_o, (selected), mrad	1
Detector area, A_d, (p. 56), mm^2	0.05
Geometric optical function, K_o, (p. 56), sr/cm	4×10^{-6}
Radiometer optical efficiency, η_o, (assumed), dimensionless	0.5
Optical gain parameter, $\eta_o K_o D_o^2$, cm sr	8×10^{-4}
Window diameter, D_w, (assumed), cm	25
Window differential pressure, ΔP, (selected), $lb/in.^2$	15
Window factor of safety, (assumed), dimensionless	10

When windows are required, they must be somewhat larger than the radiometer aperture, and 25 cm was assumed as a window diameter compatible with the 20 cm radiometer aperture diameter. Although infrared window materials are not currently available in the 25 cm diameter size, larger sizes of these materials are likely to be available in the future. Also the transmittance of a multiple pane window (which could currently be used) is likely to be similar to that for a single pane window because of the compensating differences in blockage and thickness. Single pane construction was therefore assumed for all window materials of the application range study to provide direct comparisons of materials. The window thickness required is a function of design pressure differential and factor of safety (as well as the window material strength properties). A 15 lb/in^2 pressure differential ΔP (approximately one atmosphere) was selected for the application range comparison computations. This is directly adequate for evacuated altitude chambers and many other test facilities. It is probably conservatively high for pressure controlled radiometer enclosure chambers, which might be employed with high pressure test facilities (p. 55). Although highly conservative, a tenfold factor of safety was assumed to illustrate maximum window thickness trends likely to be encountered. The above criteria yielded suitable parameters for evaluating window effects on infrared stress detectability (Table V).

The spectral factors relative to emitted signals, window transmission, and detector response impose the most important limits on detectable stress ranges. The spectral distribution of emitted signals varies primarily with the test part temperature level and secondarily with the spectral emissivity of the test part surface (particularly for uncoated metals). The window transmittance varies primarily with the type of material and secondarily with its thickness. The detector spectral response varies primarily with the type of detector employed. To evaluate the spectral aspects of infrared stress detectability, all frequency effects were assumed to be negligible.

For negligible frequency effects, the emitted signal ratio η_p would be unity (p. 46). For the specific window design criteria (Table V), the required thicknesses would be 1.80 cm for crown glass and zinc selenide, 1.58 cm for modified glass, and 0.95 cm for magnesium fluoride (p. 49). The spectral integral $(V'_{\lambda r}/\bar{\varepsilon}_\lambda)$ can be evaluated at various temperatures for the five diversely different detectors (pp. 50-54). Surface emissivity $\bar{\varepsilon}_\lambda$ can be evaluated for uncoated and coated metals (p. 55), black enamel being selected as the coating material on the basis of its suitability for high temperatures and rapid thermal response. The above procedures define the integrated parameter $V'_{\lambda r}$ indicative of signal-to-noise ratio in terms of all spectral factors (p. 49). For negligible frequency effects, the detectivity ratio η_d would be unity, and the noise filter bandwidth Δf can be normalized to one hertz (p. 60). Detectable stresses σ^* can then be computed from the above criteria and the thermoelastic constants K_M for the materials (p. 61).

The detectable stresses without windows indicate strong trends with test part temperature for the structural metals (uncoated or coated) with various infrared detectors (fig. 23). Temperature increases in the 300 to 1000°K range make detectable stresses more favorable by orders of magnitude, and detectable stresses are relatively low for all detectors at high temperature. This indicates that wide filter bandwidths could be used to achieve rapid surface scanning and that radiometers smaller than selected herein (Table V) would be useful for high test part temperatures. It also indicates that high emissivity coatings on test parts would be less important at high than at low test part temperatures. At room temperature, high emissivity coatings, large radiometers, sophisticated detectors, and relatively narrow filter bandwidths are likely to be required for accurate infrared stress measurements. However, with the above favorable conditions, the most suitable detector (mercury activated germanium at 28°K) has a detectable stress limit of approximately 50 to 230 lb/in^2 at 300°K (fig. 23). This compares favorably with the typical strain gage and photoelastic coating resolution of

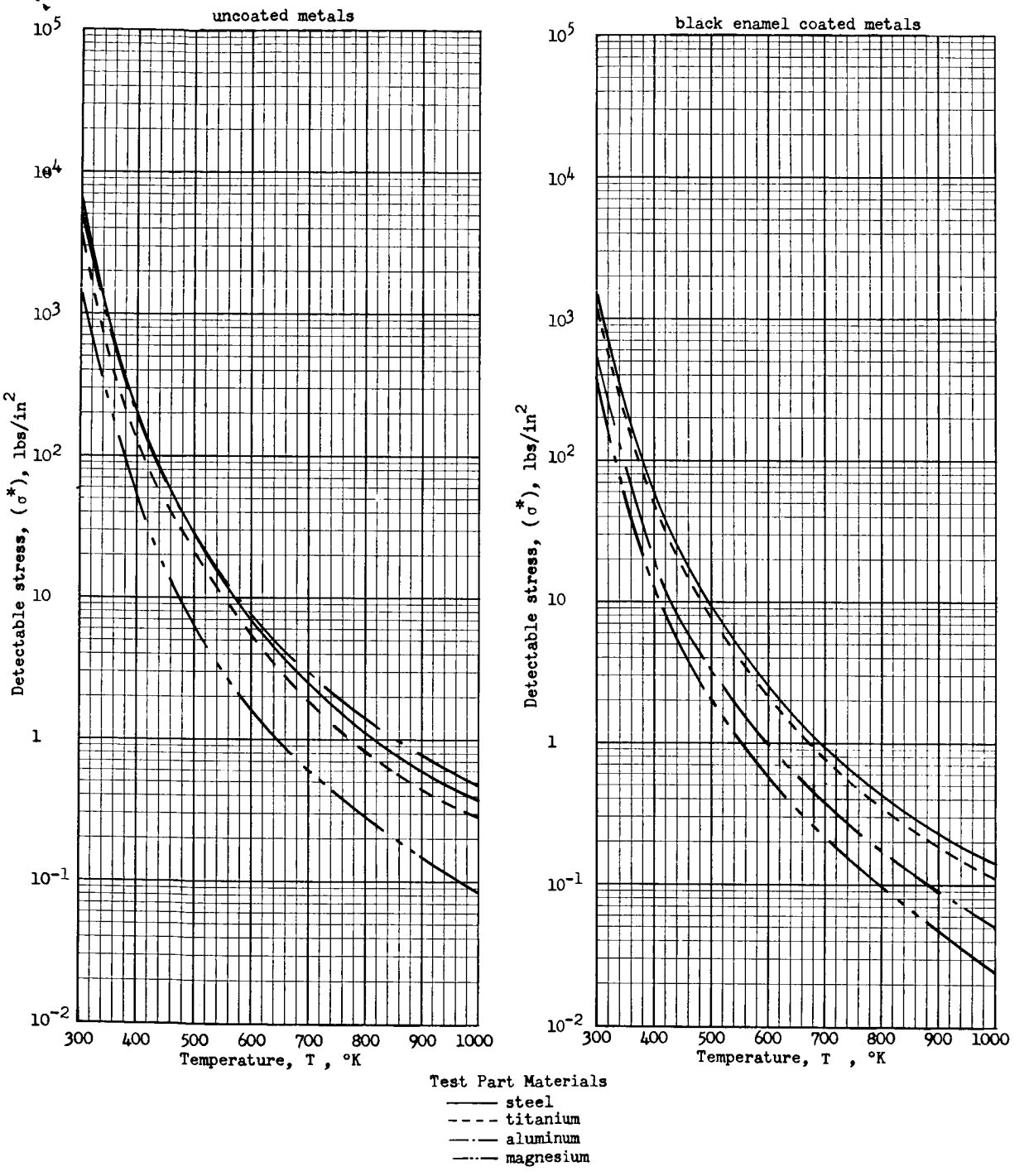

Note: Detectable stresses normalized to 1 Hz bandwidth Δf for a typical radiometer (Table V and fig. 22) with unity detector signal ratio η_d and unity test part signal ratio η_p.

(a) Lead sulfide detector at 77°K

Figure 23. - Typical infrared stress detection trends with temperature level

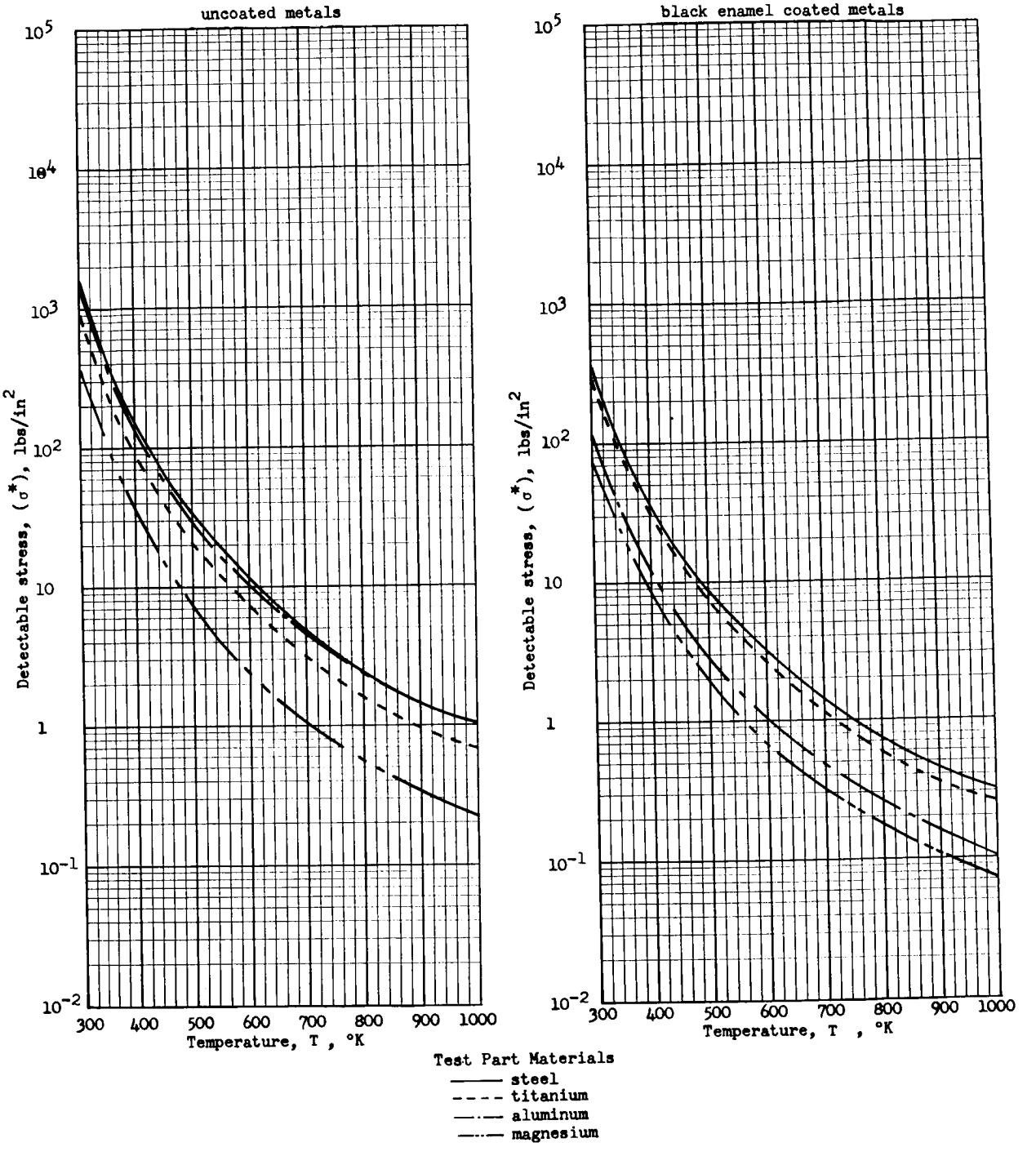

Note: Detectable stresses normalised to 1 Hz bandwidth Δf for a typical radiometer (Table V and fig. 22) with unity detector signal ratio η_d and unity test part signal ratio η_p.

(b) Indium antimonide detector at 77°K
Figure 23. - Continued.

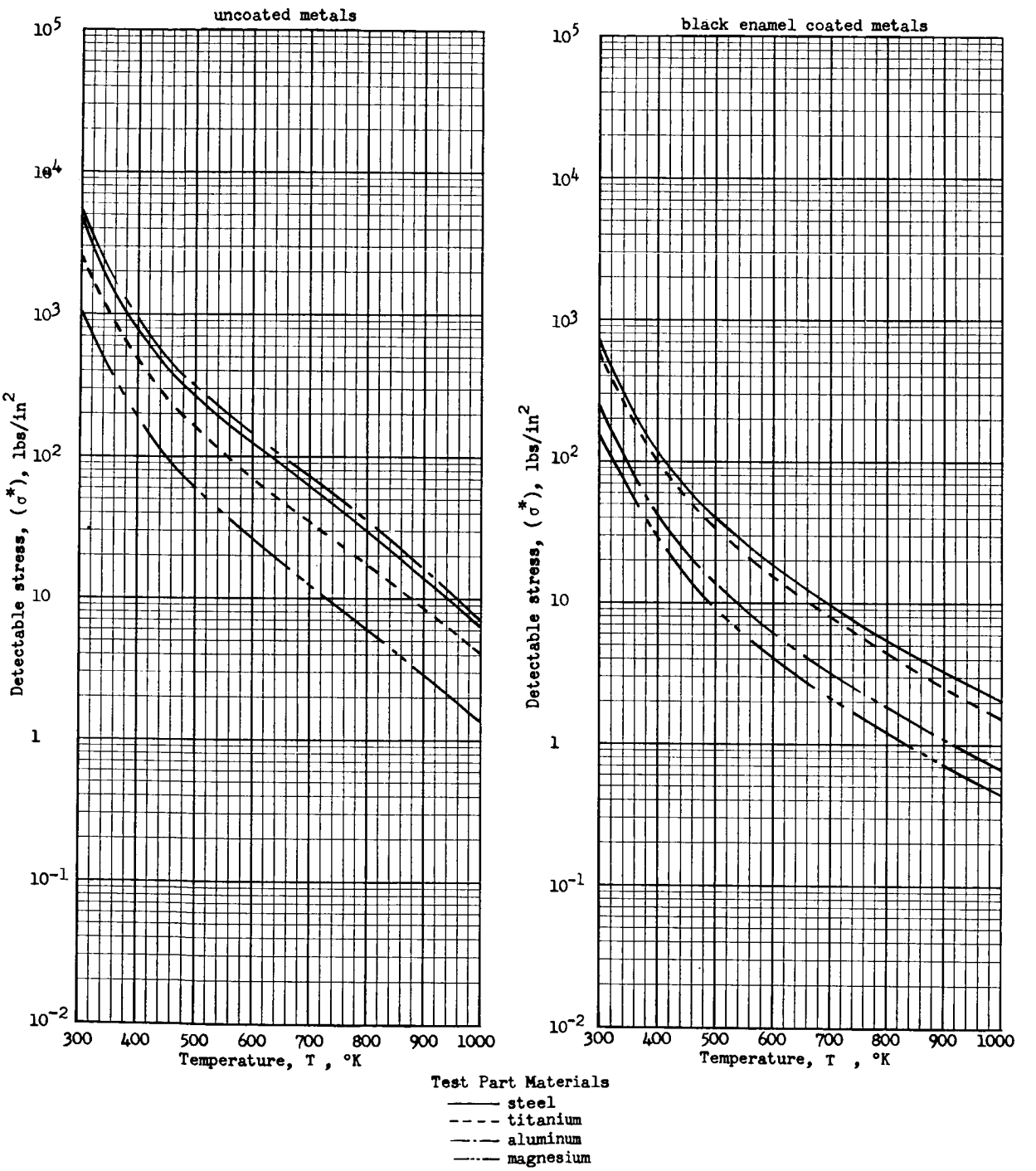

Note: Detectable stresses normalized to 1 Hz bandwidth Δf for a typical radiometer (Table V and fig. 22) with unity detector signal ratio η_d and unity test part signal ratio η_p.

(c) Gold activated germanium detector at 77°K

Figure 23. - Continued.

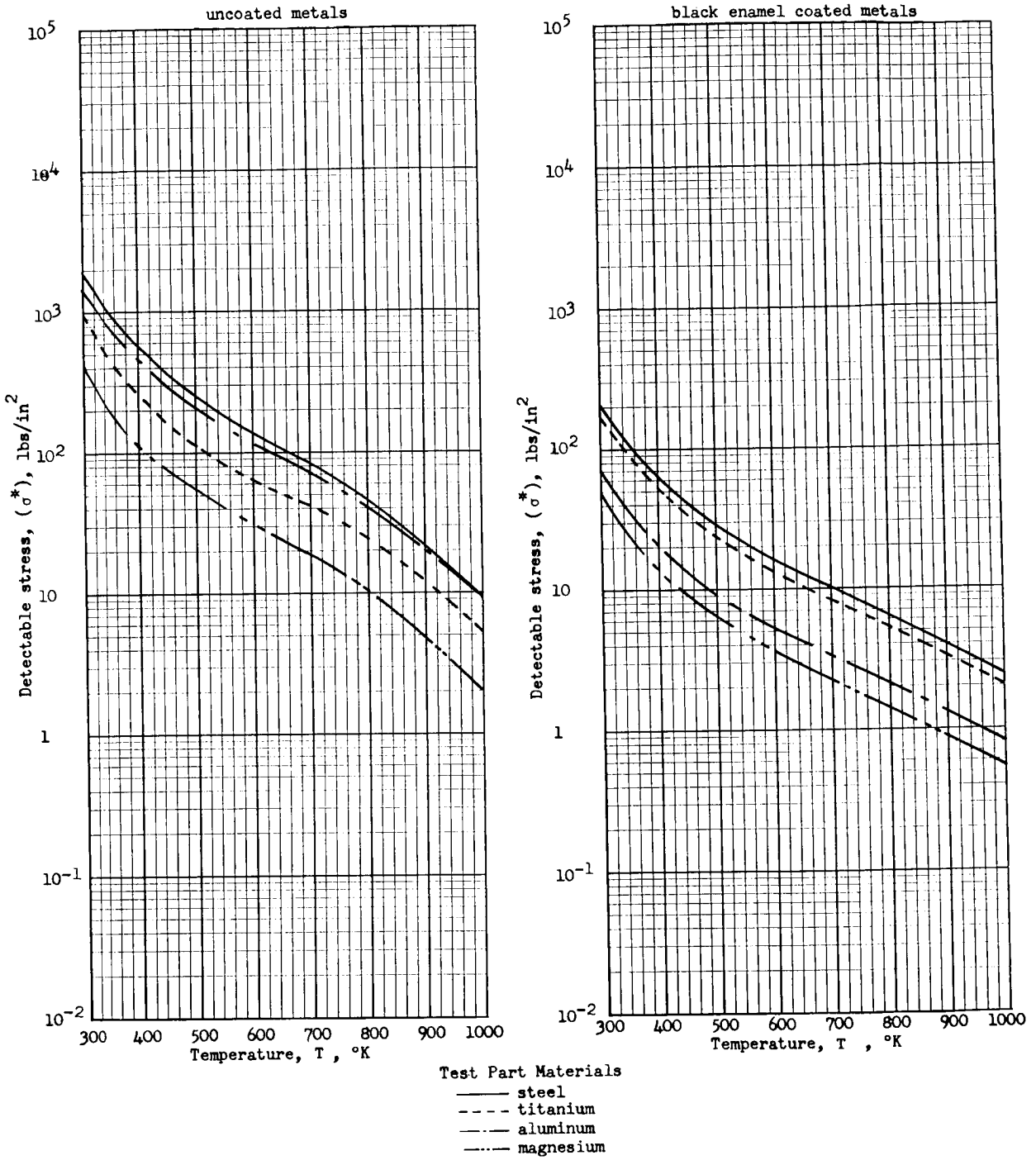

Note: Detectable stresses normalized to 1 Hz bandwidth Δf for a typical radiometer (Table V and fig. 22) with unity detector signal ratio η_d and unity test part signal ratio η_p.

(d) Mercury activated germanium detector at 28°K
Figure 23. - Continued.

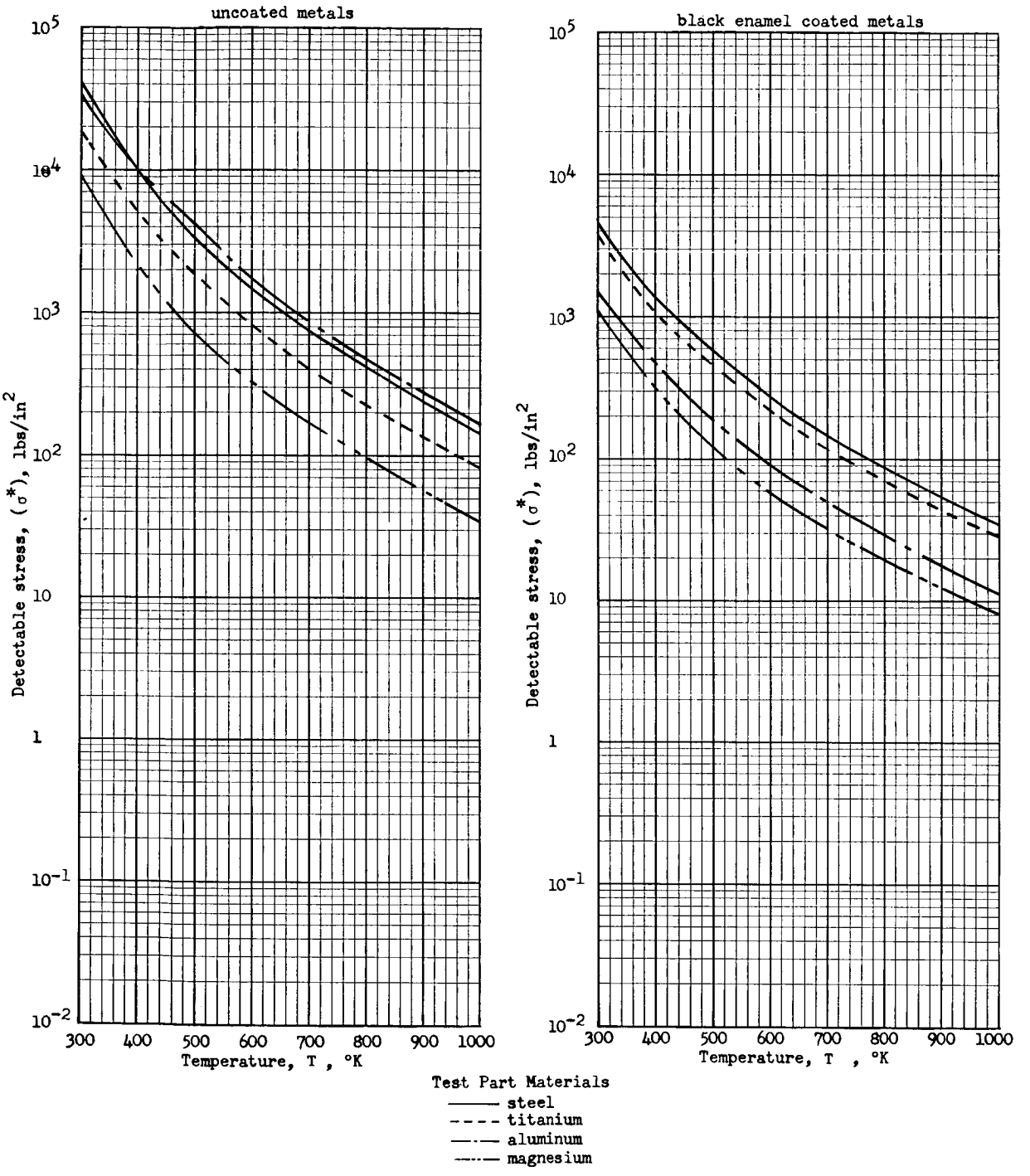

Note: Detectable stresses normalized to 1 Hz bandwidth Δf for a typical radiometer (Table V and fig. 22) with unity detector signal ratio η_d and unity test part signal ratio η_p.

(e) Unimmersed thermistor detector at 300°K
Figure 23. - Concluded.

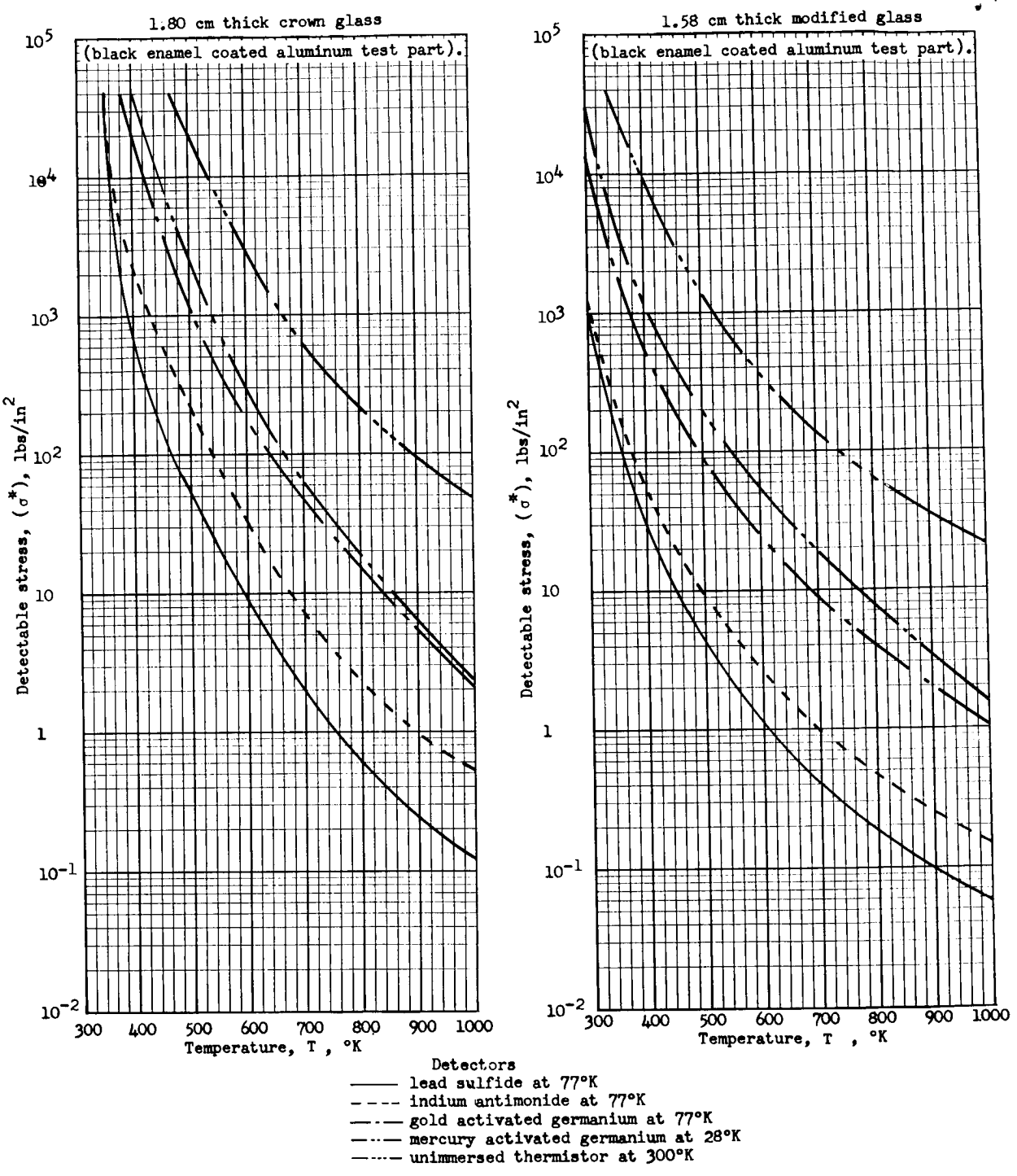

Note: Detectable stresses normalized to 1 Hz bandwidth Δf for a typical radiometer (Table V and fig. 22) with unity detector signal ratio η_d and unity test part signal ratio η_p.

(a) Glass window materials

Figure 24. - Typical window effects on infrared stress detection

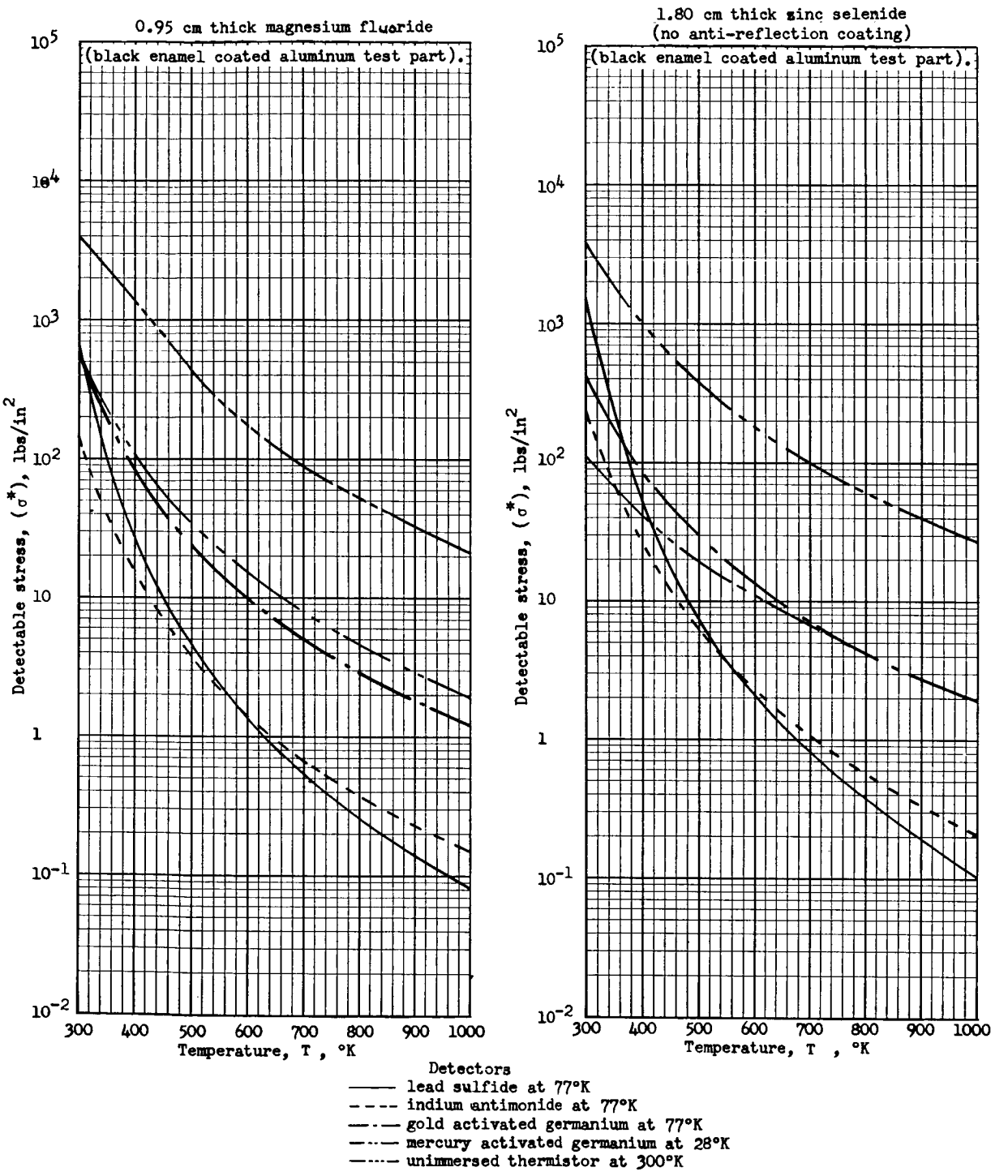

Note: Detectable stresses normalized to 1 Hz bandwidth Δf for a typical radiometer (Table V and fig. 22) with unity detector signal ratio η_d and unity test part signal ratio η_p.

(b) Infrared window materials

Figure 24. - Concluded.

approximately 130 to 580 lb/in^2 at 20 microinches per inch resolution (ref. 29). It is likely that infrared stress measurements at room temperature will be limited by other factors (such as environmental reflection effects), but accuracies of the general magnitude typical for conventional instrumentation are likely with the most sophisticated infrared techniques. Infrared stress measurements are likely to be more accurate than any conventional measurements at moderately elevated temperatures.

The detectable stresses with windows showed the basic trends in the relations between window materials, detectors, and test part temperatures (fig. 24). Ordinary optical glass (crown glass) can be used for elevated test part temperatures only, and particular detectors become practical for different temperature levels. Modified glass has somewhat less critical attenuation of lower temperature test part signals, and useful room temperature infrared stress data might sometimes be acquired through it with detectors having high response in short wave lengths. Infrared window materials would be necessary to obtain ultimate infrared stress accuracy at room temperature when windows cannot be avoided. These materials do not impose large signal transmission losses, but they are much more expensive than glasses and are limited in maximum available size. The cost and size limitations are more critical for zinc selenide than for magnesium fluoride and zinc selenide would usually be most useful for detectors with longer wave length peak response than those covered by this study (particularly if an anti-reflection coating could be used on the window). Other available materials transmitting in spectral ranges between magnesium fluoride and zinc selenide could be considered for specific applications (Appendix F).

The above radiometric limitations on infrared stress measurements were based on no signal roll-offs due to test part oscillation frequency. There are important infrared stress application range limits relative to frequency, and these can be evaluated with the technology herein (pp. 46-48). It was considered desirable to compute typical frequency ranges for coated room temperature test parts without windows (the most common test application conditions). Although higher temperature test parts would have more favorable detectable stresses (fig. 23 and 24), there would be only minor direct variations in signal roll-off frequencies with temperature. The mercury activated germanium detector at 28°K was selected for frequency roll-off analysis on the basis of its favorable response with room temperature test parts, (fig. 23). Aluminum was selected as the test part material for coating roll-off computations because it is a common structural material with a moderately high thermoelastic constant (p. 61). The factors above define detectable stresses in the absence of frequency effects for a typical radiometer (Table V) by the procedures previously discussed (p. 68)

The black enamel test part coating was selected for conductance and environmental roll-off computations on the basis of its favorable thermal response. Since these roll-offs are a function of the test part structural material properties, computations were made for various materials. For substrate conduction computations, test part thicknesses t_p of 0.1, 1, and 10 cm were selected on the basis of a typical range in which bending stresses may be significant. For lateral conductance computations, heat sink proximities x_p of 0.1, 1, and 10 were selected on the basis of a typical range which would be of interest in terms of spatial resolution of data. For environmental heat transfer computations test part thicknesses t_p of 0.01, 0.1, and 1 cm were selected on the basis of a typical range to the thinnest practical test parts (such as honeycomb sandwich facing sheets with no significant bending stresses). Heat transfer coefficients h of 10^{-3}, 10^{-2}, and 10^{-1} W/°K cm^2 were selected for the environmental computations on the basis of various typical test environments. The lowest coefficient (1.76 Btu/hr. ft^2 °F) is typical for a high emissivity test part at 300°K in a 300°K atmospheric environment without forced convection. The intermediate coefficient (17.6 Btu/hr. ft^2 °F) is typical for a high emissivity test part at 1000°K in a 300°K atmospheric environment without forced convection or of a 300°K test part in a 300°K moderate forced convection environment (such as normal atmospheric winds). The highest coefficient (176 Btu/hr ft^2°F) is typical for a test part in a relatively high forced convection environment of the same temperature (such as an atmospheric density transonic wind tunnel). With the parameters selected above, the lower frequency roll-off signal factors (C_z, C_x, and C_e) can be computed (p. 47). For lateral conduction computations, the thermal wave mode can be considered an adverse signal ratio (p. 20).

Both the black velvet and black enamel test part coatings were selected for coating roll-off computations on the basis of their different favorability aspects in test applications. Black enamel coating thicknesses of 0.3, 0.5, 0.7, and 0.9 mil were selected for computations on the basis of the range from its minimum opaque thickness to the maximum thickness likely to be required due to coating application variables. Black velvet coating thicknesses of 2, 3 and 4 mils were selected on the basis of the range from its minimum practical to its maximum probable required thickness. With the parameters selected above, the upper frequency roll-off signal factor (C_c) can be obtained (pp. 46 and 101).

A frequency range from 10^{-2} to 10^4 Hz was selected for the roll-off computations. The lower frequency (36 cycles per hour) is typical of the slowest periodic loading likely for complex structural fatigue test. The higher frequency is approximately five times the maximum frequency (2 000 Hz) normally encountered in vibration testing. The broad frequency range therefore covers all test part stress oscillation

frequencies likely to be of interest. Assigned discrete frequencies f can be combined with the frequency signal factors (identified above) to compute dimensionless frequency parameters defining emitted signal ratios η_p (p. 47). Detectable stresses σ^* can then be computed by the procedures previously discussed (p. 68).

Substrate conduction will usually impose the most critical lower frequency application range limits (fig. 25). The magnitudes of roll-off frequencies vary by a factor of approximately twenty for the various materials. The substrate conduction frequency limits are greatest for the thinnest test parts, but the bending stresses (producing substrate conduction) are usually not encountered in thin test parts. The roll-off is relatively flat, the conductance error being only ten percent at a frequency approximately two orders of magnitude less than the roll-off threshold frequency. Corrections for substrate conduction are frequently feasible (p. 16). In general, substrate conduction will frequently impose limits on structural fatigue loading tests, but will less frequently be encountered in vibration and acoustic testing.

Lateral conduction will impose considerably less severe lower frequency application range limits than substrate conduction (fig. 26). As with substrate conduction, the magnitudes of lateral conduction roll-off frequencies vary greatly for different materials. The frequency limits are greatest for radiometric fields of view in close proximity to heat sinks, but the closest proximity shown (0.1 cm) would not be of interest unless the radiometric field of view was also that small in magnitude. Lateral conduction corrections are probably feasible with an auxiliary sensor (p. 21). In general, lateral conduction will seldom impose severe test frequency limits, but it can introduce data errors perceptible only with an auxiliary sensor (p.86)

Environmental heat transfer will usually impose the least critical lower frequency application range limit (fig. 27). The magnitudes of the roll-off frequencies do not vary greatly for different materials (being different by approximately a factor of two for the metals evaluated). The frequency limits are greatest for the thinnest test parts and most severe environments. In a typical room environment, no significant roll-offs are likely to be encountered even for slow fatigue test cycling of honeycomb sandwich panels with thin facing sheets. In a wind tunnel, roll-offs could be encountered with thin skin models at frequencies of interest in flutter testing. Approximate corrections for environmental heat transfer are usually feasible (p. 24). In general, environmental heat transfer will not frequently impose important limits on infrared stress measurements.

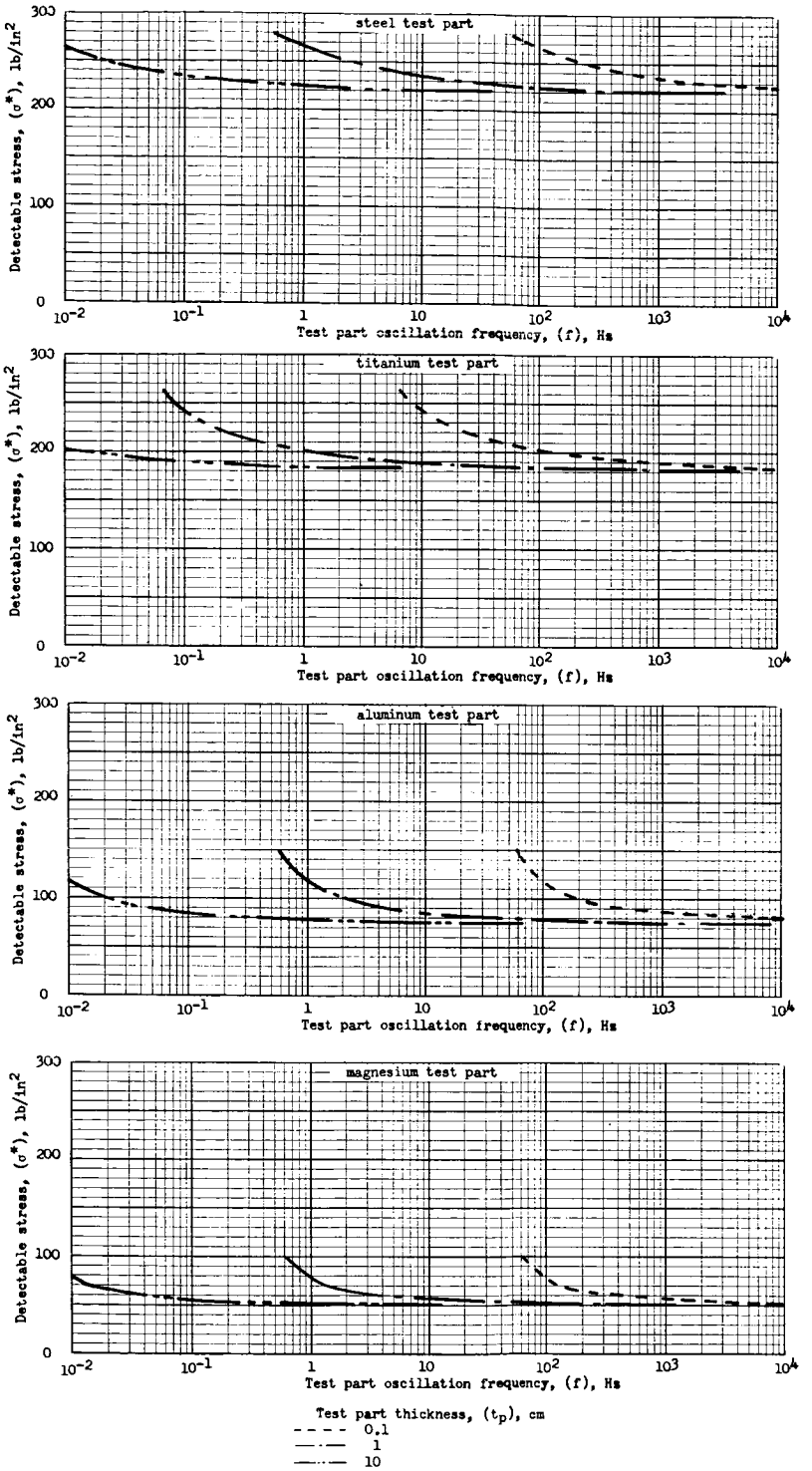

Note: Detectable stresses normalised to 1 Hz bandwidth Δf for a typical radiometer (Table V and fig. 22) with a mercury activated germanium detector at 28°K having unity detector signal ratio η_d and viewing a 300°K test part coated with black enamel, coating lag effects being omitted for clarity (fig. 28).

Figure 25. - Typical substrate conduction effects on infrared stress detection

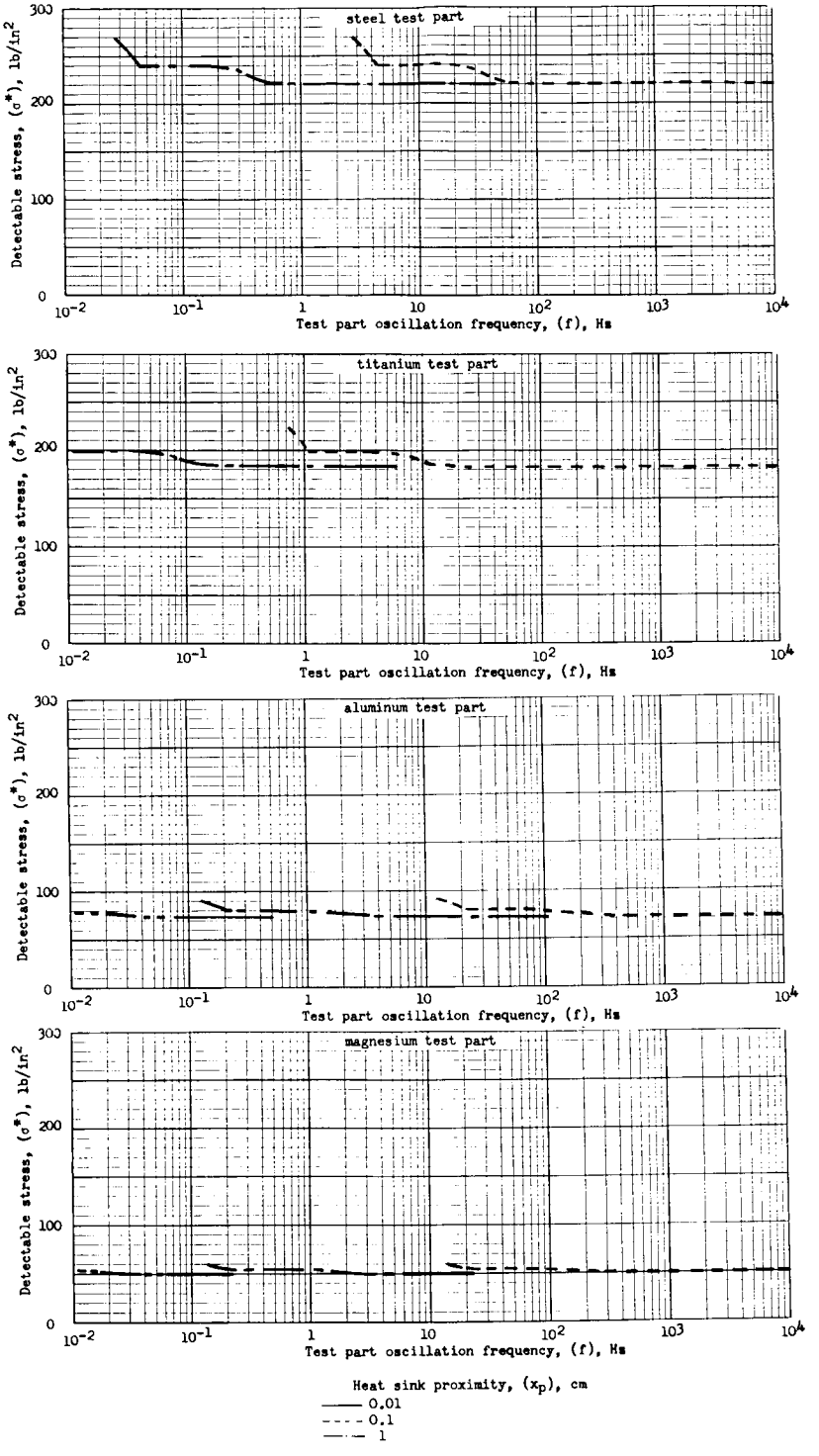

Note: Detectable stresses normalized to 1 Hz bandwidth Δf for a typical radiometer (Table V and fig. 22) with a mercury activated germanium detector at 28°K having unity detector signal ratio η_d and viewing a 300°K test part coated with black enamel, coating lag effects being omitted for clarity (fig. 28).

Figure 26. - Typical lateral conduction effects on infrared stress detection.

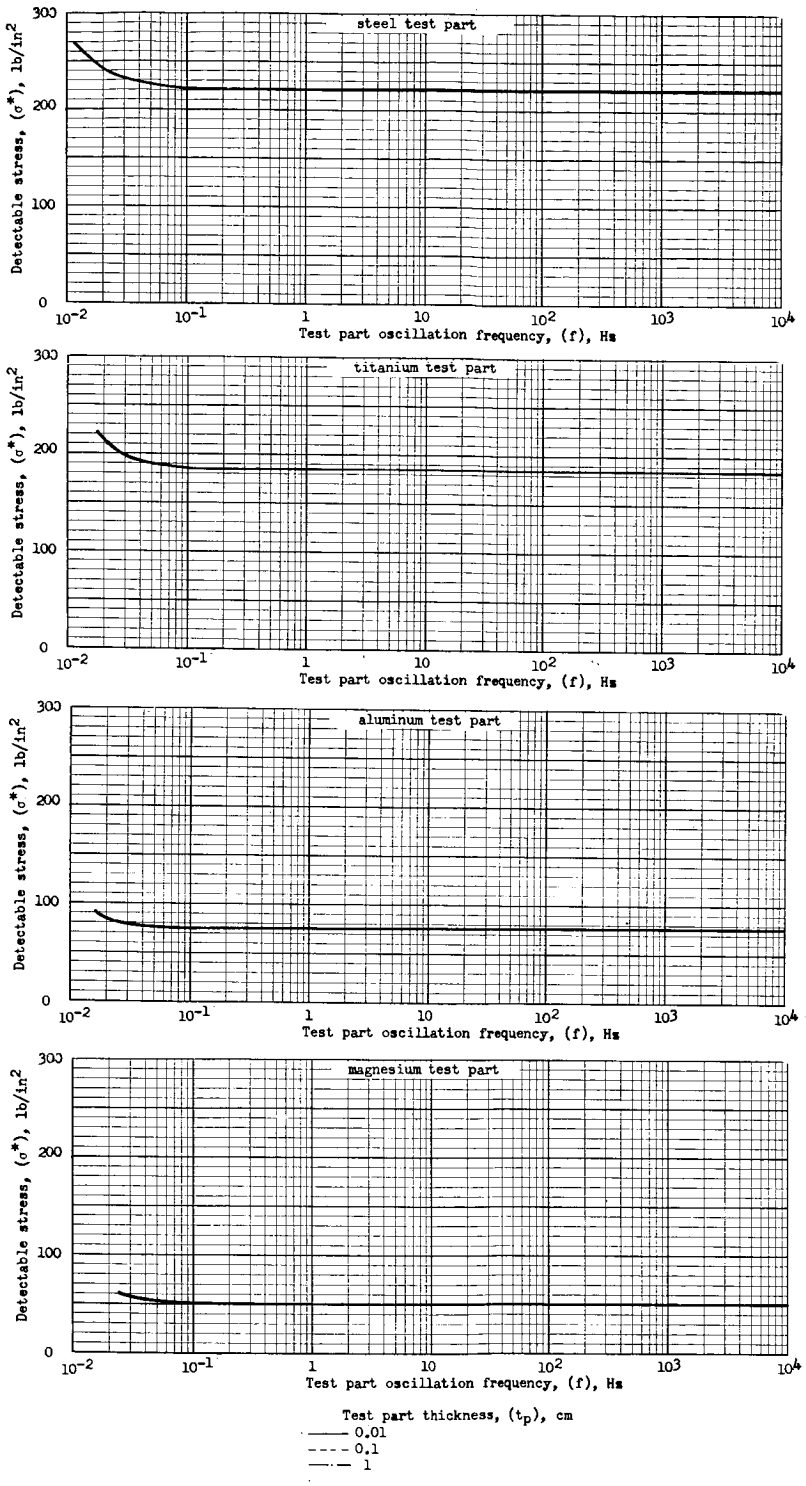

Note: Detectable stresses normalized to 1 Hz bandwidth Δf for a typical radiometer (Table V and fig. 22) with a mercury activated germanium detector at 28°K having unity detector signal ratio η_d and viewing a 300°K test part coated with black enamel, coating lag effects being omitted for clarity (fig. 28).

(a) Typical room environment

Figure 27. - Typical environmental heat transfer effects on infrared stress detection.

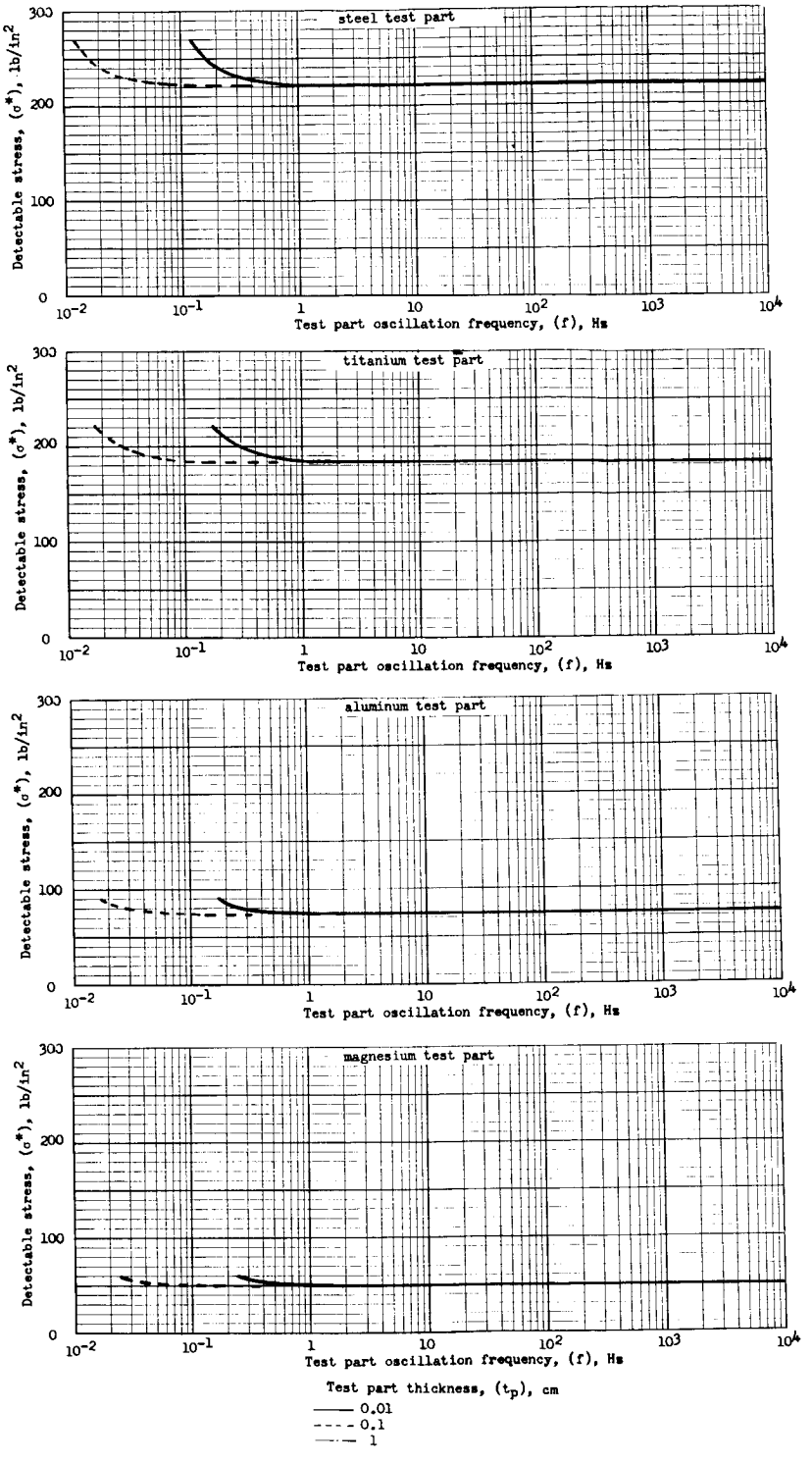

Note: Detectable stresses normalized to 1 Hz bandwidth Δf for a typical radiometer (Table V and fig. 22) with a mercury activated germanium detector at 28°K having unity detector signal ratio η_d and viewing a 300°K test part coated with black enamel, coating lag effects being omitted for clarity (fig. 28).

(b) Moderate forced convection environment
Figure 27. - Continued.

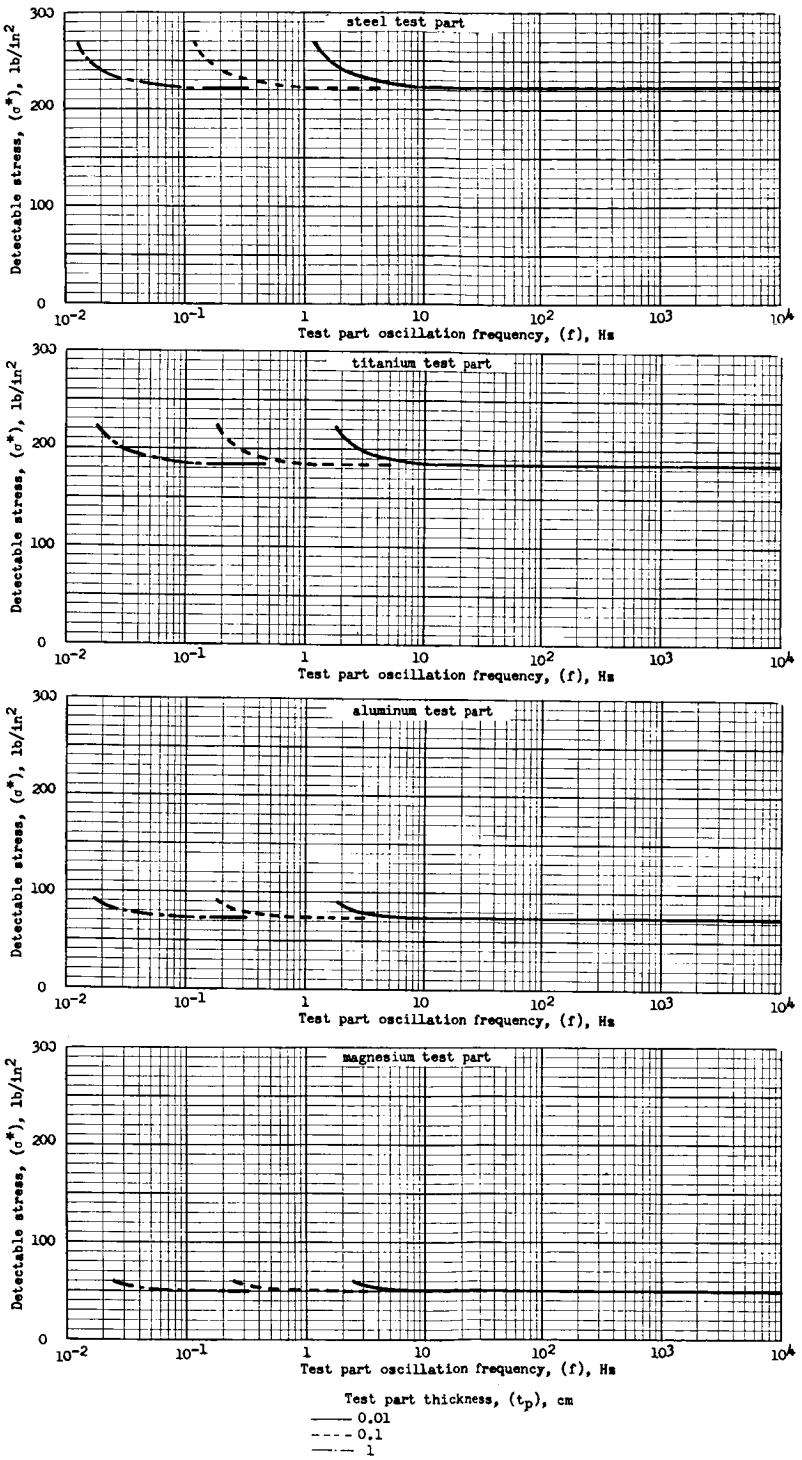

Note: Detectable stresses normalized to 1 Hz bandwidth Δf for a typical radiometer (Table V and fig. 22) with a mercury activated germanium detector at 28°K having unity detector signal ratio n_d and viewing a 300°K test part coated with black enamel, coating lag effects being omitted for clarity (fig. 28).

(c) Severe forced convection environment

Figure 27. - Concluded

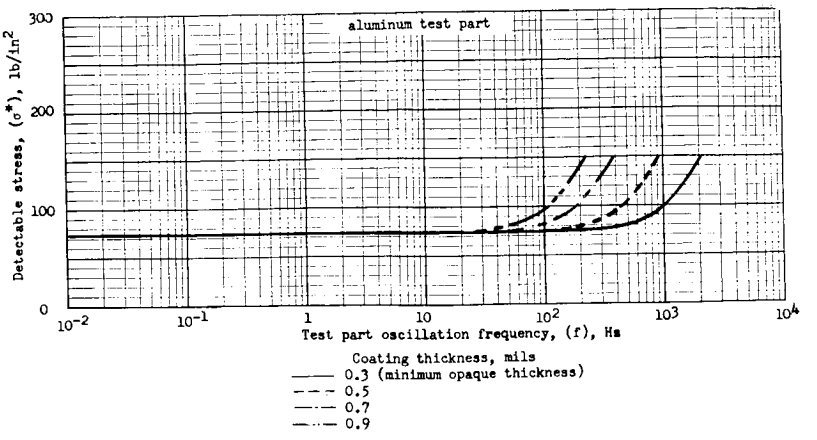

(a) Black enamel

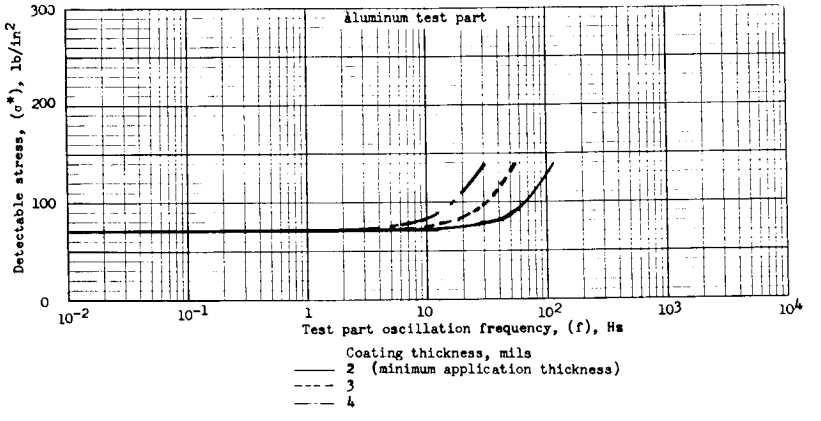

(b) Black velvet

Note: Detectable stresses normalized to 1 Hz bandwidth Δf for a typical radiometer (Table V and fig. 22) with a mercury activated germanium detector at 28°K having unity detector signal ratio n_d and viewing a 300°K coated aluminum test part, conductance and environmental effects being omitted for clarity (fig. 25, 26, and 27).

Figure 28. - Typical coating lag effects on infrared stress detection.

Coating thermal lag can impose important upper frequency application range limits (fig. 28). The roll-offs are greatly different for black velvet (which has superior radiation properties) and black enamel (which has superior thermal response). The roll-offs are usually more important in terms of data errors which could be introduced by unknown coating thicknesses than the absolute magnitudes of signal losses. Black velvet is the preferred coating when its roll-off threshold is adequately safe for the test application frequency (pp. 58-59). Black enamel is suitable for approximately one order of magnitude higher frequencies than black velvet. Corrections for coating lag are feasible when coating thickness is known (p. 26). Improved coating application and measurement techniques would be required to obtain accurate spatial infrared stress data at frequencies much greater than approximately 10 Hz (p. 85).

Recommended Future Work

High Emissivity Coating Technology - The use of coatings on test parts greatly enhance detectability levels, accuracy, and other aspects of infrared stress measurement. (See section on "Instrument System Methodology, pp. 46 and 55). Work reported herein shows that favorable frequency response can also be obtained with thin coatings of an available black enamel material. (See appendix on "Coating Response Experiments", p. 102). However, the present coating application and thickness measurement methods are not adequate for achieving thin coatings on test parts as required in the infrared stress measurement applications. Development of techniques to obtain a thin coating of uniform thickness over large surface areas is desirable. The minimum feasible thickness limits could then be evaluated for high emissivity coatings on test parts. This would define an upper frequency limitation imposed by coating thermal lag in test applications. It appears practical to measure coating thicknesses by active infrared scanning. This approach is particularly desirable for infrared stress measurement because the same radiometric instrumentation employed for stress sensing could be utilized for pre-test coating thickness measurements. Preliminary theoretical analysis (not shown herein) indicates certain favorable feasibility aspects of infrared coating thickness measurement. The initial transient response time of thin coatings is approximately one millisecond. (See appendix on "Coating Response Experiments", p. 100). This is short enough to permit practical scanning for the simple secondary (sustained) transient. The coating thermal diffusivity (and conductivity) is approximately one-tenth that of the most adverse metallic substrate (titanium), and strong infrared signatures are likely to be produced by thickness variations. Detail techniques would have to be developed for infrared thickness measurement, and they could then be applied in the coating application work. The coating research would yield improved upper frequency range limits and rapid evaluation of frequency limits for coated test parts. The proposed coating thickness measurement method is believed to be unique, and the contractor desires to retain proprietary rights to its general application in paint thickness measurement.

Suppression of Environmental Reflection - Spurious signals can be obtained from environmental reflection effects. (See section on Instrumentation System Methodology", p. 58). The spurious signals can be suppressed to some degree by high emissivity coatings on test parts and surfaces around the radiometer aperture. However, the degree of suppression is dependent on coating diffuseness as well as high coating emissivity (low reflectivity). An available black velvet coating is probably more diffuse than an available black enamel, but it also has greater thermal lag than black enamel. (See section on "Signal Emission Frequency Ranges", p. 46). Time response is not important for a coating around the radiometer aperture, and black velvet might be used there when black enamel is used on the test part (for rapid thermal response). The general aspects of environmental reflection effects are known, but the diffuseness of coatings is unknown. Specific experiments would be needed to quantitatively

define optimum techniques for suppression of environmental reflection effects. This research would yield more accurate and reliable infrared stress measurements for vibrating test parts.

Lateral Conductance Corrections - Many important infrared stress measurements applications will involve thin plates with biaxial stress fields. The lateral conduction will usually be the most important lower frequency limitation in these applications. The approximate magnitude of this limitation can be evaluated from available information. (See section on "Lateral Conduction", p. 21). However, valid lateral conduction corrections cannot be made analytically, and corrections are desirable to accurately define stresses near stress nodes, stiffeners, etc. Corrections might be made by incorporating data memory and an analog computer device in a scanning radiometer. However, such a computer would be complex, and non-scanning conduction corrections would not be obtained with this approach. More reliable corrections appear feasible by incorporating auxiliary sensing in a radiometer. The appropriate sensing would be a secondary detector with a field of view around the perifery of the primary data detector field of view. This approach is considered physically practical, and the signal correction analog computer would be simple. Further study would be required to define the specific techniques and feasible performance limits for this lateral conduction correction approach. The technique would provide automatic estimates of data accuracy (with lateral conduction) as well as the basic data corrections for important regions of test parts.

Temperature Corrections - The test part temperature has a direct effect on signal radiance. (See section on "Infrared Signal Magnitudes", p. 11). It must be known for infrared stress data reduction. Radiometric sensing of temperature is desirable to measure transients and spatial gradients without contacting sensors. An auxiliary radiometer would obviously be feasible for temperature measurement, but it is desirable to also evaluate certain techniques employing the primary radiometer. The relative accuracy required is much less for the temperature level than for the small temperature increments produced by oscillating stresses, and an auxiliary radiometric sensor may not be necessary. Quantitative evaluation of several techniques would yield definition of the method most suitable for infrared stress temperature corrections.

Calibration Techniques - The research reported herein is considered adequate to determine what test applications are suitable for infrared stress measurements, to select the most favorable measurement equipment and techniques, and to evaluate attainable data accuracy and spatial resolution in terms of test measurement ranges and primary test application factors. However, there are many secondary factors which can alter the exact relationship between the stress in a test part and the radiometric signal output during any specific infrared stress measurement. These include variations in test part thermoelastic constants and surface emissivities, infrared transmission losses, and radiometric performance

of specific instrumentation. Exact theoretical treatment of all secondary factors is impractical, and calibration will be desirable for each specific infrared stress measurement test set-up. One type of calibration can be obtained with strain gages on a highly stressed region of the test part which can be radiometrically viewed. This type of calibration would usually be desirable when strain gages can be installed on test parts because it provides an instrumentation drift check during test runs (a check of every set of spatial data with a scanning instrument). However, it may not always be possible to install strain gages on the test part, and it will usually not be practical to obtain the desired absolute calibration ranges from instrumented test parts. It is desirable to develop a device for absolute instrument calibration prior to installation of test parts. The best approach would be radiometric measurements on a specimen of the test part material being subjected known stress oscillation while at the location where the test part is to be installed. This approach would yield an absolute calibration device capable of achieving desired stress and temperature ranges with all secondary factors of the specific application present.

Signal Processing Technology - Several aspects of signal processing require evaluation to define instrument system techniques. Narrow electronic filter bands are favorable relative to signal-to-noise ratio. (See section on "Infrared Detection", p. 44). Filters can impose limits on instrument response and therefore attainable scanning speed. Optical chopping is desirable for improved signal amplification at low oscillating stress frequencies, but it can impose limits on both scanning speed and the ranges of oscillating stress over which data acquisition is feasible. The work reported herein treats sinusoidal signals only, but other wave shapes (such as multiple mode bending or panel flutter tension-tension) can be treated by harmonic analysis, electronic gate, or other methods. Evaluation of the various signal processing techniques is desirable to determine the infrared stress measurement requirements and limitations. This would yield the specific approaches for direct stress read-out instrumentation with surface scanning capabilities.

CONCLUDING SECTION

The thermoelastic effect produces nearly isentropic energy conversion, and this energy conversion is a function of changes in the sum of principal stresses within materials (p. 7). Coefficient of thermal expansion, density and specific heat are the primary material properties affecting the energy conversion, but modulus of elasticity and Poisson's ratio can introduce secondary effects which are increasingly important at elevated temperatures (p. 8). The thermoelastic constants of common structural metals (steel, titanium, aluminum, and magnesium) were measured, and were found to vary somewhat with stress increment and temperature level (p. 95). These variations are attributed to the probable unknown anistropic property effects in metals fabricated by rolling and the known isotropic effects, which include the minor theoretical variations with temperature, the variations of coefficient of expansion with temperature, and the variations of specific heat and Poisson's ratio with temperature and stress. The thermoelastic constant is of (small) significantly positive magnitude for many materials, but it is known to be negative for some materials, and it is probably insignificantly small for other materials. The thermoelastic energy conversion produces (small finite temperature increments proportional to imposed stress increments in an adiabatic element of a material with a finite thermoelastic constant (p. 7).

For an adiabatic material element subjected to oscillating stresses, the signal emitted is a function of the (peak-to-peak) stress magnitude, the thermoelastic constant, the surface emissivity, and the temperature level (p. 11). However, a material element of a test part can be considered adiabatic only when the oscillation frequency is high enough to avoid appreciable heat transfer between the element and other portions of the test part or the test part environment (pp. 16, 21, and 25). If the test part has a high emissivity coating for enhanced infrared signal emittance, the frequency must also be low enough to avoid appreciable thermal lag of the coating surface relative to the structural test part (p. 27). The non-adiabatic and coating lag effects impose unavoidable lower and upper frequency signal roll-off limitations in testing applications. The theoretical analysis for the most important lower frequency roll-off (substrate conduction) and the upper frequency roll-off (coating lag) was experimentally verified (pp. 114 and 117). Since high emissivity coatings are desirable, the thermal responses of selected coatings was measured (p. 101) so that the upper frequency signal roll-off could be quantitatively evaluated. Since thin coatings are required for rapid thermal response, the opaque thickness threshold was experimentally determined for a selected favorable coating material (p. 107). The research discussed above yielded the quantitative theoretical definition of emitted test part signals and the appropriate experimental verification.

The signal losses due to passage through air are relatively small, (p. 30). The losses due to passage through pressure barrier windows are usually significant, and window pane materials suitable for the spectral range of the emitted signals must be used (pp. 137-139). The transmission

characteristics of four diverse window pane materials were defined in terms of test facility window differential pressure and the other pertinent parameters (pp. 33 and 34). Radiometer performance depends on the collection of radiant signal energy to irradiate a detector and the conversion of radiant energy to electrical signals by the detector. The power irradiating the detector is dependent on certain geometric arrangement aspects of the optical collection system (pp. 36-37). The smaller angular fields of view yield lower signal strengths, but they are advantageous for favorable spatial resolution (small fields of view on test part surfaces). The stand-off distance (between test part and radiometer) and the required optical field depth are also factors in the spatial resolution (p. 40). Various infrared detectors have vastly different spectral responses, and signal frequency effects are also different. (pp. 121 and 122). The performance characteristics of five diversely different detectors were defined, and this was combined with the signal emission and loss analysis to evaluate a "detectable stress"(pp. 42-44). Detectable stress is the lower limit of stress oscillation likely to be detected (and the probable accuracy limit of measurements at greater stress levels).

The results discussed above were utilized to postulate a simplified instrumentation system methodology suitable for estimating the appropriate detectable stress and spatial resolution limits for any arbitrary test application requirements (pp. 46-63). Although this methodology covered only combinations of four windows and five detectors, the diverse spectral ranges of the data permit its extension to other combinations. Selected typical application ranges were defined with the methodology (pp. 66-67, 69-75, and 79-84). These data indicate that infrared stress measurement accuracies of a magnitude similar to strain gages would be feasible at room temperature, but this is for a very narrow electronic bandwidth (not generally practical), and infrared measurements may be limited by environmental reflection or other unknown effects (p. 118). Infrared stress instrumentation would be more accurate than conventional instrumentation at high temperatures (pp. 68-76). Additional research would be required to develop practical direct read-out infrared stress instrumentation (pp. 85-87).

Infrared stress measurements yield data on the sum of principal stresses. Strain gages yield data on directional tension-compression strain. Photoelastic coatings yield (most readily) data on shear strain or difference in principal strains. Combinations of these techniques could yield many (undefined) types of data not previously within the state-of-the-art. One obviously interesting combination is infrared and photoelastic, which yields complete definition of biaxial stress fields by techniques suitable for rapid spatial data acquisition.

North American Aviation, Inc.
Columbus Division
Columbus, Ohio, May 1, 1967

APPENDIX A

THERMOELASTIC EXPERIMENTS

by Milo H. Belgen and Robert K. Haning

Introduction

Various thermoelastic experiments have been reported in the literature (ref 1-5 and 30). Although these data verify the general magnitude of the thermoelastic effect, more complete data for modern structural metals were considered necessary to utilize the thermoelastic effect in structural stress instrumentation. Steel, titanium, aluminum, and magnesium were selected for testing so that a wide range of material properties would be covered. Precise measurements were desired with various magnitudes of stress increment and temperature level so that second order effects could be evaluated.

Test Specimens

Four specimens were fabricated for testing. Each specimen was 40 inches long (including end grips), and had a 0.25 x 0.40 x 35 inch (nominal) test section. The specimen cross sections were measured so that stresses could be accurately computed for known tension loads. From theoretical considerations (ref 14, pp. 266), end thermal conduction effects were known to be negligible for the selected specimen length and required test loading time periods.

Each specimen was fabricated from a different structural metal. The specific materials had different tensile yield strengths, and there were small differences in the strengths of the materials at the two planned test temperatures (Table VI).

TABLE VI.- TEST MATERIAL YIELD STRENGTHS

(from ref 28)

Materials	Yield Strength, lb/in^2	
	80°F(300°K)	200°F(367°K)
steel (AISI 4130)[a]	132 000	127 000
titanium (6Al-4V)[b]	145 000	130 000
aluminum (7075-T6)	66 000	58 000
magnesium (AZ31B-H24)	29 000	22 000

a 150 000 to 160 000 lb/in^2 heat treat
b 160 000 lb/in^2 heat treat

Test Setup

Each test specimen was successively installed in a fixture for testing. Load was applied hydraulically and measured with a calibrated load link. Pressure was provided by a small hydraulic power supply and controlled at a given level by an adjustable relief valve. The test specimen was protected from room air temperature changes by an aluminum tube wrapped with fiberglass insulation and covered with aluminum foil. A wire mesh heating element (coiled around the tube under the insulation) and infrared lamps (mounted opposite the exposed ends of the specimen) were utilized for the +200°F tests. Powerstats were used to control voltage applied to the wire heating element and lamps.

Three thermocouples were mounted on the test specimen, one at the center and one near each end. Each thermocouple was soldered to a small square of brass shim stock. A thermistor, cemented to a thin aluminum disc, was mounted on the center of the test specimen. A thin coating of high thermal conductivity compound was applied to the flat, under surface of the thermocouples and thermistor. The thermocouples and thermistor were secured to the specimen with rubber bands. The thermocouples were read out on a dial type, self-balancing temperature indicator. Thermistor resistance was measured on a 5 digit Wheatstone bridge with an electronic galvanometer.

Test Procedure

Tests were run on each specimen with loads producing 25, 50, and 75 percent of the working yield stress at approximately 80°F and at 200°F (Table VI). The specimen was considered to be temperature stabilized when the three thermocouples indicated a temperature within 1°F of each other, and thermistor drift was less than 0.005°F/min. Thermistor resistance with zero stress was noted, and the Wheatstone bridge was pre-set to the anticipated value of thermistor resistance with the specimen loaded. The needle valve at the load actuator was closed, and (with the hydraulic power supply on) the desired pressure value was set using the adjustable relief valve. The needle valve was then opened. The desired stress level was reached in approximately 3 seconds and a timer was started. A thermistor resistance reading was taken as quickly as possible (usually in 10 to 30 seconds) and the time was recorded. Time and resistance readings were taken at approximately 15 second intervals during the next 4 minutes. The load was then released to prepare for the next test run.

Data Reduction

The thermistor resistance values were converted to temperature using a calibration curve, and subtracted from the initial zero

stress temperature. These temperature increment values were plotted versus time and a curve was drawn through the points to zero time. The extrapolated value of temperature increment at zero time was used as the increment (θ) produced by the abrupt stress change (thus correcting for minor subsequent heat transfer into the insulation). The stress increment (σ) was computed from the load link reading and the measured test specimen area. The absolute temperature level (T) was computed from the average of the thermistor readings (with and without applied load). The thermoelastic constant was then computed from the relation

$$K_M = \theta/T\sigma$$

(See section on "Thermoelastic Energy Conversion", p. 7).

Test Data

The test data indicated variations of thermoelastic constants with both stress increment and temperature level (Table VII). The data scatter for repeat runs was relatively small. The maximum deviation of data from averaged values was $\pm$ 1.18% for all runs except one (magnesium at elevated temperature with the 25 percent stress increment), which had $\pm$ 2.1% scatter. Nearly half of the data was within $\pm$ 0.5% of the averaged values. The relatively small data scatter and the estimated overall accuracy of the measurements indicated that the averaged values defined consistent variations in the thermoelastic constants.

It was considered desirable to compare the measured thermoelastic constants with theoretical values computed from the material properties. The literature data on properties were found to vary significantly, particularly for three of the materials (Table VIII).

With the appropriate units conversions, the theoretical thermoelastic constants were computed from the relation

$$K_M = 100\alpha_x/\rho c_p$$

(See section on "Thermoelastic Energy Conversion", p. 8). This is applicable to stresses near zero because the material properties had been measured at zero stress.

Although the theoretical and experimental thermoelastic constants agreed relative to general magnitude, there was considerable scatter in theoretical values (fig. 29). This scatter is attributed to the cumulative errors introduced by the scatter in thermal expansion and specific heat data (Table VIII). Accurate thermal property data are usually not required for engineering design analysis, but accurate thermoelastic

TABLE VII. - THERMOELASTIC TEST DATA

Stress increment % of yield (Table V)	Thermoelastic constant, (K_M), in^2/lb			
	Individual runs		Averaged Values	
	298.75°K (±0.35°K)	367.55°K (±0.65°K)	298.75°K (±0.35°K)	367.55°K (±0.65°K)
Steel (4130)				
25	2.153×10^{-8} 2.185	2.157×10^{-8} 2.199	2.168×10^{-8}	2.178×10^{-8}
50	2.234 2.246	2.282	2.240	2.282
75	2.242	2.276 2.320	2.242	2.298
Titanium (6AL-4V)				
25	2.622×10^{-8} 2.641	2.709×10^{-8} 2.729	2.632×10^{-8}	2.719×10^{-8}
50	2.733 2.742	2.771 2.782	2.738	2.776
75	2.848 2.879 2.916	2.869 2.897	2.881	2.883
Aluminum (7075)				
25	6.404×10^{-8} 6.457 6.518	6.728×10^{-8} 6.840	6.460×10^{-8}	6.784×10^{-8}
50	6.680	6.916	6.680	6.916
75	6.768	6.859 6.943	6.768	6.901
Magnesium (AZ31B)				
25	9.724×10^{-8} 9.733	10.160×10^{-8} 10.344 10.595	9.728×10^{-8}	10.366×10^{-8}
50	9.675 9.842	9.863 9.896 10.079	9.758	9.946
75	9.495 9.587	9.776 9.823	9.541	9.800

constant data are desirable for the infrared stress instrumentation application. The experimental thermoelastic constants are considered more accurate than the theoretical computations in several ways. The measurement accuracy was greater for the thermoelastic constants than is normally attempted (or required) for thermal properties. The direct measurement of thermoelastic constants also precludes cumulative errors from several individual material property measurements.

TABLE VIII. - MATERIAL THERMOELASTIC PROPERTIES
(ref. 28 and 31)

Materials	Property Ranges		
	Expansion coefficient, in/in ^{o}F	Density lb/in^3	Specific heat $BTU/lb^{o}F$
Steel (4130)	6.3×10^{-6} 6.4	0.283	0.114 0.115
Titanium (6AL-4V)	4.6 5.2	0.160 0.162	0.135 0.135
Aluminum (7075)	12.4 12.9	0.101	0.21 0.23
Magnesium (AZ31B)	13.4 14.2	0.0639 0.064	0.234 0.25

There are considerable differences between the magnitudes of thermoelastic constants for various materials (fig. 29). This does not directly indicate comparative infrared signal strength because material strengths (and therefore normal structural design stresses) are different for the various materials (Table VI). Considering the product of thermoelastic constant and yield strength, aluminum is the most favorable of the four materials covered by this study. On the same basis, the relative infrared signals for titanium, steel and magnesium would be approximately 91, 67, and 65 percent of that for aluminum. However, there can be significant differences in the specific alloys and heat treat levels for the same basic materials. The thermoelastic signals would therefore be of the same general magnitude with the diversely different structural metals evaluated, and this implies that many other materials would also produce similar infrared stress signals.

The test data indicated variations in thermoelastic constants with both temperature and stress increment (fig. 29). The temperature variations could be due to the variations in coefficient of expansion and specific heat with temperature but available data on these properties are too limited for quantitative evaluation of this. The stress increment variations were different for the individual materials. For a tension stress increase equal to 75 percent of yield strength, the thermoelastic constant data trends were approximately 7 to 10 percent increases for steel, 9 to 14 percent increases for titanium, 3 to 6 percent increases for aluminum, and 1 to 2 percent decreases for magnesium. These trends are probably due to variations of specific heat and/or Poisson's ratio with stress. (See section on "Thermoelastic Energy Conversion", p. 9).

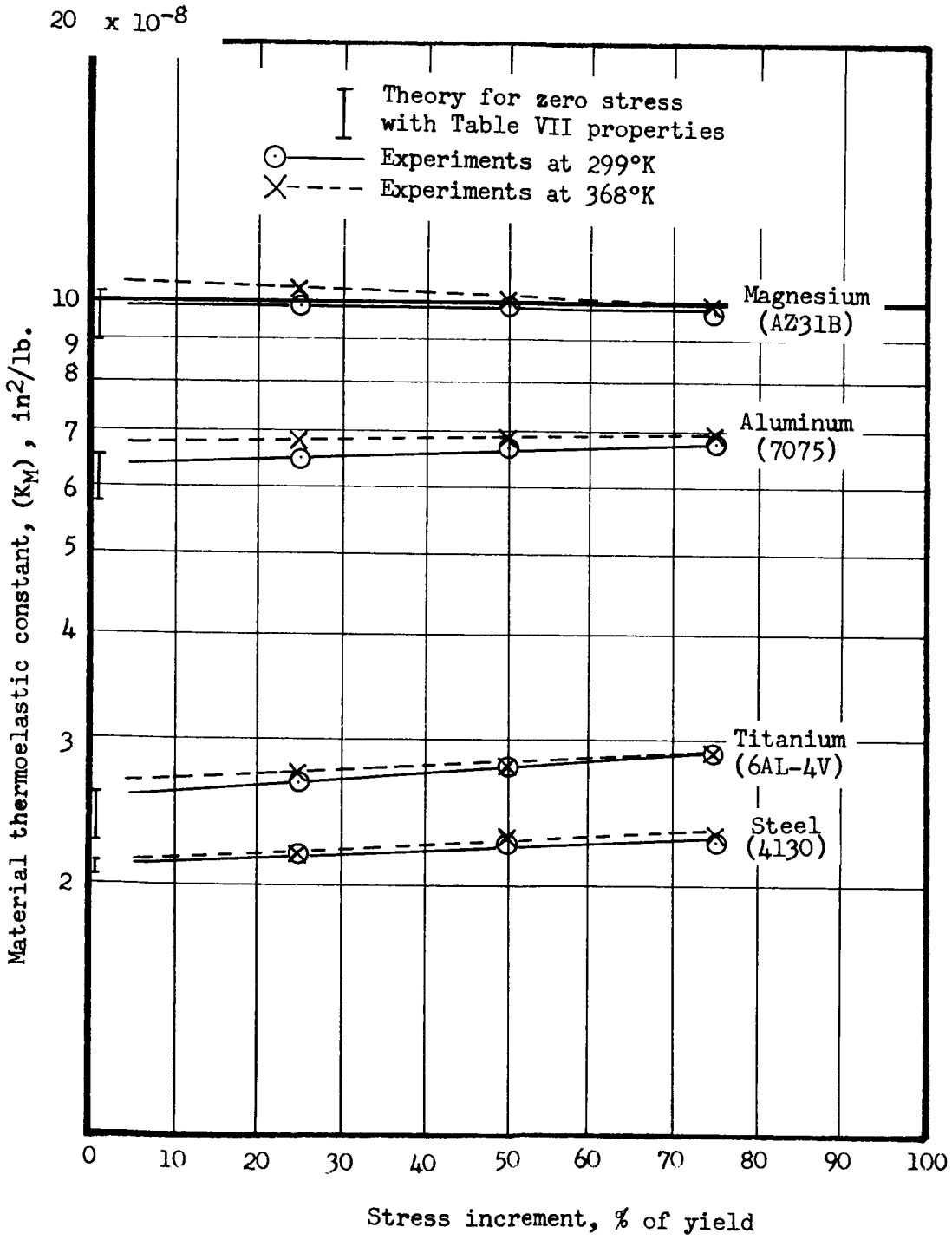

Figure 29. - Trends in thermoelastic constants for structural metals

The overall thermoelastic constant variations with stress and temperature were approximately 12.8 percent for steel, 13.4 percent for titanium, 9.0 percent for aluminum, and 3.0 percent for magnesium. These magnitudes are probably representative of the maximum variations which would be encountered for these materials in test applications with 299 to 368°K temperatures. Stresses greater than 75 percent of yield are unlikely to be required in structural test applications. Although all tests were performed with tension stress increments, there is no reason to expect different thermoelastic constants for compression stresses. When tension-compression stress oscillation is produced in a vibrating beam, some averaging effect would be expected, and this would tend to reduce thermoelastic constant variations.

Conclusions

Four diverse structural metals had thermoelastic constants which would produce similar infrared stress signal magnitudes. This indicates that infrared stress signal generation is not strongly dependent on the type of structural metal of which the test part is fabricated. It also implies that many materials would yield infrared stress signals similar to those obtained with the four materials tested.

The available thermoelastic constant data are considered adequate to evaluate infrared stress detection limits for the specific structural metals tested. (See section on "Instrument System Methodology", p. 61). Although some data corrections can be made for second order thermoelastic constant variations, specific thermoelastic calibrations are required to obtain ultimate data accuracy. (See section on "Recommended Future Work", p. 86). Materials additional to those covered in this study could be used for infrared stress measurements if practical calibration techniques were available.

APPENDIX B

COATING RESPONSE EXPERIMENTS

Introduction

Radiometric signals tend to be improved in several ways by application of high emissivity coatings to metallic test parts, but coatings may impose limitations on the useful test frequency range (See section on "Infrared Signal Magnitudes", p. 10). The frequency limitation of a coating is a function of its thermal diffusivity and its thickness squared. (See section on "Coating Thermal Response", p. 26).

Rapid thermal response is not important relative to the usual high emissivity coating applications. Because of this, no valid data were available on coating thermal diffusivities or minimum practical thicknesses, and standard high emissivity coatings were not known to have desirable combinations of emissivity and response characteristics. Coating experiments were considered necessary to define the basic coating characteristics important for the infrared stress measurement application.

The purpose of the experiments was to define the thermal response of a selected standard high emissivity coating and of several other coatings considered promising for relatively high emissivity and response. The primary data requirement was transient response characteristics of coatings. However, it was also necessary to check emissivities for non-standard coatings and thin coatings (which were not known to be opaque).

Coating Selection and Application

A specific coating was selected as representative of standard high emissivity coatings developed for high and diffuse thermal radiation over a wide wave length range. The selected coating is marketed under the trade name, "3M Black Velvet 101-C10", by the 3M Company, St. Paul, Minnesota. It has been used for many optical and infrared applications, and considerable data were available on its properties (various unpublished data, most of which was generated by the coating manufacturer). The data indicate approximately 0.92 infrared total emissivity with a relatively flat spectral distribution. The data also indicate good coating stability in common environments, including temperatures as high as 425°K. The recommended application thickness is 2 mils (or thicker), but tests of a thinner coating was considered desirable because of the possible improvement in response.

One type of coating was selected for test on the basis of its suitability for relatively high temperatures. This coating is marketed under the trade name. "Black Heat Resisting Enamel Q36K802", by Rinshed-Mason Company, Aneheim, California. It has been used to increase radiation cooling on hypersonic flight vehicles, and some unpublished data were available on its properties. The data indicate a relatively high infrared emissivity and good coating stability in common environments, including temperatures as high as 645°K.

One type of coating was selected for test on the basis of its promising aspects relative to thermal conductivity. This coating is marketed under the trade name, "Silver Conducting Paint HB0125-004", by North American Aviation, Inc., Columbus, Ohio. It has been used in applications requiring conductance of electrical current, and this indicated that its thermal conductivity would be higher than that of dielectric coatings. The coating is stable in common environments, including temperatures as high as 395°K. It was considered desirable to test both the standard formulation of this coating and a formulation with the addition of ten percent by weight of carbon black (for increased emissivity).

Based on early test results, a coating of high graphite content was added to the experiment. It was prepared by mixing 35 percent graphite (No. 2 medium powdered flakes, Joseph Dixon Crucible Co., Jersey City, New Jersey) with 65 percent acrylic (A-10 acrylic resin, Hanna Paint Mfg. Co., Columbus, Ohio) by weight, and adding thinner (MIL-T-6094) as required for spray application consistency.

All test coatings were applied by spraying and allowing them to air dry. Because of the non-standard coating compositions, the reliability of standard paint thickness meters was unknown, and it was decided to use direct physical measurements. The specific technique was a dial indicator with a spherical faced probe supported on a flat table. All known procedures for precision of this type of measurement were carried out (checks on table flatness, indicator hysteresis, probe curvature, indicator spring loading, data repeatability, etc.). With these procedures, the accuracy of coating thickness measurements was estimated to be $\pm$ 0.1 mil (or better).

Test Procedure

Aluminum (7075) was selected as the test substrate material because its low emissivity was suitable for indicating non-opaque coating effects on emissivity. The substrate specimen consisted of

a strip with 0.02 inch thickness, 0.25 inch width, and 36 inch length. The ends of the specimen were supported by a fixture incorporating a spring to keep the strip flat with a small axial tension load. Test coatings were applied as 0.25 inch square spots in the central one-third of the specimen length so that thermal conduction to the ends of the specimen would be negligible.

An electrical power supply was connected to the ends of the specimen so that it could be heated by passing electrical current through the aluminum strip coating substrate. The power supply had capacitors which could be pre-charged and then discharged to produce rapid specimen heating for transient response tests. The particular capacitor circuit had a primary power pulse duration of 0.0002 second, followed by minor current oscillation (of minor total power) for an additional 0.0007 second. The power supply could also be operated continously without the capacitors to obtain steady-state moderately elevated temperatures for emissivity tests.

An infrared radiometer system was mounted in a manner suitable for viewing of the specimen coating spots. The radiometer optics were of the Cassegrain telescope type with an eight inch diameter primary mirror. The radiometer detector was of the germanium immersed thermistor bolometer type with a one milliradian field of view (nominal for the specific optics). The radiometer was located 78 inches from the specimen so that the nominal field of view on the specimen was a 0.078 inch square, and all minor peripheral radiometric response was within an area smaller than the 0.25 inch square coating spots. Transient thermal response data were recorded by a photographic oscilloscope connected to the bolometer preamplifier (with no radiation signal chopping or electronic filtering). Steady-state emissivity data were recorded from a suitable root-mean-square meter connected to the instrument system output (with the system integral 200 Hz radiation signal chopping and narrow band electronic filtering). The equivalent observed radiometer noise was 0.8°K (peak-to-peak) during transient tests and 0.02°K (root-mean square) during steady-state tests.

Thermal response test runs were carried out by focusing the radiometer on a selected coating spot, allowing the specimen to stabilize at room temperature, discharging the electrical power supply capacitor (to produce a rapid 10°K increase os substrate temperature), and recording data during the surface temperature transient (with automatic oscilloscope triggering by the electrical pulse). Thermal response data reduction was carried out with a procedure correcting for the finite response time of the radiometer detector. The substrate temperature transient was assumed to be a step function (neglecting the minor effects of the actual transient

during the short duration period of electrical heating). Various values were assigned for the coating signal ratio parameter C_c (See section on "Coating Thermal Response", p. 26), and the coating surface temperature ratio versus time was computer for each assigned value (ref. 14, p. 266). The detector time constant (known to be 0.0010 second from a radiation chopping calibration) was applied to compute radiometer signal ratio versus time for each assigned value of C_c. The computed data were plotted to form a family of transient signal ratio curves with the coating characteristic C_c as the discrete variable. The observed test signal ratios were plotted on the same graph, and were found to define curves with the same shapes as the computed data (as should be the case for valid test and data reduction procedures). Test values of the coating characteristic C_c were obtained by interpolation of the test plots relative to adjacent computed plots for discrete values of C_c.

Thermal emissivity test runs were carried out by installing themocouples and thermal insulation on the back of the specimen, adjustment the electrical current flow through it to obtain 367 ± 1°K steady-state temperature, focusing the radiometer on a selected coating spot, and recording data (average rms radiometer signal). More accurate emissivity tests were planned for promising coatings. (See section on "Spectral Reflectivity Experiments", p.103). Simplified data reduction procedures were employed for the preliminary screening test data. The emissivity of a selected standard coating spot was estimated to be 0.92 from literature data (See section on "Coating Selection and Application", p.97). Signal increments for other coating spots were applied with the known radiometer constants to computed emissivity increments. No corrections were made for increments of environmental reflection from coating spots (known to be small for the specific test conditions).

Test Data

There was considerable scatter in the test data, particularly the transient data (fig. 30). This was attributed primarily to uncertainties in coating spot thicknesses arising both from the known measurement accuracy limitations and unknown thickness variations over individual coating spots. The transient data plots were shown at the slope known from theoretical considerations, with a relatively heavy weighting assigned to the thicker coating data (expected to be the most accurate). The total emissivity plots were shown with the data point trends but these trends are not considered definitive, and more valid emissivity data were obtained for selected coatings. (See section on "Spectral Reflectivity Experiments," p. 107).

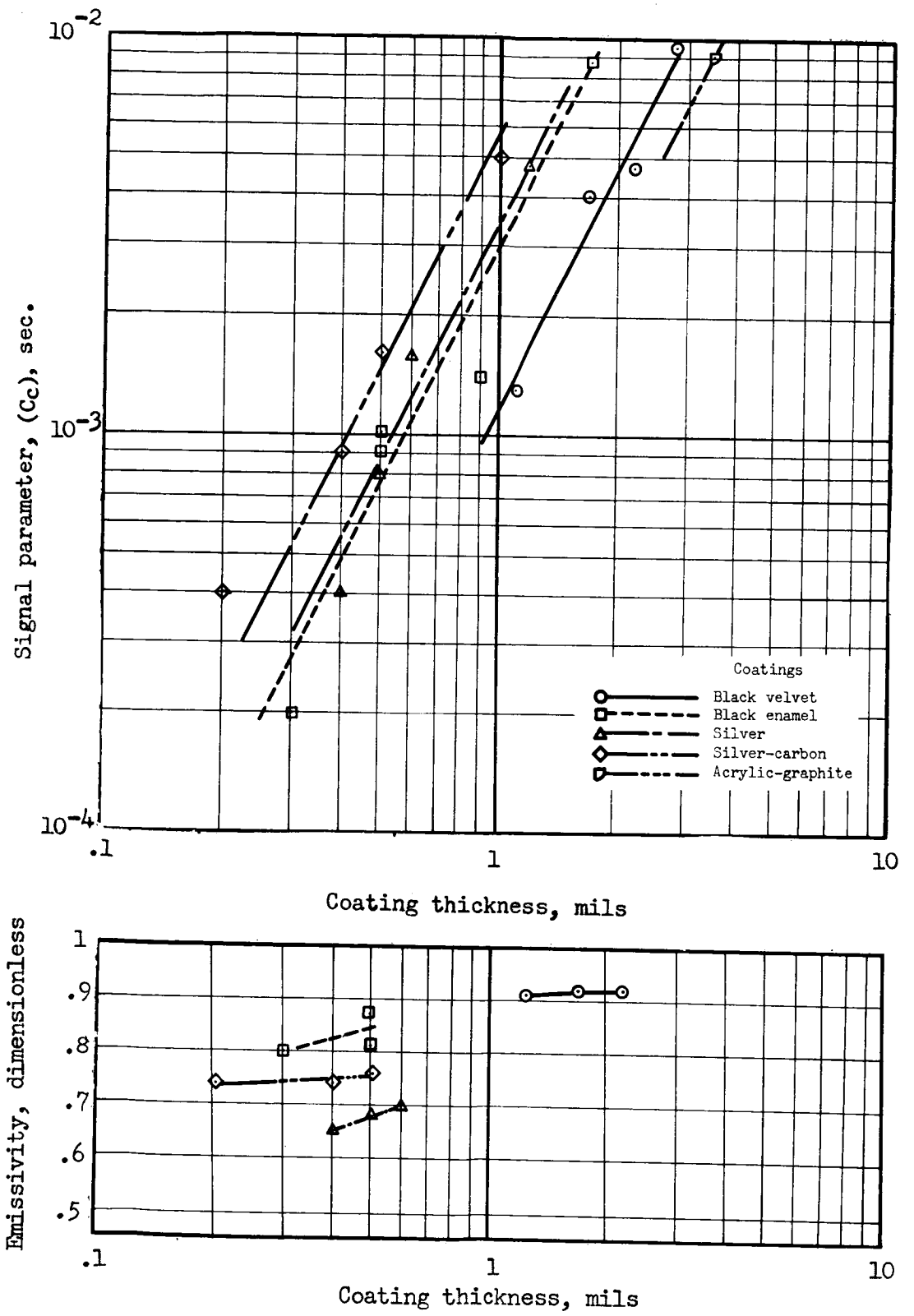

Figure 30. - Transient response and thermal emissivity for various coatings

The standard high emissivity coating (black velvet) had relatively favorable thermal response properties, but it was found to be unsuitable for application in thin layers. Although the 1.1 mil test spot retained high emissivity, it had visible voids exposing the substrate. Additional attempts to produce thin layers with this material indicated that approximately 2 mils thickness is necessary for reliable uniformity over extended coating surface areas. On this basis, a minimum coating thermal response signal parameter of 0.0046 second was considered applicable for black velvet (2 mils thick).

Although the black enamel coating had less favorable thermal response and emissivity properties than the standard coating, it was suitable for application in thin layers. Because of this, a coating thermal response signal parameter range of 0.00027 to 0.00107 second was considered applicable for black enamel (with the 0.3 to 0.6 thickness range of threshold thermal emissivity effects).

The silver base coatings were less favorable than black enamel in both response and emissivity. Although these coatings undoubtedly had higher thermal conductivity than any others tested, they apparently had lower thermal diffusivity.

The acrylic-graphite coating had more favorable (higher) thermal diffusivity than any other coating tested, but it was found impractical to apply in thin layers.

Conclusions

It appears likely that additional research would yield a coating with high emissivity and diffusivity which could be applied in thin layers. Based on the available data, it is believed such a coating could give a tenfold increase of the upper frequency ranges presently feasible (with the black enamel coating). However, the black enamel currently has the advantages of proven favorable thermal response and known suitability for elevated temperatures and other common environments

Coatings for infrared stress measurements must be uniform over large test part surface areas (See section on "Coating Thermal Response", p. 27). Research on coating application and thickness measurement is presently considered more important than development of better coatings (See section on "Recommended Future Work", p.58). The black enamel is considered the best coating available for the rapid response, but the black velvet is probably the best coating for suppression of environmental reflection effects. (See section on "Instrumentation System Methodology," p. 58)

APPENDIX C

SPECTRAL REFLECTIVITY EXPERIMENTS

by Milo H. Belgen and Robert K. Haning

Introduction

The strength of infrared stress signals is directly proportional to test part surface emissivity (See section on "Infrared Signal Magnitudes), p. 10). High emissivity coatings can improve signal strength and other aspects of infrared stress measurements, but coating thermal lag also imposes upper frequency testing limitations (See section on "Signal Emission Frequency Ranges", p. 48). It is desirable to use thin coatings for minimum thermal lag, but surface emissivity can be degraded when coatings are too thin to be opaque (See section on "Coating Response Experiments", p. 101).

Some literature data were available on emissivity of metals and coatings. It was considered necessary to supplement these data with experiments, particularly for the thin coatings most important to infrared stress measurements. An available black enamel was selected as the test coating material because of its favorable thermal response. The purpose of the analysis and experiments was to define spectral emissivities of uncoated and coated metals (including the black enamel thickness of threshold emissivity degradation due to non-opaque coating effects).

Test Specimens

Sixteen specimens were fabricated from four structural metals in the form of disks of approximately 0.98 inch diameter and 0.043 inch thickness. The faces of the specimens were polished to obtain flat smooth surfaces without oxide films. Specimens of three metals were selected for testing without coatings to supplement the available literature data on metals. The remaining thirteen specimens were used as the substrates for coated metal tests.

All coating work was done with a material marketed under the trade name, "Black Heat Resisting Enamel Q36K802", by Rinshed-Mason Company, Aneheim, California. Coating spray application techniques were evaluated with axilliary aluminum specimens which were cross sectioned for microscopic examination of coating thickness uniformity. Specific techniques of mixture thinning, spray gun control and number of passes were found to yield the approximate coating thicknesses desired with relatively small thickness variations over the areas required for small specimens. The observed thickness variations were found to exist primarily at the edges

TABLE IX. - SPECTRAL REFLECTANCE TEST SPECIMENS

Substrate Material	Coating thickness, mils	
	Central region[a]	Face average[b]
Aluminum (7075)	0.27 0.35 0.58 0.80 0.93 1.23 1.53	0.13 0.29 0.52 0.73 0.75 1.21 1.59
Magnesium (AZ31B)	0[c] 0.21 0.61	0[c] 0.11 0.71
Titanium (6AL-4V)	0[c] 0.20 0.64	0[c] 0.28 0.75
Steel (4130)	0[c] 0.23 0.66	0[c] 0.30 0.80

a Electronic micrometer measurements for central 1/4 inch diameter areas of specimens.

b Volume measurements of an accuracy limited by non-uniform coating thicknesses.

c Uncoated metallic specimens.

of the specimens and in the direction of spray gun motion. The effect of these variations on the data were suppressed (as discussed below) to the degree feasible.

Before coating application, the thickness of each specimen was measured with an electronic micrometer (10^{-5} inch precision), and the volume of each specimen was measured by the water bouyancy weight increment method with a precision scale. Coatings were then applied with a spray gun motion direction defined by an edge indexing mark on the back of each specimen. The desired approximate coating thicknesses were achieved by repeating pre-determined application techniques (discussed above). After coating application, the thickness and volume of each

specimen was again measured. The change in specimen thickness was considered a direct indication of the coating thickness in the central (1/4 inch diameter) area of a specimen. The change in specimen volume was considered an indication of average coating thickness over the entire coated face area of a specimen.

The two methods of coating thickness measurement agreed within 0.1 mil for most of the specimens, and disagreed a maximum 0.18 mil for any one specimen (Table IX). The degree of agreement between central region and face average thicknesses were considered an indication that specimen coatings were relatively uniform. However, the central region (micrometer) measurements were selected as more accurate than the face average (volume) measurements for spectral reflectivity data analysis. The reflectivity instrumentation field of view is a rectangular spot 1/2 inch long (as discussed below), and the known coating non-uniformities at the edges of specimens (discussed above) would not affect reflectivity data. The central region thicknesses were therefore considered more accurate than the average thicknesses. Although the precision of the electronic micrometer was 10^{-5} inches, the absolute accuracy of coating thickness measurements was estimated to be ± 0.05 mil on the basis of several possible sources of cumulative errors.

Test Procedure

The specimen thermal radiation property measurements were made by the heated cavity (Gier-Dunkle hohlraum) reflectometer method (ref. 31, pp. 970-971). For this method the specimen is mounted flush with the inside wall of a heated cavity. The specimen is water cooled on the back side so that it remains at room temperature. A relative radiometric signal is measured by viewing the specimen and an adjacent region of the heated cavity wall with a spectrometer. Since the heated cavity wall is known to be a diffuse radiator material with relatively small specimen and viewing port areas, the wall radiation is representative of total radiant energy incident on the specimen. Since the specimen is water cooled in a heated cavity, its emitted radiant energy is relatively small, and the radiation from the specimen is representative of the incident radiant energy reflected by the specimen. The relative signal is therefore dependent on the specimen reflectivity. During these particular tests, the specimen mounting was for an angle of spectrometer viewing perpendicular to the specimen surface.

The spectrometer used for the test was a type in common usage for the near infrared wave length range (Perkin-Elmer Corporation Model 13U). Considering the heated cavity temperature limit and the spectrometer wave length response characteristics, the test set-up would yield best accuracy in a 2 to 15 micron range, but would also yield (less accurate) data in the 15 to 25 micron range. The spectrometer was operated in its automatic slow spectral scan mode so that no significant instrument time response errors would occur.

With the specific test arrangement, the spectrometer field of view on the specimens was a rectangular spot 1/2 inch long. This spot was located at the center of the specimens, and its width was varied during spectral scans to produce optimum radiant signal energy for the spectrometer. Since there were known small coating thickness variations in the direction of spray gun application motion (discussed above), specimens were mounted with an orientation tending to suppress the effects of these variations on reflectivity data. Specimen indexing marks were positioned opposite one end of the rectangular field of view. With this orientation the spot width variations during spectral scans were in the direction of the most uniform coating thickness.

Data Reduction

Although emissivity is the property most important for infrared stress measurements, reflectivity experiments were performed to enhance the test accuracy, particularly for the high emissivity coatings considered most important. Emissivity values were computed by subtracting the observed test reflectivity values from unity. The results of these test observations and computations are commonly considered normal emissivity, but this is known to be only approximately correct for several reasons (ref. 32).

The uncoated metal literature data (ref. 33 and 34) were reported as measured emissivities. The black velvet literature data (ref. 35) were reported as emissivities computed from reflectivity tests (as discussed above).

All data were smoothed to eliminate minor spectral variations which would impair presentation clarity. This did not exclude any maximums or minimums, and it did not alter data over more than 0.5 micron wave length ranges.

Test Results

The thinnest black enamel coatings tested were not opaque at the longest wave lengths (Table X and fig. 31). Based on these data, the opaque thickness threhold for black enamel was estimated to be 0.3 mil. The ±0.05 mil uncertainity in coating thicknesses (discussed above) would not significantly alter the estimated threshold, especially since observed non-opaque effects were small in the 0.2 to 0.3 mil thickness range. The above conclusions were qualitatively confirmed by minor non-opaque effects observed with a 0.15 mil thick coating during vibrating beam tests (See section on "Infrared Stress Measurement Experiments", pp. 112-114)

TABLE X. - BLACK ENAMEL OPAQUE THICKNESS THRESHOLDS

Symbol (fig.31)	Coating Thickness, mils	Substrate material
Opaque Coating Thicknesses		
1	0.35 to 1.53 0.61 to 0.66	aluminum steel, titanium, and magnesium
Non-opaque Coating Thicknesses		
2	0.27	aluminum
3	0.23	steel
4	0.20 to 0.21	titanium and magnesium

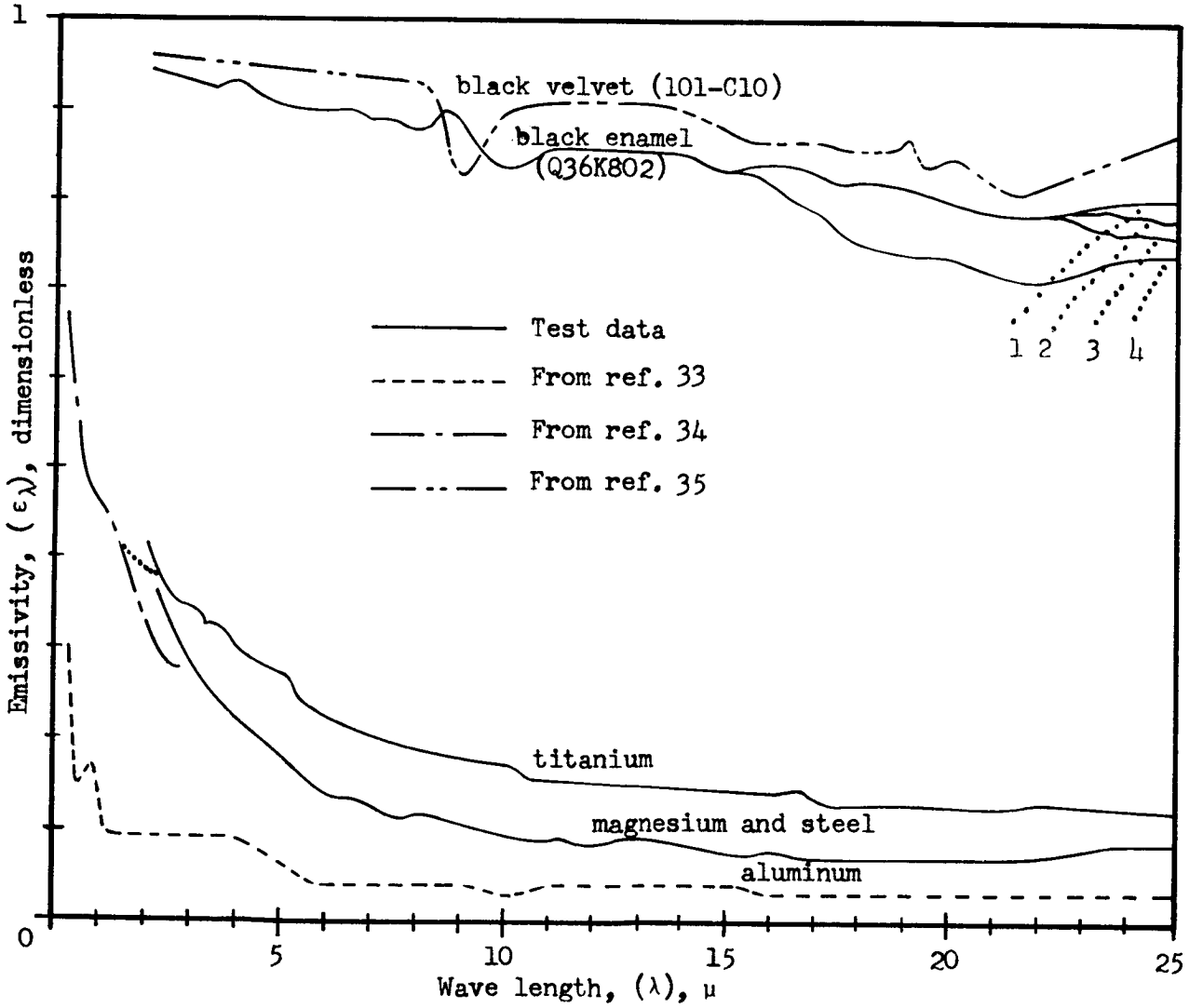

Figure 31.- Spectral emissivity of uncoated and coated structural metals

The emissivities of both coatings evaluated are much greater than uncoated structural metals (fig. 31). The data shown are for polished metals, and metallic emissivities increase with roughness, oxidiation, and other factors. However, these emissivity increases have limited usefulness for infrared stress measurements because they are not usually uniform or of known magnitude. Metals with heavy surface oxide usually have high emissivities, but heavy oxide coatings can cause thermal lag errors in high frequency signals.

Conclusions

The emissivities of structural metals can be increased with coatings. An available black enamel coating is opaque in thicknesses greater than 0.3 mil, and faster thermal response can be obtained with it than with an available black velvet coating. (See section on "Coating Response Experiments", p.101). However, black velvet has slightly higher emissivity and is probably more effective than black enamel relative to suppression of environmental reflection effects. (See section on "Instrumentation System Methodology, p. 48).

APPENDIX D

INFRARED STRESS MEASUREMENT EXPERIMENTS

Introduction

Four types of frequency roll-offs can be encountered with infrared stress test parts. (See section on "Signal Emission Frequency Ranges", p. 47). The most important lower frequency roll-off is caused by substrate conduction with test parts subjected to bending deformations. The only upper frequency roll-off is caused by coating thermal lag with test parts having high emissivity coatings for improved radiation signal emission.

Theoretical relations have been defined for the conductance and coating frequency roll-offs. (See section on "Test Part Signal Generation", pp. 12-17 and 26-27). The transient response characteristics of coatings have been experimentally evaluated. (See section "Coating Response Experiments", pp. 97-102). It was considered desirable to perform infrared stress measurement experiments with vibrating test parts so that validity of the theoretical relations could be checked.

Test Parts

Three beams with uniform rectangular cross sections were fabricated from aluminum (7075-T6). The specific cross sections were approximately 3 x 4, 3/8 x 1, and 0.08 x 1 inch sizes. The length of each beam was selected so that it could be clamped in a fixture and vibrated as a cantilever at approximately 20 to 30 Hg in a resonant mode practical for the specific beam thickness. The first bending mode was used for the thickest beam, and the second bending mode was used for the two thinner beams.

Portions of beams which would have relatively high and uniform stress oscillation during vibration were selected as test instrumentation areas. The area near the beam root was selected for the thickest beam (first bending mode). Although a stress gradient would exist along the beam in this area, it was considered negligible for the small (0.1 inch) measurement areas on the long (64 inch) beam. An area approximately equally distant from the beam root and tip was selected for each of the thinner beams (second bending mode). Since the selected location is a stress node (maximum) region, there would be no significant stress gradients in this area.

Beam thicknesses were measured with micrometers at the selected test instrumentation areas. High emissivity coatings were then applied to one face of each beam at the selected areas. An available black

enamel coating material was used because of its favorable thermal response and known opaque thickness threshold (Appendix B and C). The specific material is marketed under the trade name, "Black Heat Resisting Enamel Q36K802", by Rinshed-Mason Company, Aneheim, California. Coating spots of five different discrete thicknesses were applied at the same distance from the root of the thick beam. Micrometer measurements of the beam were made after coating application, and the thickness increments (0.15, 0.80, 1.20, 1.50, and 2.20 mils) were recorded as coating thicknesses for this beam. Although the coating thickness data were rounded only to the $\pm$0.05 mil apparent measurement precision, the accuracy of the data was estimated to be approximately $\pm$0.2 mil because of several sources of cumulative errors (not discussed herein). A single coating spot was similarly applied and measured on each thin beam. These measurements indicated coating thicknesses of 0.35 and 0.40 mils, and the data were estimated to be accurate to $\pm$0.1 mil because more favorable techniques (not discussed herein) could be used for the thin beams.

A strain gage and thermocouple was installed on each beam. Each of these sensors was at the same distance from the beam root as the coating spot (or spots), but was on the opposite face of the beam. The strain gages had beam root-to-tip alignment in conformance with the unidirectional stresses which would be produced by vibration. The strain gage on the thinnest beam was calibrated by weight loading so that curvature effects with the finite gage thickness would be included in data reduction. Since the curvature correction was small (approximately 3 percent) for the thinnest beam, no such calibrations or corrections were made for the other two beams.

Test Procedure

Each of the three beams was successively clamped horizontally in a rigid fixture with an unsupported projecting length suitable for the desired natural frequency and vibration mode (discussed above). An electromagnetic shaker (of a size suitable for each beam) was mounted behind the beam and near its root so that relatively high resonant motions and stresses could be obtained. The thin beam motion modes were visually observed with vibration, and their lengths were adjusted so that there was no significant angular oscillation movement at coating spots during substrate conduction test runs. There was angular movement of the coating spots near the root of the thick beam during test runs, but it was considered too small to affect test data.

An infrared radiometer system was mounted in a manner suitable for viewing beam coating spots perpendicular to their surface. The radiometer optics were of the Cassegrain telescope type with an eight inch diameter primary mirror. The radiometer detector was of the germanium

immersed thermistor bolometer type with a one milliradian field of view (nominal for the specific optics). The radiometer was located 100 inches from the beam so that the nominal field of view on the beam was a 0.1 inch square, and all minor peripheral radiometric response was within an area smaller than the 0.5 inch square coating spots (even with the maximum de-focusing movement of the thin beams). The internal optical chopper of the radiometer was disconnected and locked in its open position. The output of the bolometer preamplifier was connected to a 3.5 Hz bandwidth noise filter (wave analyzer). Prior to vibrating beam tests, the radiometer system (including the noise filter) was checked with an external optical chopper to verify flat signal response in the 20 to 30 Hz frequency range.

Strain gages and thermocouples were connected to conventional read-out instruments suitable for indicating the instantaneous oscillating strain magnitude and frequency and the average instantaneous temperature level of the beam surface opposite the coating spots. Radiometric noise was checked (without vibration) before and after each vibration test run, and it was found to remain constant (0.3 millivolts signal output noise). All vibration test data were recorded at steady-state conditions.

Coating lag roll-off test runs were performed by sequentially viewing each of the five coating spots on the thick beam. The shaker power was carefully adjusted to obtain the same strain gage signal output during each of these runs. With this procedure, the accuracy of attaining the same stress magnitude at all coating spots was favorable for excluding two known possible sources of error. Repeating stresses for individual runs would be dependent on instrument precision (rather than absolute accuracy), and minor variations of thermoelastic constants with stress would not effect data reduction accuracy.

Substrate conduction roll-off test runs were performed sequentially on the three beams of different thicknesses. Data were recorded at various arbitrary stress levels during these runs. The 0.80 mil coating spot only was used for these runs on the thick beam (for reasons discussed below).

Some qualitative checks were made for reflected environmental radiation effects with the thinnest (0.198 cm) beam. The beam was moved outward in its mounting clamp approximately six inches. This longer beam was vibrated in its second natural mode and the beam motion at the coating spot was observed visually. As expected from the vibration mode shape, the coating surface was then found to be undergoing an oscillating rotary motion of significant magnitude (approximately ± 5 deg. at 20 000 lb/in^2 peak-to-peak stress). The radiometer was moved to a position opposite the spot in its new location so that its viewing angle was perpendicular to the coating surface when the beam was not vibrating. With

this arrangement, the rotary beam surface movement during vibration caused the location of its primary environmental reflection environment to oscillate well beyond the sides of the radiometer aperture. Environmental reflection increments were then produced by placing materials of relatively high and/or low emissivity on each side of the radiometer. The results were observed qualitatively as radiometric signal increments at a constant stress oscillation level (approximately 20 000 $lb/in.^2$).

Data Reduction

All strain gage data were reduced to stress (peak-to-peak) by conventional methods. An elastic modulus of 10^7 lb/in^2 was used for this data reduction (ref. 28).

All radiometric signals were corrected by subtraction of the observed 0.3 millivolt noise before reporting herein as observed radiometer signals. The signals were further corrected (as shown herein) to equivalent 300°K signals. These corrections were made with the assumption that signals vary as the fourth power of absolute temperature, which is exactly correct only for a thermal detector with completely flat spectral response (ref. 5). The test radiometer had a germanium immersion lense, which alters the flatness of its spectral response. However, the relatively small corrections for minor deviations of test temperatures from 300°K were considered valid to improve overall test data accuracy.

Coating lag and substrate conduction signal roll-off parameters were computed with the assumption of unity signal ratio for the 0.80 mil thick coating spot on the 7.62 cm thick beam. The original basis for this data reduction was the assumption that the theoretical roll-off analysis was correct. However, the relatively small signal ratio changes observed for adjacent test data points indicated that the assumption was approximately correct (as discussed below).

Test Results

The test data indicated a small signal loss for the thinnest coating and signal losses increasing with thickness for the other coatings (Table XI and XII).

The test data for coatings thicker than 0.80 mil agreed fairly well with the theory (fig. 32). The scatter of these data was attributed to the estimated ± 0.2 mil uncertainty in the measured coating thicknesses (discussed above). The slight signal loss for the thinnest (0.15 mil) coating was attributed to non-opaque effects on its surface emissivity which would not be expected for the 0.80 mil coating. (See section on "Spectral Reflectivity Experiments", p. 106). The small difference between the signal ratios for the two thinnest coatings indicated that the 0.80 mil coating lag was small, and its signal ratio was approximately unity as assumed for data reduction.

Table XI.- COATING LAG TEST DATA

Strain gage indication, (σ) lb/in^2	Vibration frequency, (f) H_z	Coating thickness, mils	Radiometer output signal, mV	Beam temperature, ^oF
22700	21.2	0.15	4.1	80
		0.80	4.2	80
		1.20	3.9	80
		1.50	3.7	78
		2.20	3.2	78

Table XII.- COATING LAG SIGNAL ROLL-OFF PARAMETERS

Frequency Parameters			Radiometer Signal Parameters	
Coating Thickness	Coating factor, (C_c), sec[a]	Frequency parameter ($C_c f$) dimensionless	Corrected signal (σ=22 700 lb/in^2) mV[b]	Signal ratio, (η_c) Dimensionless
0.15	6.8×10^{-5}	0.0014	4.10	0.98[d]
0.80	1.90×10^{-3}	0.040	4.20	1.00[c]
1.20	4.3×10^{-3}	0.091	3.90	0.93[d]
1.50	6.7×10^{-3}	0.142	3.76	0.90[d]
2.20	1.45×10^{-2}	0.308	3.26	0.77[d]

[a] From fig. 30, p. 101 for black enamel coating.

[b] Corrected to equivalent 300°K signal.

[c] Assumed to be unity for ($C_c f$) of 0.040 as shown in fig. 5, p. 26.

[d] Computed from signal ratios relative to the 0.80 mil coating signal.

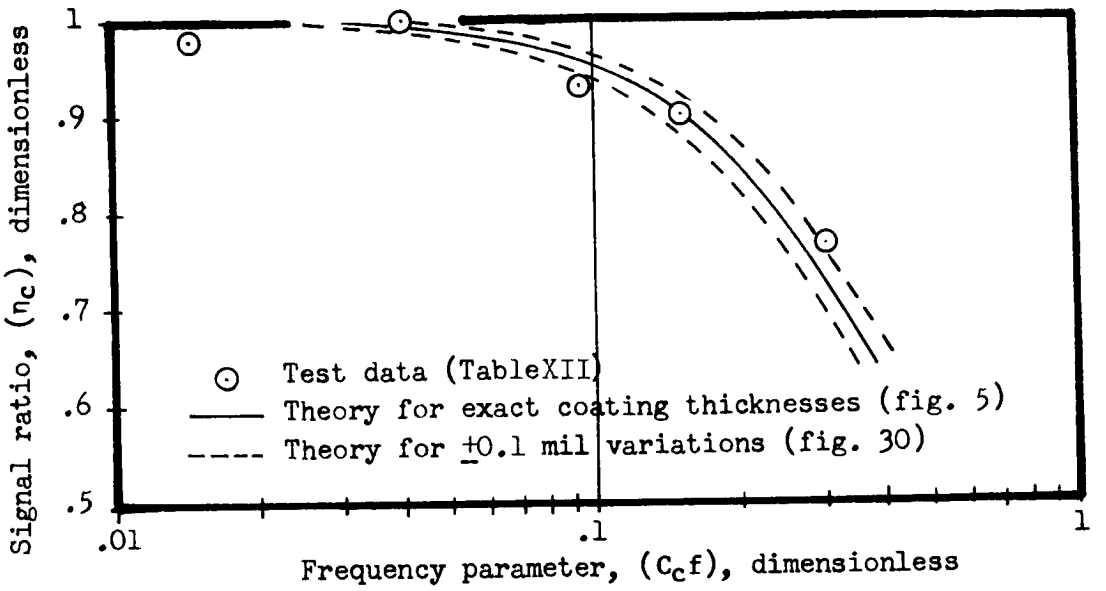

Figure 32.- Test and theoretical coating lag signal roll-offs

If the thickness of the coating on a test part is known, the frequency threshold of coating lag signal roll-off can be accurately predicted to assure reliability of test data acquired at lower frequencies. If the coating thickness is known exactly enough, data corrections for coating lag could be made for test frequencies as much as ten times the roll-off threshold. However, the signal ratio variations for ±0.1 mil coating thickness variations (fig. 32) show the importance of exact thickness in such corrections. Conventional coating thickness measurement techniques are not suitable for rapid measurements on large surface areas with thin coatings.

The coating lag roll-off tests verified the validity of assuming that coating lag would not affect signals from the two thinner beams for substrate conduction testing. The thickest of these coatings was 0.40 ±0.1 mils, and its maximum coating response factor C_c would therefore be 0.00048 seconds. (See section on "Coating Response Experiments", p. 101). At the 26.6 Hz maximum test frequency (shown below), the coating frequency parameter $C_c f$ would be 0.0128. This is below the roll-off threshold by a factor of more than two (fig. 32). The third beam coating was 0.35 ±0.1 mil thick, and would be less critical relative to thermal response. It was also known to be thick enough to be essentially opaque. (See section on "Spectral Reflectivity Experiments, p. 107).

The substrate conduction test data indicated increasing signal losses with decreasing beam thicknesses (Table XIII and XIV). The scatter in radiometric signal data was approximately the same magnitude as the observed 0.3 millivolt radiometer noise (fig. 33), and this was considered the primary source of data scatter.

TABLE XIII - SUBSTRATE CONDUCTION TEST DATA

Beam Thickness (t_p), cm	Vibration frequency, (f), Hz	Strain gage indication, (σ), lb/in^2	Radiometer output signal, mV	Beam temperature, ^oF
7.62	21.2	5 440	0.8	74
		13 530	2.0	74
		22 700	4.2	80
		30 150	5.2	81
0.950	25.8	16 320	2.3	70
		29 900	4.3	70
		43 500	6.4	72
0.198	26.6	10 350	0.9	72
		20 650	2.1	72
		31 000	2.9	73

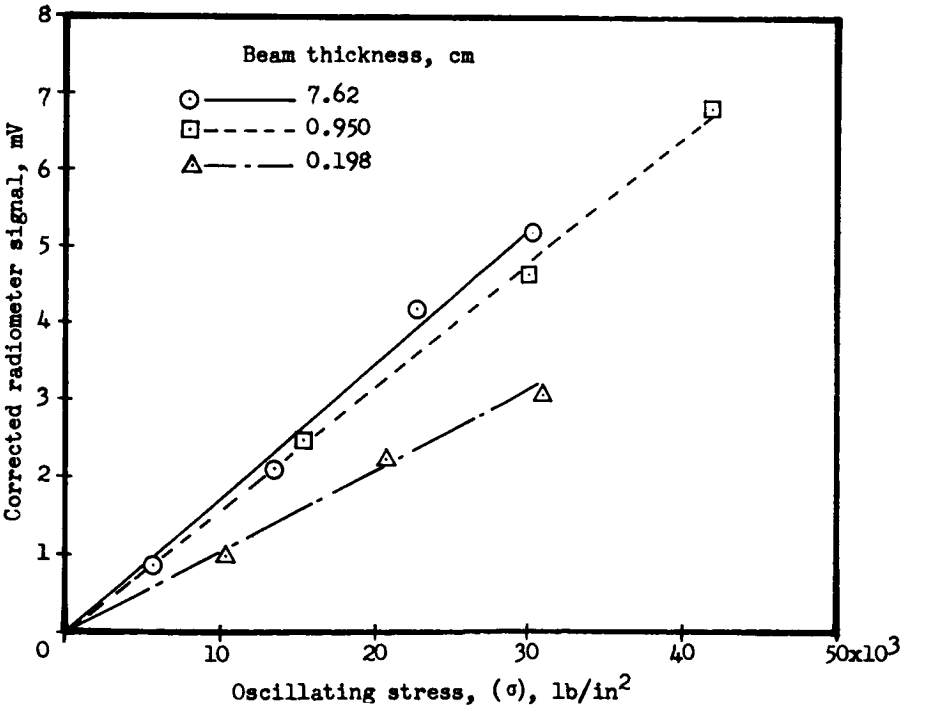

Figure 33.- Radiometer signals for various beam thicknesses

Table XIV. - Substrate Conduction Signal Roll-Off Parameters

Beam Thickness, (t_p) cm	Frequency Parameters		Radiometer Signal Parameters		
	Conduction factor (C_z) sec^a	Frequency parameter, (C_zf) dimensionless	Oscillating stress (σ) lb/in^2	Corrected signal mV^b	Signal ratio, $(\sigma=25\ 000\ lb/in^2)$ dimensionless
7.62	118.5	2510	5 440 13 530 22 700 25 000 30 150	0.84 2.09 4.20 4.37[c] 5.16	1.00[d]
0.950	1.842	47.6	16 320 25 000 29 900 43 500	2.48 4.02[c] 4.64 6.80	0.91[e]
0.198	0.0800	2.13	10 350 20 650 25 000 31 000	0.96 2.23 2.63[c] 3.06	0.61[e]

a Computed from relation $C_z = t_p^2/\alpha_p$ for $\alpha_p = 0.49\ cm^2/sec$ as shown in fig. 15 and Table II, pp. 46-47

b Corrected to equivalent 300°K signal.

c From fig. 33 for 25000 lb/in^2 stress.

d Assumed to be 1.00 for C_zf of 2510 as shown (approximately) in fig. 2, p. 16.

e Computed from 25,000 lb/in^2 signal ratios relative to the 7.62 cm thick beam signal.

The substrate conduction test data agreed fairly well with the theory (fig. 34). There was a relatively small difference (9 percent) in signal ratios for the two thickest beams with almost two orders of magnitude difference in the frequency parameter. This indicated that the substrate conduction was small for the thickest beam, and its signal ratio was approximately unity as assumed for data reduction.

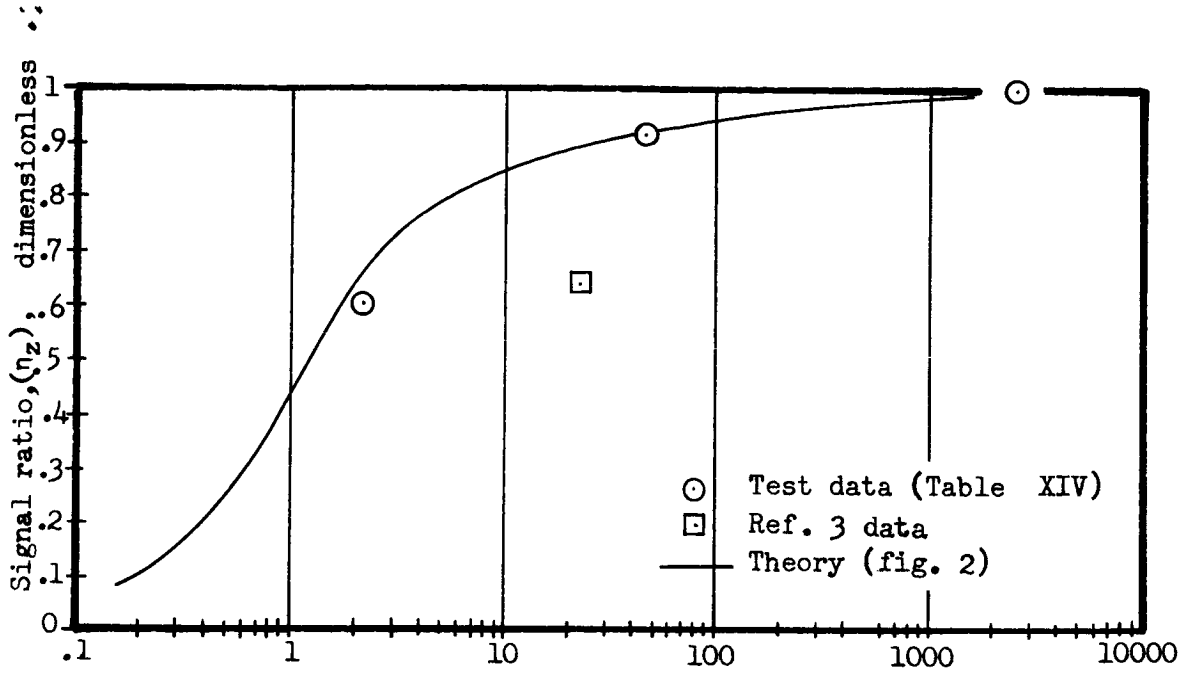

Figure 34.- Test and theoretical substrate conduction signal roll-offs.

The deviation of the thinnest beam data point from theory (fig. 34) appears to be only partially due to radiometric measurement inaccuracy. Since measurement errors were believed to be negligible for beam thicknes, stress oscillation frequency, and stress magnitude (from strain gages), the probable major cause of the deviation is a beam material thermal diffusivity different from the handbook value used for data reduction. Although the actual location of the intermediate data point indicates a similar diffusivity difference, the estimated overall test accuracy was not sufficient to define this in the relatively flat roll-off range. The agreement of radiometric data with theory is considered reasonable in terms of the estimated test accuracy and expected material property uncertainties.

Data reported in the literature (ref. 3) did not agree with the theory (fig. 34). These data had been obtained from tests of a vibrating beam with thermocouples attached to its surface. Although thermocouple response checks had indicated that adverse instrumentation lag would not be obtained, it appears that some subtle instrumentation response effect could have been encountered. No source of major errors has been identified for the radiometric data reported herein, and these data are more extensive than previously reported. The radiometric data are therefore considered the most reliable and an adequate check of the theory.

The 0.80 mil coating on the thickest beam yielded a signal of approximately 1.76×10^{-4} mV per lb/in^2 (fig. 33). The observed 0.3 mV radiometer noise therefore indicated a detectable stress σ^* of 1700 lb/in^2. This can be compared with detectable stress computed from the known test application factors. The selected data point was for no signal losses by coating lag or substrate conduction (as discussed above). It was also known that there were no other signal roll-offs (pp. 46-47), and η_p was therefore unity. The data were for a 300°K test part with no windows, and the spectral integral for an unimmersed thermistor under these conditions would be 1.3×10^7 $\sqrt{\text{Hz}}$/cm sr (pp. 49 and 54). However, the test detector had a germanium immersion lense, and a typical threefold increase in detectivity from this would indicate a spectral integral $V'_{\lambda r}/\epsilon_\lambda$ of 3.9×10^7 $\sqrt{\text{Hz}}$/cm sr for the test detector. The black enamel coating on the test part surface has an emissivity $\bar{\epsilon}_\lambda$ of approximately 0.87 for a signal in the 5 to 15 micron spectral range of the 300°K signal (pp. 11 and 55). The spectral integral parameter $V_{\lambda r}$ would therefore be 3.73×10^7 $\sqrt{\text{Hz}}$/cm sr (pp. 49). The actual radiometric field of view was 1 mrad, but the typical effect of the immersion lense would yield an equivalent unimmersed field of view ϕ_o of 0.5 mrad (p. 55). The radiometer focal length f_o was 30.4 cm (12 in.), and these factors define a geometric optical function K_o of 1.4×10^{-6} sr/cm (p. 56). The radiometer optical efficiency η_o was estimated to be 0.5. The aperture diameter D_o was 20.3 cm (8 in.). The above factors define an optical gain parameter ($\eta_o K_o D_o^2$) of 2.89×10^{-4} sr cm (p. 56). The detector time constant was 1 msec, and the detectivity ratio η_d would be 1.38 for the 21.2 Hz test frequency (p. 60). The test noise filter band Δf was 3.5 Hz. The test beam material was aluminum which would have a thermoelastic constant K_M of 6.65×10^{-8} in^2/lb (p. 61). The above factors would indicate a detectable stress σ^* of 1800 lb/in^2 (p. 61). This agrees fairly well with the 1700 lb/in^2 detectable stress indicated by the observed radiometer noise.

Reflected environmental radiation checks (carried out as discussed above) showed that suprious signals could be produced by non-uniform radiation environments near the radiometer aperture. No spurious effects were observed from the normal uncontrolled room background (factory type room without air conditioning and containing a diverse distant background of walls and objects). However, placement of a polished aluminum sheet (low emissivity) adjacent to one side of the radiometer produced approximately 30 percent radiometric signal increase. With black optical cloth draped three feet beyond both sides of the radiometer aperture, no spurious signals were observed for several arbitrary placement locations of the aluminum sheet. No attempt was made to quantitatively measure environmental reflection effects, but a uniform radiation environment around the radiometer aperture appeared to suppress spurious signals.

Conclusions

Coating thermal lag signal roll-off tests confirmed the validity of the theoretical analysis. Coating lag can cause significant errors in high frequency infrared stress measurements. Improved techniques for coating application and thickness measurement are required to obtain ultimate reliability, accuracy, and frequency ranges with infrared stress measurements. (See section on "Recommended Future Work", p. 85).

Substrate conduction signal roll-off tests confirmed the validity of the theoretical analysis.

The observed radiometer noise was in fairly good agreement with the detectable stress computed by the methods developed during the research reported herein. (See section on "Instrumentation System Methodology", pp. 46-63).

Reflected environmental radiation can produce spurious signals when test part motion and stress oscillation is at the same frequency. High emissivity coatings on the test part and around the radiometer aperture tend to suppress these spurious signals, but the quantitative effects of environmental reflection on infrared stress signals are not presently known. Additional research on this is required to assure ultimate accuracy and reliability of infrared stress data. (See section on "Recommended Future Work", p. 85).

APPENDIX E

INFRARED DETECTOR ANALYSIS

by J. A. Daily

Introduction

Infrared stress detection and spatial resolution limits are dependent on the type of infrared detector utilized in the radiometer (See section on "Optical Collection", pp. 37-38 and "Infrared Detection", pp. 42-43). Six different detectors are discussed herein, and their basic parameters and diverse spectral response, which affect the design and performance of the radiometer, are reviewed.

Detector Performance Parameters

Assuming that the radiometer performance is detector limited, its sensitivity is inversely proportional to the detector's specific detectivity. Thus large values of specific detectivity are desirable, but these values vary in magnitude and spectral response depending on the detector material, mode of operation, operating temperature, and field of view. The spectral response curves (fig. 35) depict the specific detectivity of the six detectors operating with a 180 deg. field of view.

Also of prime importance to the design and performance of the radiometer, is the detector frequency response (fig. 36) and noise spectra (fig. 37). Table XV includes most of the basic parameters of the chosen detectors and is included for ease in rapid comparison of the detectors (ref. 13, 15, 36, 37 and 38).

Detector Comparison

Thermistor Bolometer - The thermistor bolometer has found wide application in the detection of infrared from low temperature objects (long wavelength operation), one of the principal applications being in radiometers. The thermistor bolometer differs from the rest of the detectors being studied in that it is a thermal detector rather than a photon detector. Although the thermistor flake is a voltage biased semiconductor, the term "thermistor" denotes "thermally sensitive resistor". Incident radiation physically warms the thermistor flake changing its resistance

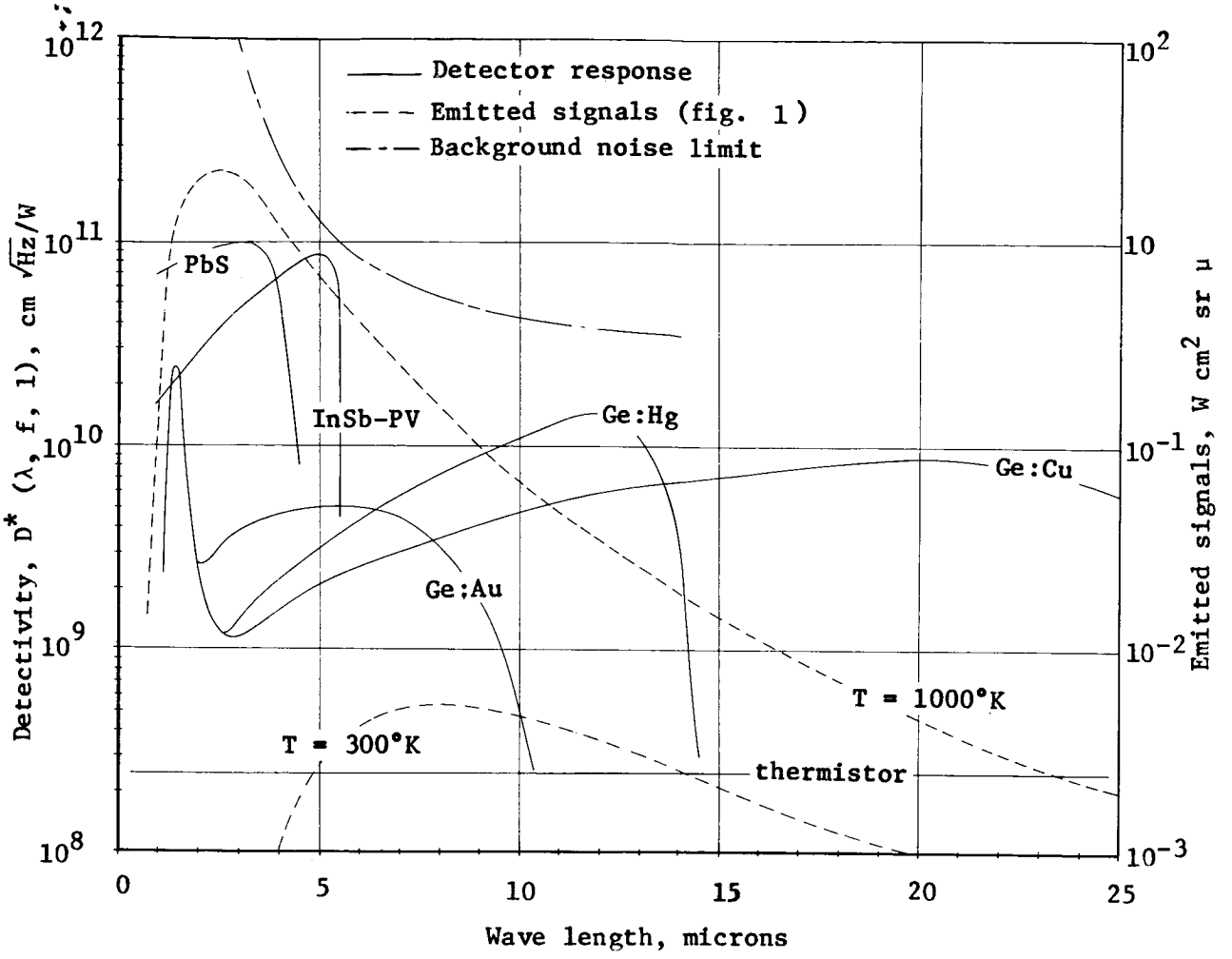

Figure 35.- Spectral response

TABLE XV.- CHARACTERISTIC DETECTOR PARAMETERS

Material	Photon or thermal	Mode of operation	Film or single crystal	N-type, P-type, intrinsic, or extrinsic	Operating temp., °K	Wavelength of peak response, microns	Cut-off wavelength (50% down), microns	Peak detectivity, cm $\sqrt{Hz}$/W	Response time, μs	Resistance per square, ohm	Noise mechanism	Min. practical area, mm^2
thermistor Bolometer	thermal	bolometer	-	-	300	flat	-	2.5×10^8 (90 Hz)[b]	1000	2.4×10^6	Thermal	.01
PbS	photon	photo conductive	film	intrinsic	77	2.5	3.3	8.0×10^{10} (90 Hz)[b]	455	5×10^6	current	.05
InSb-PV	photon	photo voltaic	single crystal	PN	77	5.3	5.5	8.8×10^{10} (900 Hz)[b]	1	1×10^3	current below 100 Hz gr above[a]	.01
Ge:Au	photon	photo conductive	single crystal	P-type	77	5.0	7.1	1.75×10^{10} (900 Hz)[b]	1	1×10^6	current below 40 Hz gr above[a]	.05
Ge:Hg	photon	photo conductive	single crystal	extrinsic	28	11.4	14	1.3×10^{10} (900 Hz)[b]	0.1	1×10^6	current below 400 Hz gr above[a]	.05
Ge:Cu	photon	photo conductive	single crystal	P-type	10	20	27	8.75×10^9 (900 Hz)[b]	0.1	1×10^5	current below 1000 Hz gr above[a]	.05

[a]Generation-regeneration noise.

[b]Chopping frequency.

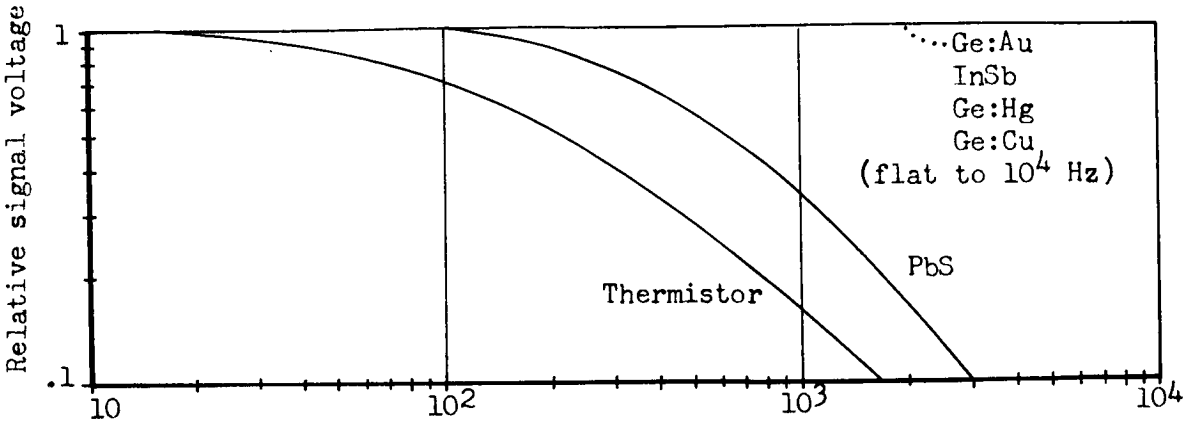

Frequency, Hz

Figure 36. - Frequency response

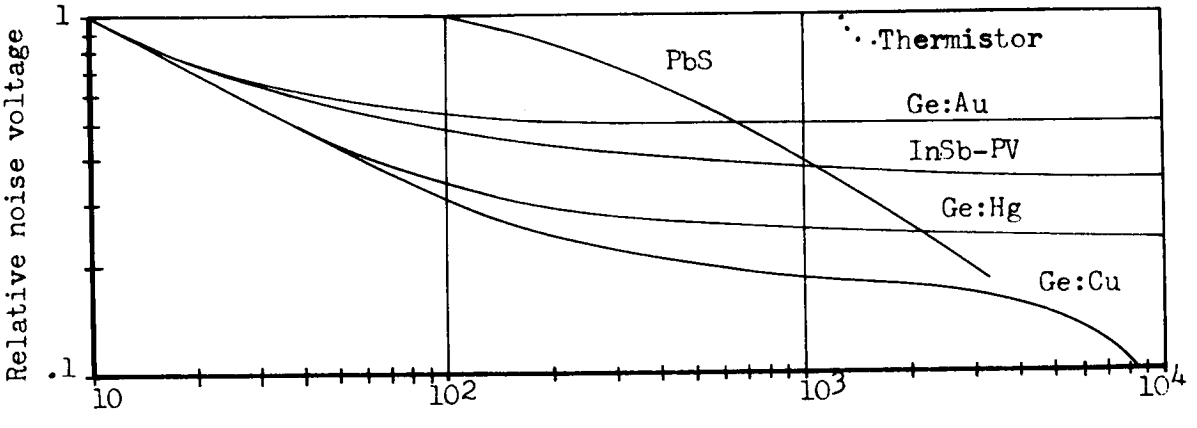

Frequency, Hz

Figure 37. - Noise spectra

exponentially with temperature. When the radiation is removed the thermistor flake returns to its original temperature with a decay dependent upon the thermal conductance between the flake and its heat sink mount. Thus inherently its time constant is long and, since its output is dependent on the total incident energy absorbed, its spectral response is flat.

Thermistor detectors can be constructed with a wide selection of sensitive areas (down to approximately 0.1 mm x 0.1 mm) and a variety of response times (1.0 to 50 milliseconds). Since the specific detectivity is proportional to the square root of the response time, the user should select the detector having the longest response time consistent with his frequency response requirements in order to obtain the highest

possible specific detectivity. The spectral response curve (fig. 35) and frequency response curve (fig. 36) are for a detector with a 1,000 microsecond time constant. Since most bolometers are limited by thermal noise, the noise spectrum (fig. 37) is frequency independent.

Performance of thermistor bolometers have been improved by utilizing immersion optics (D^* increased by factor of 3 to 4). Also significant performance improvement has been obtained by the superconducting bolometer. For instance the Andrews niobium nitride superconducting bolometer operating at 15°K provided a D^* value of $48 \times 10^8 cm\sqrt{Hz}/watt$ with a response time of 500 microseconds. However the stringent temperature control requirements (in the order of $\pm$ 0.0001°K) for stable operation, have prohibited its operational use.

The thermistor bolometer is characterized by a flat spectral response, a low specific detectivity, and a long time constant. It was selected for further study (fig. 12) because it is the best flat spectral response detector.

Lead Sulfide Detector (PbS) at 77°K - Lead sulfide is a highly versatile polycrystalline film, photoconductor and is by far the most extensively used of the infrared detectors. It was the first to be developed to the stage of large-quantity production. Lead sulfide exhibits a very high specific detectivity (best of all detectors at 2 micron radiation wavelength), but operation is limited to the shorter wavelengths. By cooling the detector to 77°K (liquid nitrogen temperature), the long-wavelength cutoff is extended from 2.5 microns (295°K) to 3.3 microns.

A wide selection of detector sizes (down to 0.2 mm x 0.2 mm) from either the chemical deposition or sublimation manufacturing technique are readily available on the commercial market. The detector cooled to 77°K exhibits a time constant of about 500 microseconds. Since these detectors exhibit higher values of specific detectivity for longer time constants, the user should select a detector having the longest response time constant suitable for the application. The spectral response curve (fig. 35) and frequency response curve (fig. 36) are for a detector with a 455 microsecond time constant. The detector is current noise limited; however, the noise spectrum (fig. 37) follows a power law that differs from a simple inverse frequency dependence.

The lead sulfide detector operating at 77°K is characterized by a very narrow spectral response with a long-wavelength cutoff at 3.3 microns, a very high peak specific detectivity, and a relatively long time constant. It was selected for further study (fig. 12) because of its high specific detectivity and its spectral compatibility with crown glass windows (fig. 8).

Indium Antimonide PV Detector (InSb-PV) at 77°K - Photovoltaic indium antimonide detectors are designed for use where the ultimate in performance in the 2 to 5.5 micron spectral region is required. When cooled to liquid

nitrogen temperature, 77°K, these detectors develop a short circuit current which is directly proportional to the number of effective incident photons and an open circuit voltage which is proportional to the log of the number of effective incident photons. Like all photodiodes, photovoltaic indium antimonide detectors do not require the use of a bias current for signal generation. Photovoltaic indium antimonide detectors have an inherent advantage over their photoconductive counterparts in the important areas of speed and sensitivity. It is approximately ten times faster and the theoretical specific detectivity is higher by a factor of $\sqrt{2}$. In actual production state-of-the-art, the specific detectivity advantage is even greater.

Photovoltaic indium antimonide detectors are available in production quantities with round or rectangular areas ranging from less than 10^{-4}cm^2 up to an including 1 cm^2. Performance of the detector depends on the detector area. Responsivity and peak specific detectivity values are:

Area, cm^2	Peak specific detectivity		responsivity, V/W
10^{-4} to 10^{-2}	8.8 x 10^{10}	cm$\sqrt{\text{Hz}}$/watt	10^5 volts/watt
0.01 to 0.1	6.6 x 10^{10}	cm$\sqrt{\text{Hz}}$/watt	10^4 volts/watt
0.1 to 1.0	5.5 x 10^{10}	cm$\sqrt{\text{Hz}}$/watt	10^3 volts/watt

The spectral response curve (fig. 35) and frequency response curve (fig. 36) are for a detector with a time constant of less than one microsecond under non-RC limited conditions. The noise spectrum (fig. 37) is dominated by generation-recombination noise above 100Hz .

The photovoltaic indium antimonide detector operating at 77°K is characterized by a relatively narrow spectral response (2.8 to 5.5 microns), a very high peak specific detectivity, and a short time constant. It was selected for further study (fig. 12) because of its high specific detectivity and its spectral compatibility with modified glass windows (fig. 8).

Gold Doped Germanium (Ge:Au) at 77°K.- Gold doped germanium was the first impurity activitated germanium detector in use. Photoconductive gold doped germanium provides longer wavelength operation and a relatively high specific detectivity. By cooling the detector to 77°K (liquid nitrogen temperature), the long-wavelength cutoff has been extended to 7.1 microns.

Detector sizes range from 0.3 mm x 0.3 mm to 5 mm x 5 mm commercially. As shown in the spectral response curves (fig. 35), the gold doped germanium detector has an intrimsic peak at the 2 micron wavelength. This is characteristic of all the germanium detectors and is usually removed by filtering. When the gold doped germanium is cooled to 77°K, the time constant is less than one microsecond (fig. 36). The detector noise spectrum (fig. 37) is dominated by current noise below 40 Hz, with generation-

recombination noise dominating at higher frequencies.

In order for gold-doped germanium detectors to be background limited, the operating temperature must be reduced to around 60°K. Liquid nitrogen can still be used by utilizing a vacuum forepump to reduce the vapor pressure above the liquid nitrogen. At 65°K, the specific detectivity increases by a factor of approximately 2.3 and the spectral response remains essentially the same.

The gold doped germanium detector at 77°K is characterized by a medium width spectral response with a long-wavelength cutoff at 7.1 microns, a relatively high specific detectivity, and a short time constant. It was selected for further study (fig. 12) because it provides the broadest spectral response of all the photon detectors utilizing liquid nitrogen as a coolant.

Copper Doped Germanium (Ge:Cu) at 10°K - The copper doped germanium detector is a single crystal, extrinsic, photoconductive device developed as the need for longer wavelength detectors arose. The device is capable of detection of infrared radiation from 2 to 27 microns. The detector is 300°K background limited and has a response time of less than 0.1 microsecond when cooled below 14°K.

Aperture sizes from 0.3 mm to 3 mm diameter are standard. Standard fields of view range from 10° to 150°. For various fields of view, the following peak specific detectivity values have been measured.

Field of view, deg.	Peak Specific Detectivity, $cm\sqrt{Hz}/watt$
180	0.9×10^{10}
120	1.0×10^{10}
90	1.3×10^{10}
60	1.8×10^{10}
30	3.3×10^{10}

The spectral response curve (fig. 35), frequency response curve (fig. 36), and noise spectra curve (fig. 37) are for a copper doped germanium detector cooled to 10°K.

A broader spectral response is available with photoconductive zinc doped germanium. When cooled to 4.2°K, this detector exhibits a long-wavelength cutoff at 39.5 microns. However, its stringent temperature requirements presently prohibit operational use.

The copper doped germanium detector operating at 10°K is characterized by a very broad spectral response with a long-wavelength cutoff at 27 microns, a relatively high specific detectivity, and a short time constant. It exhibits the broadest spectral response of all photon detectors now

operational.

Mercury Doped Germanium Detectors at 28°K - The mercury doped germanium detector is a single crystal, extrinsic, photoconductive device ideally suited for the detection of infrared radiation in the 8 to 14 micron spectral "window" of the atmosphere. These detectors have the highest detectivity with the least stringent cooling requirements for infrared detectors sensitive through the 2 to 14 micron region. For these reasons, much research and development has been accomplished with this detector and it is now readily available for commercial use.

Mercury doped germanium is 300°K background limited when operated below 40°K, and is normally used for detection of near ambient irradiance. When cooled below 30°K, the long time constant of 20 microseconds is eliminated and the response time is less than a microsecond. Aperture sizes from 0.3 mm to 3 mm diameter are standard. Also, standard fields of view range from 10 to 150 deg. For various values of field of view, the following peak specific detectivity values have been obtained:

Field of view, deg.	Detectivity, $cm\sqrt{Hz}/watt$	
	0.2 mm^2 > Area	0.2 mm^2 < Area
120	1.4×10^{10}	0.8×10^{10}
80	1.9×10^{10}	1.1×10^{10}
40	3.6×10^{10}	2.0×10^{10}
20	7.0×10^{10}	4.0×10^{10}

for operating temperatures below 28°K and electric fields below 30 volt/cm. The detector depicted in the spectral curve (fig. 35), the frequency response curve (fig. 36), and the noise spectra curve (fig. 37) has a response time of less than one microsecond.

With the exception of spectral response, the performance characteristics of mercury doped germanium detectors vary with operating temperature. By operating at 28°K or cooler, stable operation is obtained (Fig. 38). The problem of remaining under this temperature during peak load conditions has essentially been resolved, even for closed-cycle coolers. For instance, Norelco now provides an airborne IR system with a double-expansion Stirling-cycle cooler utilizing helium as the working gas which is capable of a no load operating temperature of 14°K. Norelco's previous single-expansion Stirling-cycle cooler was capable of a no load operating temperature of 23°K which provided only marginally stable detector operation under peak load conditions.

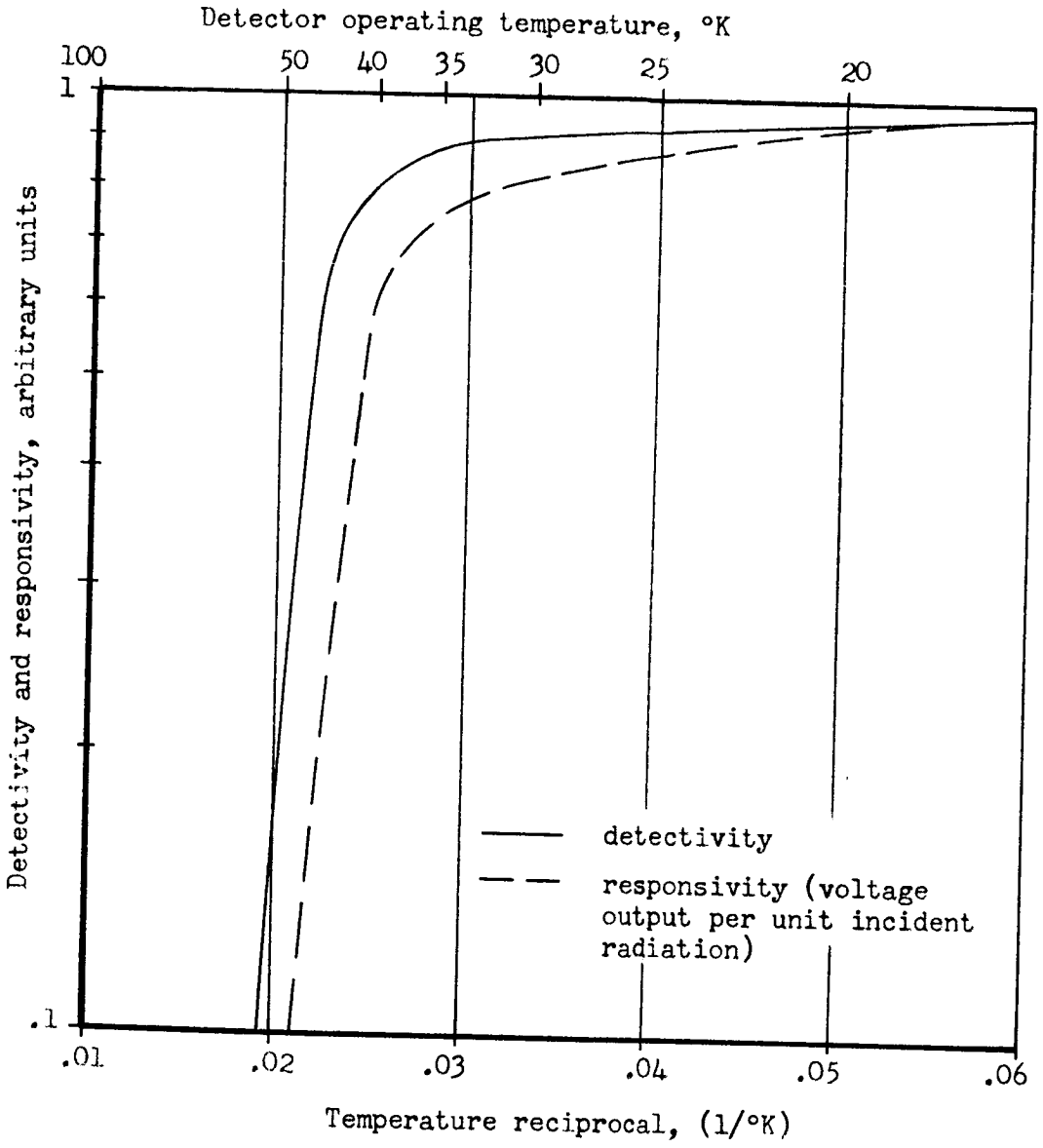

Figure 38 - Effect of operating temperature on performance of Ge:Hg detector (300°K background and optimum bias)

The mercury doped germanium detector operating at 28°K is characterized by a relatively broad spectral response with a long-wavelength cutoff at 14 micron, a relatively high specific detectivity, and a short time constant. It was chosen for further study (fig. 12) because its spectral response best matches the irradiance spectrum of room temperature objects (fig. 1).

Detector Cold Shielding - A method for increasing the specific detectivity of a background noise limited detector is to decrease the extraneous background noise input. This can be done by decreasing the field of view with cold shielding. Necessary, however, is that the cold shielding be sufficiently cool so that its photon noise is negligible compared to the background noise which it eliminated. Using photovoltaic indium antimonide as an example (fig. 39), the specific detectivity increases as the field of view decreases and is proportional to the theoretical cosecant trend for the large field of view values.

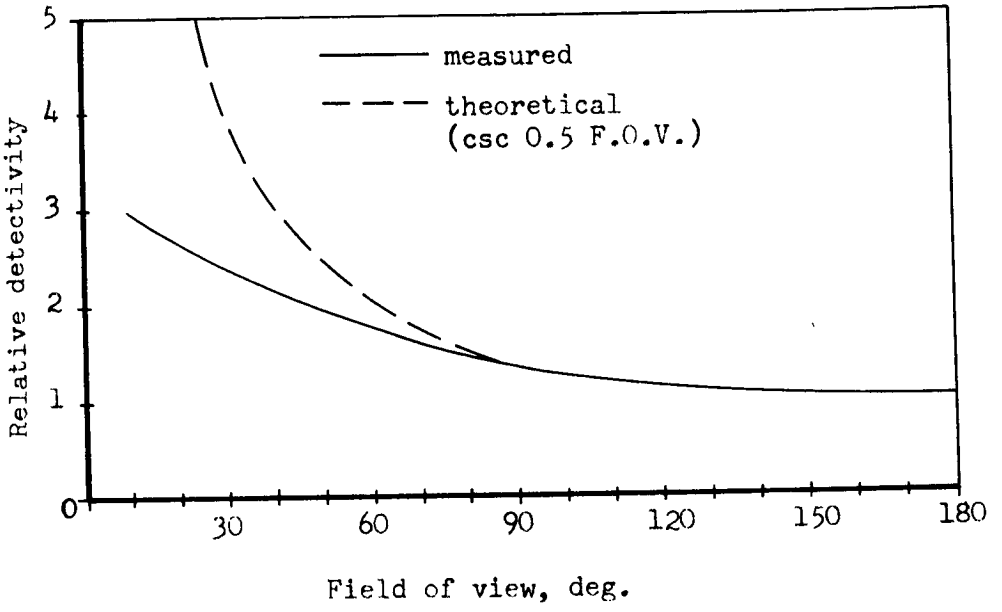

Figure 39. - Effects of cold shielding on InSb-PV detector performance (77°K operating temperature)

Wind Tunnel Window Emission - Assuming that the window is undisturbed by its environment except for temperature, the window will emit energy proportional to that absorbed after reaching a steady-state condition. This window emission as seen by the radiometer is essentially a noise source and will thus reduce the signal to noise performance or sensitivity of the overall sensor. On a macroscopic basis, the percentage of absorption is equal to unity (100%) minus the percentage of transmission minus the percentage of reflection. Assuming negligible reflection, the window emittance is proportional to unity minus the transmission (fig. 40).

Radiometer Bandwidth - This radiometer parameter is of extreme importance and is usually a design compromise. Since the infrared detector is a large noise source, minimum bandwidth is dictated. However, an

adequate bandwidth is necessary to preserve the integrity of the detected signal. The different items determing the frequency response requirements of the radiometer (i.e. scan rate, stress signal frequency, maximum bit rate, minimum frequency, possible use of a narrow band filter, etc.) require further study. (See section on "Recommended Future Work", p. 87). After sufficient analysis of the various alternate methods of detection and signal processing, a minimum but adequate bandwidth can be determined in terms of test application requirements. (See section on "Signal Processing Factors, p. 60).

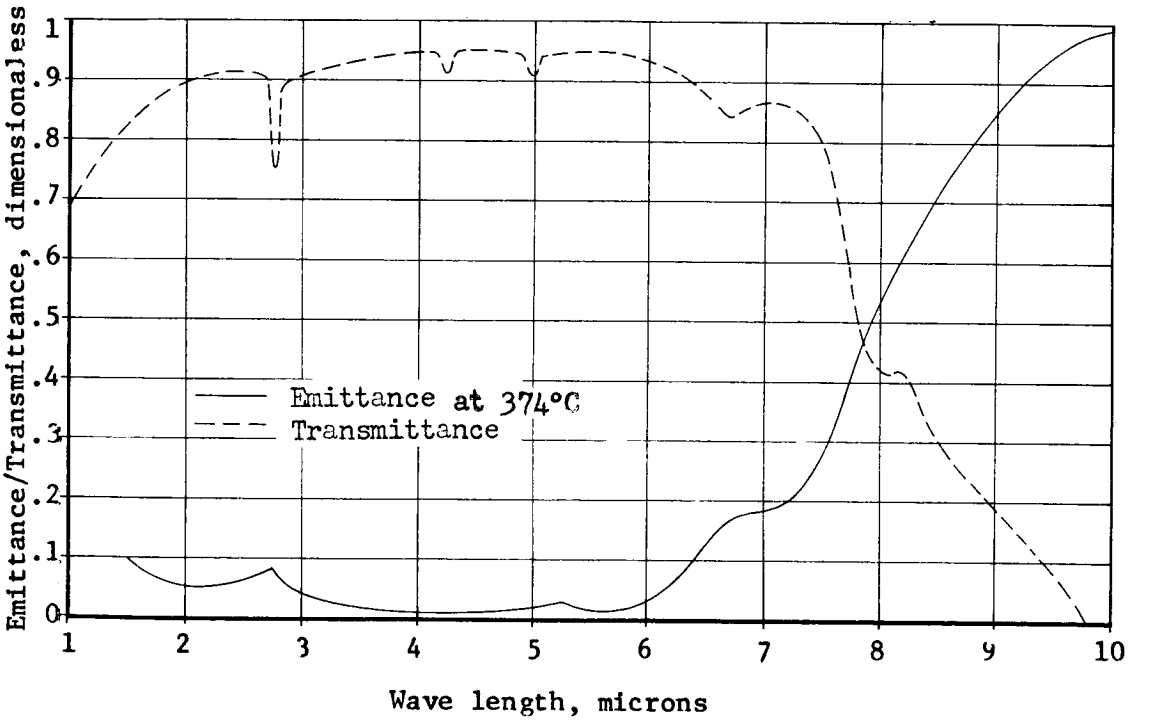

Figure 40.- Typical window emittance effects (0.04 inch thick "Irtran 1" material)

APPENDIX F

WINDOW DESIGN ANALYSIS

by Ralph T. Rauch and Milo H. Belgen

Introduction

Pressure barrier windows are required for some test facilities important to infrared stress measurements. (See section on "Pressure Barrier Window Attenuation" p. 31). It was considered desirable to identify the factors considered in the selection and design of the four window materials to be used in the infrared study.

Most test facilities have windows employing common glass materials (such as crown glass), which transmit radiant energy only at relatively short wave lengths. If exterior radiometers are employed for infrared stress measurements in such test facilities, it may be necessary to install window panes employing a material more suitable for radiant energy transmission. This would frequently be practical without major modifications of window frames. Various test facilities have round, square, or rectangular optical windows, depending on their specific functional purpose. It was therefore considered desirable to present general design criteria for all of these common window configurations.

Window Design Criteria

Geometric Factors.- Window thickness (t_w) is the geometric factor important relative to infrared transmittance losses, and it is also an important factor relative to the stress (σ_w) and deflection (δ_w) produced by pressure loading (ΔP). For the round windows, the diameter (D_w) is the additional geometric factor pertinent to stress and deflection. For rectangular (or square) windows the width (X_w) and length (Y_w) are the additional geometric factors pertinent to stress and deflection.

Type of Loading.- Test facility windows are nearly always subject to a uniformly destributed load in the form of a differential pressure (ΔP).

Mounting or Condition of Support.- Test facility windows are universally mounted so that when loaded their edges can rotate with as little restraint as possible. For this reason the analysis herein was based on windows with simply supported edges.

Strength Considerations.- The integrity of a window pane is dependent on the material strength being higher (by a factor of safety) than the maximum stress (σ_w) produced in the pane by the pressure loading (ΔP). For the high silica glasses the factor of safety based on the modulus of rupture is generally taken as ten, although lower factors of safety have been successfully applied. Some indication of the factor of safety desirable for specific applications can be gained from the following data (ref. 39).

Factor of Safety	Number of Failures[a]
1	500
2	22
2.5	8
3	4
4	1.3
10	0.150

[a]Probable number of annealed windows which will fail at initial occurrence of design load (of each 1000 pieces)

Eastman Kodak Company recommends a factor of safety of four when designing windows utilizing "Irtran" materials. In addition to modulus of rupture, Poisson's ratio (ν) is a material property pertinent to window strength because of its effect on stresses produced by pressure loading.

Deflection Considerations.- Strength or integrity as related to potential failure is the primary basis for window design, but the pane deformation under pressure loading is important relative to edge rotation in the frame and other design considerations. This can be evaluated in terms of the deflection (δ_w) at the center of the pane. Modulus of elasticity (E) is the most important material property relative to deflection, and Poisson's ratio (ν) is an additional pertinent property.

Design Analysis Methods

Circular Flat Windows.- The maximum stress at the center of a circular flat plate that is simply supported around the edge and uniformly loaded is expressed by the relations

$$\sigma_w = K_{\sigma 1}(D_w/t_w)^2 \Delta P$$

$$K_{\sigma 1} = 0.09375(3+\nu)$$

(ref. 40), where $K_{\sigma 1}$ is the stress factor. Stresses can usually be computed from the 0.3055 stress factor applicable for 0.26 Poisson's ratio.

Such computations would involve less than ± 3 percent errors for many diverse optical and infrared window materials.

Maximum deflection in a circular flat plate that is simply supported all around the edge and uniformly loaded is expressed by the relations

$$\delta_w = K_{\delta 1}(D_w^4/Et_w^3)\Delta P$$

$$K_{\delta 1} = 0.001172\ (1-\nu)(5+\nu)$$

(ref. 40), where $K_{\delta 1}$ is the deflection factor. Approximate deflections can be computed from the 0.004561 deflection factor applicable for 0.26 Poisson's ratio. However, such computations could be in error by as much as 7 to 15 percent for window materials having a 0.20 to 0.36 range of Poisson's ratio. More exact deflection factors can be readily computed with the equation above if necessary.

Rectangular Flat Windows.- Maximum stress, σ_w, at the center of a rectangular plate that is simply supported all around the edges and uniformly loaded is expressed by the relations

$$\sigma_w = K_{\sigma 2}X_w^2\Delta P$$

$$K_{\sigma 2} = 0.75 - 6\pi^2 \sum_{m=1,3,5}^{\infty} m^2\left[2\nu B_m - (1-\nu)A_m\right] \sin \frac{m\pi}{2}$$

$$A_m = -\frac{2(2 + G_m \tanh G_m)}{\pi^5 m^5 \cosh G_m}$$

$$B_m = \frac{2}{\pi^5 m^5 \cosh G_m}$$

$$G_m = \frac{m\pi Y_w}{2X_w}$$

(ref. 40), where $K_{\sigma 2}$ is the stress factor. When numerical values are substituted into the above equations, the stress factor can be evaluated

as a function of Poisson's ratio. (Table XVI).

TABLE XVI.- STRESS FACTOR EQUATIONS FOR RECTANGULAR PLATES

Length-to-width ratio, (Y_w/X_w), dimensionless	Stress factor, $K_{\sigma 2}$, dimensionless
1	$(0.2213 + 0.2208\nu)$
2	$(0.5788 + 0.1044\nu)$
3	$(0.7041 + 0.0300\nu)$
4	$(0.7380 + 0.0091\nu)$

By inspection of these equations it is apparent that the greatest variation of stress factor with Poisson's ratio occurs when length-to-width ratio is unity. However, the percentage error introduced by assuming 0.26 Poisson's ratio is less than $\pm$ 8% for the 0.20 to 0.36 range of Poisson's ratio. Stress factors can readily be computed on the basis of this assumption (fig. 41).

Shearing forces Q_X and Q_Y along the edges of simply supported rectangular plates are expressed by the relations

$$Q_X = K_{QX} X_w \Delta P$$

$$K_{QX} = 0.5 - 0.4053 \sum_{m=1,3,5}^{\infty} \frac{1}{m^2 \cosh G_m}$$

$$Q_Y = K_{QY} X_w \Delta P$$

$$K_{QY} = 0.4053 \sum_{m=1,3,5}^{\infty} \frac{(-1)^{\frac{m-1}{2}}}{m^2} \tanh G_m$$

(ref. 40), applicable to the center of the long and short sides, respectively. The values of shearing force factors K_{QX} and K_{QY} can be computed (fig. 41).

The reactions at the edges of a rectangular plate are expressed by the relations

$$V_X = K_{VX} X_w \Delta P$$

$$V_Y = K_{VY} X_w \Delta P$$

applicable at the center of the long and short sides, respectively. The values of reaction factors can be computed (fig. 41).

In the design of a frame for a rectangular plate it may be important to make the frame sufficiently rigid to keep the corners from rising. If the corners are not prevented from rising the calculated stress at the center of the plate will have to be multiplied by the factor,

$$K_{\sigma k} = \frac{X_w^4 - 0.4167\, X_w^2 Y_w^2 + Y_w^4}{X_w^4 - 0.8333\, X_w^2 Y_w^2 + Y_w^4}$$

(ref. 40). Values for this factor can be computed (fig. 42). If it is found necessary to hold the corners of the window down, the required force at each corner is expressed by the relation

$$R = K_R X_w^2 \Delta P$$

(ref. 40). The values of this force factor can be computed (fig. 43).

The maximum deflection at the center of a rectangular plate that is simply supported all around the edges and uniformly loaded is expressed by the relations

$$\delta w = K_{\delta 2} (X_w^4 / E t_w^3) \Delta P$$

$$K_{\delta 2} = (1-\nu^2)\left\{\frac{5}{32} - \frac{48}{\pi^5} \sum_{m=1,3,5}^{\infty} \frac{(-1)^{\frac{m-1}{2}}}{m^5} \frac{2 + G_m \tanh G_m}{2 \cosh G_m}\right\}$$

(ref. 40), where $K_{\delta 2}$ is the deflection factor. It is generally unnecessary to go beyond the second term of the series in numerical calculations because of the rapid convergence, and numerical values can be computed (fig. 44).

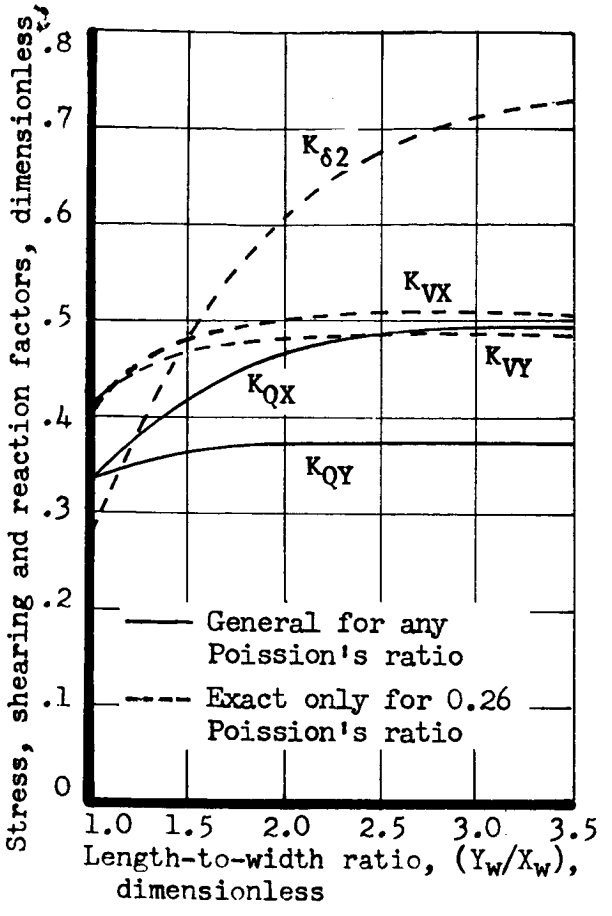

Figure 41.- Strength design factors for rectangular plates

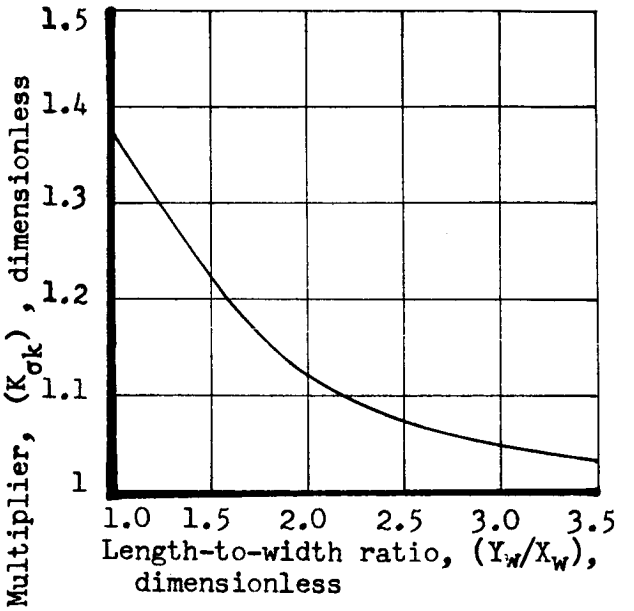

Figure 42.- Stress multiplier for rectangular plates

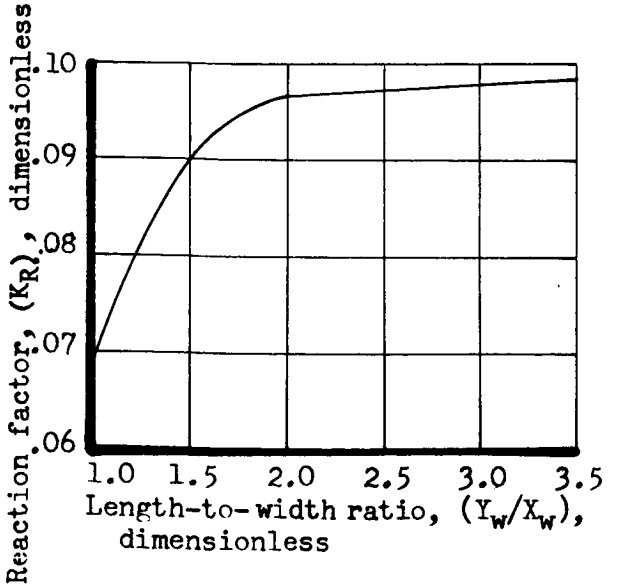

Figure 43.- Reaction factor for rectangular plate

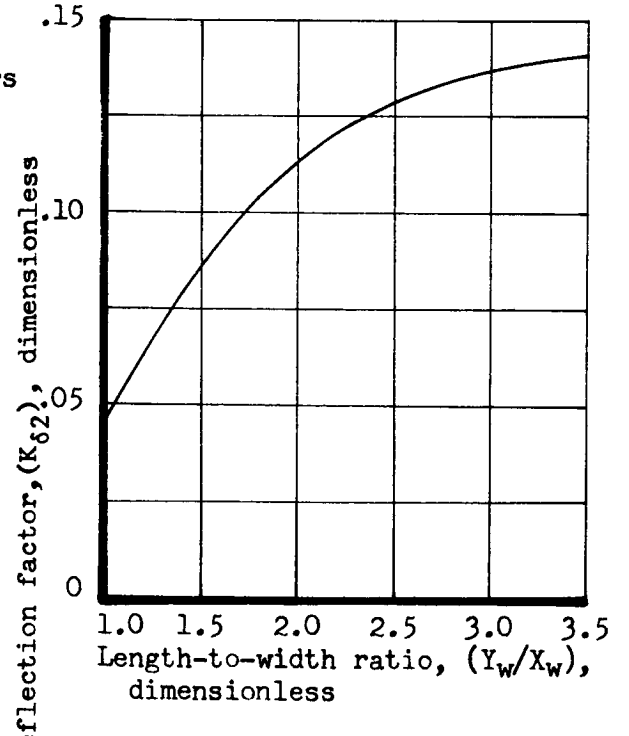

Figure 44.- Deflection factor for rectangular windows

Window Material Selection Factors

Modulus of Rupture in Bending.- It is desirable to select a material that has a modulus of rupture sufficiently high to keep the windows reasonably thin over an acceptable range of sizes and differential pressures. This modulus varies with material, the form of the section and the length-to-depth ratio for window pane materials.

Modulus of Elasticity.- Deflection is inversely proportioned to the modulus of elasticity. Therefore, a high modulus is desirable to keep deflections practical over the range of sizes and pressures likely to be encountered in the design of wind tunnels and test cells.

Poisson's Ratio.- This property has some effects on stresses and deflections for flat plates. However, the effects are relatively small for the 0.20 to 0.36 range of Poisson's ratios, which might be encountered with window materials. Therefore, this property normally has little weight in the selection of window materials.

Coefficient of Linear Expansion.- This property is used mostly to evaluate differential expansion between the window pane and its frame. Differential thermal expansion provisions can be incorporated in the frame design more readily if the pane and frame have nearly the same expansion coefficient.

Coefficient of Thermal Conductivity.- This property of the material is a factor in the temperature differential (between the two faces of the window pane) which may be obtained during test facility operation. A high conductivity is desirable to minimize temperature differentials. However, the window pane thermal stresses are dependent on the material thermal stress resistance factor as well as the thermal conductivity.

Thermal Stress Resistance Value.- This property is important relative to the thermal stresses produced by temperature differentials (between the two faces of a window pane). It is defined as the temperature difference between the two faces of a window pane which will cause a tensile stress of 1000 lb/in^2 on the cooler of the two faces. (See Table XVII footnote). A high value is desirable for minimum thermal stress.

Softening Point.- A softening point high enough for the window operating temperature of the specific application is required. The higher the softening point, the more generally adaptable the material will be for diverse facilities.

Hardness.- It is desirable that a window pane material be of high enough hardness for normal handling without damage. In some applications (such as wind tunnels), high hardness may be particularly important

from the standpoint of resisting abrasion from particles in the air stream.

Corrosion Resistance.- The material corrosion resistance must be adequate for all normal window pane usage conditions.

Water Solubility.- It is desirable (but not essential) that window pane materials be insoluble in water.

Workability.- It is desirable (but not essential) that window pane materials can be worked with reasonable ease by conventional methods currently used by manufacturers of optical equipment.

Available Size.- It is desirable (but not essential) that window pane materials be available in sizes somewhat larger than required radiometer aperture diameters. Multiple pane windows can be employed if other favorable properties of the material justify the additional complexity.

Cost.- Since all materials practical for transmitting long wave length infrared radiation are much more costly than ordinary glasses, this is a uniquely important factor in the selection of infrared window pane materials.

Selection of Materials for Infrared Stress Study

Since the existing windows of test facilities will usually be one of the common optical glasses, it was considered desirable to define infrared stress measurement limits for this type of material. Crown glass was selected as the specific material because of its widespread use for schlieren and other test facility window functions. However, its useful transmission range is typical of nearly all common glasses, which are essentially opaque at wave lengths beyond approximately 2.7 microns.

The other materials were selected on the primary basis of transmitting longer infrared wave lengths than crown glass. Although many materials transmit longer wave lengths, most of them are not useful as window pane materials. Some are excessively costly, not available in useful sizes, or are unacceptably soluble in water. Others do not have a high enough modulus of rupture, hardness, or softening point to be practical for pressure barrier window panes. However, there are materials which can be considered for windows with various spectral transmission ranges (Table XVII).

It was considered desirable to select the second window pane material primarily on the basis of availability in large sizes at low cost. There are a number of such materials which transmit wave lengths as long as approximately 3.5 to 4.5 microns (Table XVII). A specific modified glass material (Corning Glass works designation Cortran TM 9753) was selected as representative of the maximum spectral range feasible for materials with favorable physical properties and available at low cost

in sizes adequate for large radiometer apertures. There are other materials available with similar characteristics, and minor improvements of this general category of materials is likely in the future. However, development of low cost materials for long wave lengths (greater than 5 microns) currently appears improbable.

Of the few materials currently available for long wave lengths Irtran 1 is the most useful (Table XVII). It has an unusually high modulus of rupture (more than triple that of crown glass), and has no specific unfavorable physical characteristics related to window applications. It transmits to approximately 9 microns, a range compatible with most of the infrared detectors. It is currently available in sizes adequate for relatively large radiometers, and larger sizes are likely to be available in the future. Although it is costly in comparison with glasses, it is not impractically costly in relation to the total cost of a radiometer system.

For wave lengths beyond the 9.5 micron limit of Irtran 1, two materials (Irtran 2 and Irtran 4) can be considered as window materials (Table XVII), depending on the specific spectral transmission range required. Irtran 2 has a high modulus of rupture (more than double that of crown glass), and has no specific unfavorable physical characteristics related to window applications. It transmits to 14.5 microns, a range compatible with all infrared detectors except those responding in the longest wave lengths. Its available size and cost considerations are the same as for Irtran 1. Irtran 2 would usually be the best window pane material for wave lengths beyond 9 microns. Although Irtran 4 transmits to longer wave lengths (22 microns) and has a modulus of rupture about the same as crown glass, it does not have the hardness desirable for pressure barrier windows (Table XVII). It is also more limited relative to maximum size and more costly than Irtran 1 and 2. However, Irtran 4 was selected for the infrared stress application range study to provide a large increment of long wave length transmission characteristics.

Infrared transmission characteristics were evaluated in more detail for the window pane materials selected for further study. (See section on "Pressure Barrier Window Attenuation", p. 31).

TABLE XVII.- PROPERTIES OF OPTICAL AND INFRARED MATERIALS

(From ref. 13,22,23,25,26,27, and 41)

Manufacturer	Designation or Material	Transmission range,[a] microns		Modulus of rupture, lb/in^2	Poisson's ratio (ν)	Modulus of elasticity, (E), ($10^6 lb/in^2$)	Expansion coefficient, α_x, ($10^{-6}/°C$)	Knoop hardness	Water solubility, room temp., (g/100g)	Softening point, (°C)	Thermal stress resistance,[b] (°C)	Thermal conductivity, (10^{-3}cal/sec cm (°C)	Available size			Relative Cost
		min	max										Diameter, (in.)	Thickness or length, (in.)	Volume (in^3)	
Optical Glass																
	crown glass[c]		2.7	6 500	0.22	10.0 x 10^6	9.4	300-600	0	1343	16.6	3	unlimited	2.12		low
High Silica Glasses																
Corning Glass Works	fused quartz	0.3	3.5	7 000	0.22	10.4	0.8	461	0	1500	200	2.82	18½	0.75		low
Corning Glass Works	7905		3.5	10 000	0.22	9.6	0.8	477	0	1500	200	3.30	20	0.63		low
General Electric Co.	101-106	0.2	3.5	7 000	0.22	10.4	0.55	470	0	1670	272	3.30	20	0.63		low
Amersil Company	Infrasil	0.2	4.5	7 000	0.22	10.4	0.55	470	0	1700	272	3.30	20	0.63		low
Modified Glasses																
Corning Glass Works	01060		3.0		0.22	9.1	9.7	460	0	610	17.7	-	20	0.63		low
	9753[c]		3.8	8 000	0.28	14.3	6.36	560	0	981	16.9	3.00	20	0.63		low
	9754		4.2	8 000			6.36	560	0	-	-	-			80	low
Bausche and Lomb	RIR 20		5.5	5 700		12.0-14.0	9.6	542	0	760	12.5	3.20			80	low
	RIR 2		4.5	6 100		10.2	8.4	576	0	800	18.7	-			625	low
Polycrystalline Materials																
Eastman Kodak Co.	Irtran 1[c]	0.5	9.0	21 800		14.0	11.0	576	0	900	9.8	35.0	8	1		high
	Irtran 2	0.7	14.5	14 100	0.25	14.0	6.9	354	0	800	15.5	37.0	8	1		high
	Irtran 3	0.4	11.5	5 300	to	14.3	20.0[f]	200[g]	0	1000	5.3[j]	19.0	6	0.5		high
	Irtran 4[c]	0.5	22.0	6 100	0.36	10.3	7.7	150[g]	0	300[i]	18.9	31.0	6	0.5		very high
	Irtran 5	0.4	9.5	19 200		48.2	12.0	640	0	800	-	10.4	6	0.5		very high
	Irtran 6	1.5	31.0	4 500[d]		5.3[e]	5.9	45[g]	0	300[i]	-	10.0	3	0.5		very high
Single Crystal Materials																
Harshaw Chemical	T-12	2.0	9.0	570[d]	0.2	5.8[e]	18.9[f]	250	0.2[h]	-	14.6	23-28	5½	4		high
	calcium fluoride	0.4	11.5	5 300	0.2	11 to 15	24.0[f]	158[g]	0.0017	-	5.1[j]	23.2	9	5		high

[a] Approximate ranges based on various criteria in different literature (and not intended as a material comparison criteria except relative to large differences).

[b] Temperature differential, H_W, producing 1000 lb/in^2 stress as defined by the equation, $H_W = \frac{2000(1-\nu)}{E\,\alpha_x}$

[c] Materials selected for infrared stress application range study.

[d] Undesirably low modulus of rupture for pressure barrier window applications.

[e] Undesirably low modulus of elasticity.

[f] Undesirably high coefficient of thermal expansion.

[g] Undesirably low hardness, which may require care and protection in handling and usage.

[h] Slight solubility in water.

[i] Relatively low softening point.

[j] Relatively low thermal stress resistance.

REFERENCES

1. Todhunter, Isaac; and Pearson, Karl: A History of the Theory of Elasticity and the Strength of Materials. Vol. I. Dover Publications, Inc., 1960, p. 386.

2. McFarland, Keith: Adiabatic Temperature Effects in Strain Gage Systems. Paper presented at the Western Regional Strain Gage Committee Meeting, Aerospace Industries Association of Am., Inc., (Los Angeles, Calif.), 1961.

3. Dillon, O. W., Jr.; and Tancher, T. R.: The Experimental Technique for Observing the Temperatures due to the Coupled Thermoelastic Effect. Int. J. Solids Structures, Vol. 2, No. 3, July 1966, pp. 385-391.

4. Belgen, Milo H.: Structural Stress Measurements with an Infrared Radiometer. Preprint 17.19-1-65, ISA, Oct. 1965.

5. Belgen, Milo H.: Structural Stress Measurements with an Infrared Radiometer. ISA Trans., Vol. 6, No. 1, Mar. 1967, pp. 49-53.

6. Biot, M. A.: Thermoelasticity and Irreversible Thermodynamics. J. Appl. Phys., Vol. 27, No. 3, March 1956, pp. 241-242.

7. Flugge, W., ed: Handbook of Engineering Mechanics. McGraw-Hill Book Co., Inc., 1962, p. 38-2.

8. Anon.: American Institute of Physics Handbook. Second Ed., McGraw-Hill Book Co., Inc., 1963, p. 3-87.

9. Anon.: McGraw-Hill Encyclopedia of Science and Technology. Vol. 12, McGraw-Hill Book Co., Inc., 1960, p. 574.

10. Anon.: Encyclopaedic Dictionary of Physics, No. 2. Pergamon Press, Ltd., 1961, pp. 21-22.

11. Chalmers, Bruce; and King, R.: Progress in Metal Physics. Vol. 7, Pergamon Press, Ltd., 1958, p. 251.

12. Goodman, Stanley: and Russell, Stanton B.: Poisson's Ratio of Aircraft Materials for Large Strains. WADC TR 53-7, 1953.

13. Jamieson, John A.; McFee, Raymond H.; Plass, Gilbert N.; Grube, Robert H.; and Richards, Robert G.: Infrared Physics and Engineering. McGraw-Hill Book Co., Inc., 1963.

14. Jacob, Max: Heat Transfer. Vol. I. John Wiley & Sons, Inc., 1949.

15. Holter, Marvin R.; Nudelman, Sol; Suits, Gwynn H.; Wolfe, William L.; and Zissis, George J.: Fundamentals of Infrared Technology. The Macmillan Co., 1962.

16. Mechtly, E. A.: The International System of Units, Physical Constants and Conversion Factors. NASA SP-7012, 1964.

17. Carslow, H.S.: and Jaeger, J.C.: Conduction of Heat in Solids. Second ed., Oxford at the Clarendon Press, 1959.

18. McAdams, William H.: Heat Transmission. Second ed., McGraw-Hill Book Co., Inc., 1942.

19. Anon.: ASHRAE Guide and Data Book, Fundamentals and Equipment. American Society of Heating, Refrigerating, and Air-Conditioning Engineers, Inc., 1965.

20. Wyatt, P.J.: Stull, V.R.; and Plass, G.N.: The Infrared Absorption of Water Vapor. Space Systems Division Report SSD-TDR-127, Vol. II (ASTIA No. AD 132395), Aeronutronic Division, Ford Motor Company, 20 September 1962.

21. Wyatt, P.J.; Stull, V.R.; and Plass, G.N.: The Infrared Absorption of Carbon Dioxide. Space Systems Division Report SSD-TDR-127, Vol. III (ASTIA No. AD 400959), Aeronutronic Division, Ford Motor Company, 1963.

22. Ballard, Stanley S.; McCarthy, Kathryn A.; and Wolfe, William L.: Optical Materials for Infrared Instrumentation. Report 2389-11-S, Nonr 1224 (12), Research Inst. Willow Run Laboratories, Univ. of Michigan, January 1959.

23. Ballard, Stanley S.: McCarthy, Kathryn A.; and Wolfe, William L.: Optical Materials for Infrared Instrumentation (Supplement). Report 2389-11-S1, Nonr 1224(12), Research Inst. Willow Run Laboratories, Univ. of Michigan, April 1961.

24. Anon.: Properties Data Sheets for Polished Crown Glass (No. 1045). Pittsburgh Plate Glass Co., August 22, 1962.

25. Anon.: Properties Data Sheets for Modified Glass (Cortan TM 9753). Corning Glass Works, 17 December 1962.

26. Anon.: Properties of Polycrystalline Magnesium Flouride (Irtran 1). Eastman Kodak Company, September 1963.

27. Anon.: Properties of Polycrystalline Zinc Selenide (Irtran 4). Eastman Kodak Company, September 1963.

28. Anon.: Metallic Materials and Elements for Flight Vehicle Structures. DOD MIL-HDBK-5, August 1962.

29. McMaster, Robert C.: Nondestructive Testing Handbook, Vol. II. The Ronald Press Company, 1959, pp. 53.1-54.42.

30. Rocca, Roberto; and Bever, M.B.: The Thermoelastic Effect in Iron and Nickel as a Function of Temperature. Trans. AIME (J. Metals), Vol. 188, Feb. 1950, pp. 327-333.

31. Anon.: Aerospace Structural Metals Handbook. Air Force Materials Laboratory Contract AF33(616)-7792, Dec. 1963, (available from Office of Technical Services).

32. Dunn, S. Thomas; Richmond, Joseph C.; and Parmer, Jerome F.: Survey of Infrared Measurement Techniques and Computational Methods in Radiant Heat Transfer. J. Spacecraft Rockets, Vol. 3, No. 7, July 1966.

33. Anon.: Thermophysical Properties Research Center Data Book. Vol. I, Chapter 3. Purdue University, Dec. 1963, Figure 1056.

34. Goldsmith, Alexander; Waterman, Thomas E; Hirschhorn, Harry J.: Handbook of Thermophysical Properties of Solid Materials. Vol. 2. The Macmillan Company, 1961, p. 905.

35. Anon.: Emittance Graphs for 3M Velvet Coating. 3M Company, St. Paul, Minnesota, April 7, 1964.

36. Kruse, Paul W.; McGlauchlin, Laurence D.; and McQuistan, Richmond B.: Elements of Infrared Technology. John Wiley & Sons, Inc., 1962.

37. Wolfe, W.: and Limperis, T., ed: Infrared Quantum Detectors. Report 2389-50-T, Nonr 1224(12), Research Inst. Willow Run Laboratories, Univ. of Michigan, July 1961.

38. DeWaard, Russel; and Wormser, Eric M.: Thermistor Infrared Detectors. NAVORD 5495 (ASTIA No AD 160106), 30 April, 1958.

39. Anon.: Glass Performance Under Wind Load. Pittsburg Plate Glass Co., February 1962.

40. Timoshenko, S.; and Woinowsky-Krieger: Theory of Plates and Shells. Second Ed., McGraw-Hill Book Co., Inc., 1942.

41. Hoesterery, H. F.: Materials for Infrared Windows. Electronics, Vol. 32, No. 3, Jan., 1959.

NASA-Langley, 1968 —— 32 CR-1067

"The aeronautical and space activities of the United States shall be conducted so as to contribute . . . to the expansion of human knowledge of phenomena in the atmosphere and space. The Administration shall provide for the widest practicable and appropriate dissemination of information concerning its activities and the results thereof."

—NATIONAL AERONAUTICS AND SPACE ACT OF 1958

NASA SCIENTIFIC AND TECHNICAL PUBLICATIONS

TECHNICAL REPORTS: Scientific and technical information considered important, complete, and a lasting contribution to existing knowledge.

TECHNICAL NOTES: Information less broad in scope but nevertheless of importance as a contribution to existing knowledge.

TECHNICAL MEMORANDUMS: Information receiving limited distribution because of preliminary data, security classification, or other reasons.

CONTRACTOR REPORTS: Scientific and technical information generated under a NASA contract or grant and considered an important contribution to existing knowledge.

TECHNICAL TRANSLATIONS: Information published in a foreign language considered to merit NASA distribution in English.

SPECIAL PUBLICATIONS: Information derived from or of value to NASA activities. Publications include conference proceedings, monographs, data compilations, handbooks, sourcebooks, and special bibliographies.

TECHNOLOGY UTILIZATION PUBLICATIONS: Information on technology used by NASA that may be of particular interest in commercial and other non-aerospace applications. Publications include Tech Briefs, Technology Utilization Reports and Notes, and Technology Surveys.

Details on the availability of these publications may be obtained from:

SCIENTIFIC AND TECHNICAL INFORMATION DIVISION

NATIONAL AERONAUTICS AND SPACE ADMINISTRATION

Washington, D.C. 20546